Diss. ETH No. 21765

Modeling Stratospheric Aerosols Using a Coupled Aerosol-Chemistry-Climate Model

A thesis submitted to attain the degree of

DOCTOR of SCIENCES of ETH ZURICH
(Dr. sc. ETH Zurich)

presented by

Jianxiong Sheng

MSc Mécanique des Fluides, Université Paris VI

born on 8 October 1980

citizen of China

accepted on the recommendation of

Prof. Dr. Thomas Peter, examiner

Dr. Eugene Rozanov, Dr. Mian Chin, co-examiners

2014

Abstract

The presence of the stratospheric aerosol layer, also known as the Junge layer, was first discovered in the early 1960s. This aerosol layer contains mainly binary H_2SO_4/H_2O solution droplets, which scatter solar radiation, absorb the outwelling infrared radiation, and thus affect the atmospheric circulation and global climate. It also hosts heterogeneous chemistry in the stratosphere, which leads to nitrogen deactivation and chlorine activation with implications for subsequent ozone depletion, and the level of UV irradiance at the surface.

However, there are significant uncertainties in our understanding of the Junge layer, from the question which sulfur-containing gases besides carbonyl sulfide contribute to the maintenance of the layer, via the difficulties in properly describing the temporal evolution of particle size distributions and geographic spreading of aerosols after major volcanic eruptions, all the way to the radiative impacts on global climate. Substantial improvements in current modeling approaches are required to advance our quantitative understanding of the stratospheric aerosol layer and its interaction with atmospheric radiative, dynamical and chemical processes. In response to this challenge, this work has developed the coupled aerosol-chemistry-climate model SOCOL-AER, which is based on the size-bin resolving aerosol model AER and the chemistry-climate model (CCM) SOCOL. This new and in its capabilities unprecedented aerosol-CCM interactively includes all relevant aerosol microphysics, chemistry, transport, sedimentation and aerosol radiative feedbacks. By using this novel model, further aims of this thesis are the quantification of the relative contributions of anthropogenic and natural sulfur emissions to the Junge layer, and to investigate the evolution of particle size distributions after the eruption of Mt. Pinatubo, which serves as a natural analogue of for geoengineering measures involving stratospheric sulfur injections.

Simulations of the global atmospheric sulfur budget and of the sensitivity with respect to various sulfur emission scenarios have been conducted using SOCOL-AER. The model successfully reproduces all of main features of stratospheric aerosols under non-volcanic conditions, including seasonal cycle of aerosol extinctions compared to SAGE II and HALOE, and particle size distribution compared to in situ stratospheric aerosol measurements at Laramie, Wyoming. Only at the upper edge of the Junge layer does the model show a systematic underestimation of the tapering extinction ratios, likely due to meteoritic material which has not been implemented in the model. The calculated stratospheric aerosol burden is about 109 gigagram sulfur under volcanically quiescent conditions, showing excellent agreement with SAGE II. The validated model is used for sensitivity studies concerning anthropogenic SO2

emissions in China and India. These emissions may influence stratospheric aerosols more pronouncedly compared to emission changes in Western Europe or the US. This indicates that deep convection in the Western Pacific region may enable tropospheric sulfur emissions in the tropics, particularly during the summertime, to enter the stratosphere. However, even vastly enhanced tropospheric emissions from these regions in the future are predicted to contribute less than 8% to the background stratospheric aerosol burden. More importantly, even small eruptive volcanoes can contribute significantly to the background stratospheric aerosol burden. Calculations with SOCOL-AER suggest that volcanic contributions to the global stratospheric aerosol burden from medium-sized eruptions, such as that of Nabro in 2011, may lead to a doubling of background levels under quiescent conditions.

This work approaches another major uncertainty, namely the vertical distribution of initial sulfur injections during major volcanic eruptions. To this end, more than 300 atmospheric simulations of the Pinatubo eruption have been performed using the AER 2-D sulfate aerosol model in order to optimize the initial sulfur mass injection, which in previous modeling studies has often been chosen arbitrarily (e.g., applying a rectangular-shaped emission profile). The simulations are generated by the combinations of a 4-parameter vertical mass distribution, determined by a total injection mass and a skew-normal distribution function. The results suggest that (a) the initial mass loading was only 14 Mt of SO2, in contrast to the usually applied 20 Mt; (b) the injection vertical distribution extended from the tropical tropopause to 30 km; (c) it has a strong skewness toward the lower stratosphere. The rigorous approach to construct this optimized distribution is unprecedented. This provides a universal emission scenario for global 3-D simulations,which has been derived systematically from the observational data.

Based on the optimized emission scenario, this work in its last part employs SOCOL-AER to investigate the size-resolved stratospheric aerosol distributions after the eruption of Mt. Pinatubo. The coupled aerosol-chemistry-climate model SOCOL-AER is employed to investigate the impact of the aerosol radiative heating, sedimentation scheme, coagulation efficiency, and quasi-biennial oscillation (QBO) on the stratospheric aerosol loading after the eruption of Mt. Pinatubo. The aerosol module includes comprehensive sulfur chemistry and microphysics, in which the particles are size-resolved by 40 size bins spanning radii from 0.39 nm to 3.2 um. Radiative forcing is calculated online from the aerosol module according to Mie theory. The simulation shows excellent agreement with the Stratospheric Aerosol and Gas Experiment II (SAGE II) measurements, the high-resolution infrared radiation sounder (HIRS), and in situ measurements by optical particle counters above Laramie, Wyoming. It turns out that in particular an accurate sedimentation scheme is essential in order to prevent particles diffusing too rapidly to high latitudes. The use of a sophisti-

cated particle coagulation scheme plays a lesser role. The aerosol radiative feedback and the QBO help to sustain the aerosol in the tropical reservoir and affect the maximum of stratospheric aerosol burden, improving the agreement with observed distributions, but do not per se influence the decay rate of the aerosol burden. Overall, the results demonstrate the necessity of the combination of detailed resolution of individual processes and comprehensive coupling in order to achieve a proper prediction of atmospheric and climate effects following large volcanic eruptions or sulfur injections related to geoengineering.

Zusammenfassung

Die Existenz der stratosphärischen Aerosolschicht, auch bekannt unter dem Namen Junge-Schicht, wurde erstmals in den frühen 1960er Jahren entdeckt. Binäre Schwefelsäure-Wasser-Tröpfchen machen den Hauptbestandteil dieser Aerosolschicht aus. Durch die Streuung kurzwelliger und die Absorption langwelliger Strahlung beeinflussen sie Atmosphäre und Klima. Heterogene Reaktionen, die auf der Oberfläche der Aerosolpartikel ablaufen, führen zu einer Deaktivierung von Stickstoffverbindungen und einer Aktivierung von Chlorverbindungen. Stratosphärische Sulfat-Aerosole haben somit auch Auswirkungen auf den stratosphärischen Ozonabbau und folglich auf die einfallende UV Strahlung am Erdboden.

Trotz langjähriger Forschung ist unser Verständnis der Junge-Schicht noch lückenhaft. Zu den offenen Fragen gehören unter anderem: Welche schwefelhaltigen Verbindungen neben Karbonylsulfid tragen zur Existenz der Junge-Schicht bei? Wie lassen sich die zeitliche Entwicklung der Grössenverteilung sowie die Ausbreitung der Aerosolpartikel nach einem Vulkanausbruch angemessen beschreiben? Wie gross ist der Einfluss der Aerosole auf den globalen Strahlungshaushalt? Um unser quantitatives Verständnis der stratosphärischen Aerosolschicht zu verbessern sowie deren Wechselwirkungen mit Strahlung, Dynamik und Chemie zu verstehen, ist es notwendig, existierende Modellsysteme zu erweitern und neue Ansätze zu erarbeiten. Dazu wurde im Rahmen der vorliegenden Arbeit das vollständig gekoppelte Aerosol-Chemie-Klima-Modell SOCOL-AER einwickelt. Das neue Modellsystem basiert auf dem nach Partikelgrössen auflösenden Aerosolmodell AER und dem Chemie-Klima-Modell (engl. chemistry-climate model, CCM) SOCOL, und vereint erstmalig alle relevanten Rückkopplungsmechanismen zwischen Aerosol-Mikrophysik, Chemie, Transport, Sedimentation und Strahlung. Mithilfe von SOCOL-AER werden in dieser Arbeit die relativen Beiträge anthropogener und natürlicher Schwefelemissionen zur Junge-Schicht bestimmt sowie die Entwicklung der Grössenverteilung der Aerosolpartikel nach dem Ausbruch des Pinatubo untersucht. Vulkanausbrüche bilden ein natürliches Analogon zu geotechnischen Klimaschutzmassnahmen mittels Einbringen von Schwefel in die Stratosphäre.

Im Rahmen dieser Arbeit wurden zunächst etliche Modellsimulationen mit SOCOL-AER zum globalen atmosphärischen Schwefelbudget unter Berücksichtigung verschiedener Schwefel-Emissionsszenarien durchgeführt. Ein Vergleich mit Beobachtungsdaten zeigt, dass das Modell die wesentlichen Merkmale der stratosphärischen Aerosolschicht unter nicht-vulkanischen Bedingungen erfolgreich reproduziert. Daten der Aerosolextinktion von SAGE II und HALOE wurden dabei zur Evaluierung des Jahresgangs herangezogen, während die Grössenverteilung der Aerosolpar-

tikel mit stratosphärischen in-situ Messungen über Laramie, Wyoming, verglichen wurde. Einzig am Oberrand der Junge-Schicht zeigt das Modell eine systematische Unterschätzung des Extinktionsverhältnisses. Letzteres ist höchstwahrscheinlich auf das Fehlen von Aerosol-Vorläufersubstanzen meteoritischen Ursprungs im Modell zurückzuführen. Die simulierte Gesamtmenge des stratosphärischen Schwefelaerosols unter nicht-vulkanischen Bedingungen beträgt 109 Gg Schwefel und stimmt damit sehr gut mit Abschätzungen basierend auf SAGE-II Satellitenbeobachtungen überein. Des weiteren wurden mit dem Modell Sensitivitätsstudien zu anthropogenen SO2 Emissionen aus China und Indien durchgeführt. Asiatische Emissionen haben das Potenzial die stratosphärische Aerosolschicht stärker zu beeinflussen als Emissionen aus Westeuropa oder den USA. Aufgrund hochreichender Konvektion über dem tropischen Westpazifik können Schwefelemissionen, insbesondere während der Sommermonate, verstärkt aus der Troposphäre in die Stratosphäre transportiert werden. Jedoch hat sich gezeigt, dass Schwefelemissionen aus China und Indien, selbst unter der Annahme einer deutlichen Zunahme der zukünftigen Emissionsmenge, weniger als 8% zur stratosphärischen Hintergrundaerosolbelastung beitragen. Andererseits tragen schon kleine Vulkanausbrüche deutlich zur stratosphärischen Aerosolschicht bei. Modellrechnungen mit SOCOL-AER zeigen, dass Vulkanausbrüche mittlerer Grösse wie der des Vulkans Nabro im Jahr 2011 bereits zu einer Verdopplung der stratosphärischen Aerosolmenge vergleichen mit vulkanisch ungestörten Zeiten führen können.

Diese Arbeit adressiert einen weiteren grossen Unsicherheitsfaktor in Modellstudien, nämlich die vertikale Anfangsverteilung des Schwefeleintrags durch grosse Vulkaneruptionen. In bisherigen Modellstudien wurde die Anfangsverteilung oftmals willkürlich gewählt, z.B. mittels eines rechteckigen Emissionsprofils. Zur Optimierung der anfänglichen Schwefelverteilung wurden hier mehr als 300 Simulationen der Pinatubo-Eruption mit dem 2-dimensionalen Aerosolmodell AER durchgeführt, bei denen die 4 Parameter der vertikalen Massenverteilung, welche wiederum durch die emittierte Gesamtmasse und eine schiefe Normalverteilung beschrieben wird, sukzessive variiert wurden. Die Ergebnisse deuten auf folgende Anfangsverteilung hin: (a) Die anfängliche Gesamtmasse betrug anstatt der bislang angenommen 20 Mt nur etwa 14 Mt SO_2. (b) Der Schwefeleintrag erfolgte zwischen der tropischen Tropopause und 30 km Höhe. (c) Die vertikale Verteilung zeigt eine starke Asymmetrie mit Betonung auf der unteren Stratosphäre. Aufgrund der hier durchgeführten Optimierung steht nun erstmals eine durch die Beobachtungen systematisch abgestützte Anfangsverteilung zur Verwendung in globalen 3-dimensionalen Modellen zur Verfügung.

Die so optimierte Anfangsverteilung wurde im letzten Teil dieser Arbeit verwendet, um die hoch aufgelöste Grössenverteilung der stratosphärischen Aerosolschicht

nach dem Ausbruch des Pinatubo genauer zu untersuchen. Mithilfe des vollständig gekoppelten Aerosol-Chemie-Klima-Modell SOCOL-AER wurde der Einfluss der Aerosol-induzierten Strahlungserwärmung, des Sedimentationsschemas, der Koagulationseffizienz sowie der quasi-zweijährigen Schwingung (engl. quasi-biennial oscillation, QBO) auf die stratosphärische Aerosolbeladung nach dem Ausbruch des Pinatubo untersucht. Das Aerosolmodul berücksichtigt eine umfassende Schwefelchemie sowie Aerosolmikrophysik. Die Grössenverteilung der Aerosolpartikel wird mittels 40 Grössenklassen von 0.39 nm bis hin zu 3.2 m Partikelradius beschrieben. Der Strahlungsantrieb wird während der Simulation fortlaufend durch das Aerosolmodul gemäss Mie-Theorie berechnet. Die Simulationsergebnisse zeigen sehr gute Übereinstimmung mit SAGE II (Stratospheric Aerosol and Gas Experiment II) und HIRS (High-resolution Infrared Radiation Sounder) Satellitenbeobachtungen sowie mit in-situ Messungen mittels optischer Partikelzähler über Laramie, Wyoming. Es zeigt sich, dass insbesondere eine akkurate Beschreibung der Sedimentation von grosser Bedeutung ist, um eine zu schnelle Diffusion der Partikel in Richtung der hohen Breiten zu verhindern. Die Beschreibung der Koagulation von Aerosolpartikeln spielt hingegen eine untergeordnete Rolle. Die Berücksichtigung der Aerosol-induzierten Strahlungsrückkopplung sowie der QBO helfen, die Aerosolbeladung innerhalb der Tropen aufrecht zu erhalten, und beeinflussen das Maximum der stratosphärischen Aerosolbelastung. Beide Effekte führen zu einer besseren Übereinstimmung mit beobachteten Aerosolverteilungen, beeinflussen per se aber nicht die Abbaurate der Aerosolbeladung. Insgesamt zeigen die Ergebnisse dieser Arbeit die Notwendigkeit, detaillierte Prozessmodellierung mit komplexen, vollständig gekoppelten 3-dimensionalen Modellen zu kombinieren, um zuverlässige Vorhersagen der Auswirkungen grosser Vulkanausbrüche oder künstlicher Schwefelemissionen im Zuge geotechnischer Klimaschutzmassnahmen auf Atmosphäre und Klima zu erlangen.

Contents

Chapter 1

Introduction

In early 1960s, the pioneering works of *Junge et al.* [1961], *Junge and Manson* [1961] and *Chagnon and Junge* [1961] discovered the existence of an aerosol layer in the stratosphere using balloon and aircraft measurements. This stratospheric aerosol layer, also known as the Junge layer, was later found to contain mainly binary sulfuric acid solution (H_2SO_4/H_2O) droplets [*Rosen*, 1971]. The life cycle of stratospheric aerosol (under non-volcanic conditions) includes processes of sulfur-containing gases and preexisting particles entering the stratosphere through the tropical tropopause, the transport and transformation of the aerosol within the Brewer-Dobson circulation, and the removal of the aerosol through isentropic mixing and sedimentation [*SPARC*, 2006]. A schematic of the stratospheric aerosol life cycle is shown in Figure 1.1.

The aerosol plays a significant role in the Earth's radiative and chemical processes [*McCormick et al.*, 1995]. The aerosol can efficiently scatter solar radiation, thus increase the planetary albedo. At the same time, the aerosol absorbs the outwelling infrared radiation. The net effect is that the sulfate aerosol reflects solar radiation back to space and increases the Earth albedo, causing global mean cooling of the ground and the troposphere, while it heats the stratosphere. After major volcanic eruptions such as Pinatubo, the aerosol can cause a global surface cooling of approximately 0.5 K [*Dutton and Christy*, 1992], and up to 3 K warming in the tropical lower stratosphere [*Randel et al.*, 2009], see Figure 1.2. Moreover, the sulfate aerosol is important for the stratospheric chemistry hosting heterogeneous reactions, which result in nitrogen deactivation and chlorine activation with implications for subsequent ozone depletion [*Solomon*, 1999], the radiation balance of this layer and the level of UV irradiance at the surface.

However, there are significant uncertainties in our understanding of the stratospheric aerosol layer, from the question which sulfur-containing gases besides carbonyl sulfide contribute to the maintenance of the layer, via the difficulties in properly describing the temporal evolution of particle size distributions and geographic spreading of aerosols after major volcanic eruptions, all the way to the radiative impacts on global climate.

Uncertainties under volcanically quiescent conditions. *Junge* [1974] explained the stratospheric aerosol layer as a result of penetration of tropospheric sulfur dioxide (SO_2) into the stratosphere, which was later revised by *Crutzen* [1976] and *Turco et al.* [1980] proposing carbonyl sulfide (OCS) as a dominant source of stratospheric aerosols. *Chin and Davis* [1995] re-evaluated production of stratospheric aerosols from OCS oxidation to be 2 to 5 times smaller than *Crutzen* [1976], *Turco et al.* [1980], *Sze and Ko* [1979], and *Sze and Ko* [1980], revealing a possible overestimation of OCS contribution to the stratospheric background aerosol burden

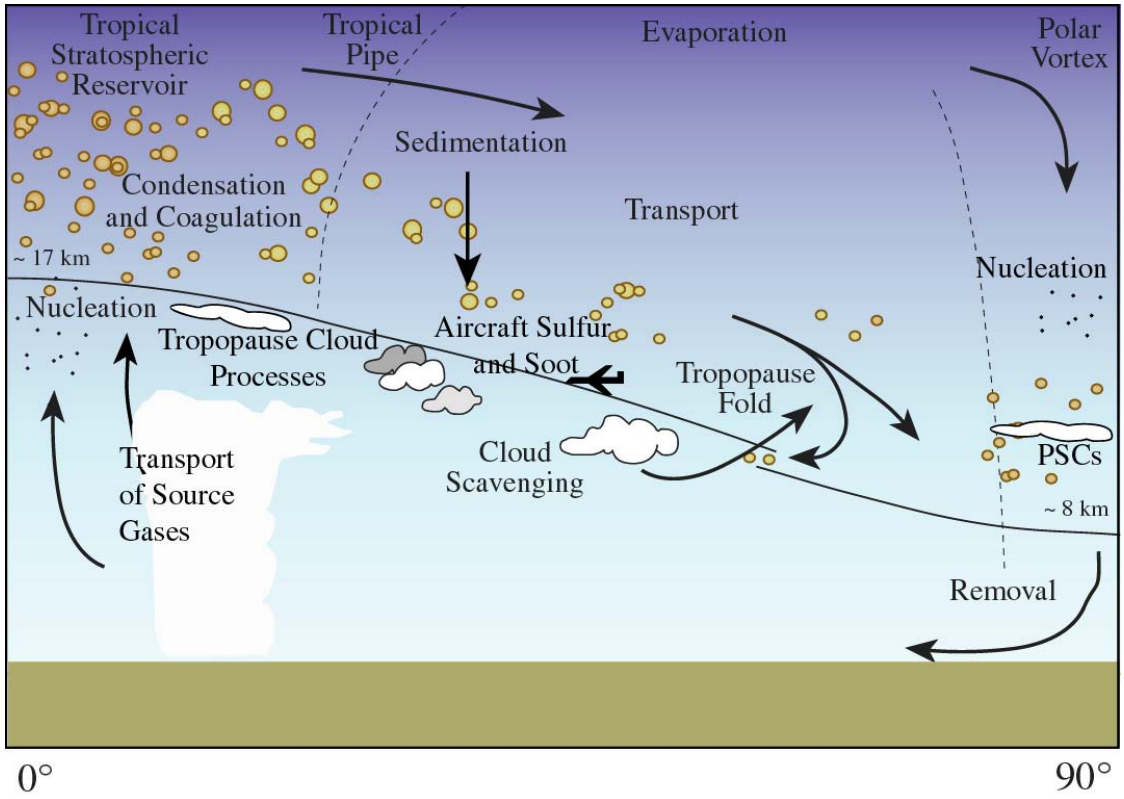

Figure 1.1 – Schematic of the stratospheric aerosol life cycle. From *Hamill et al.* [1997].

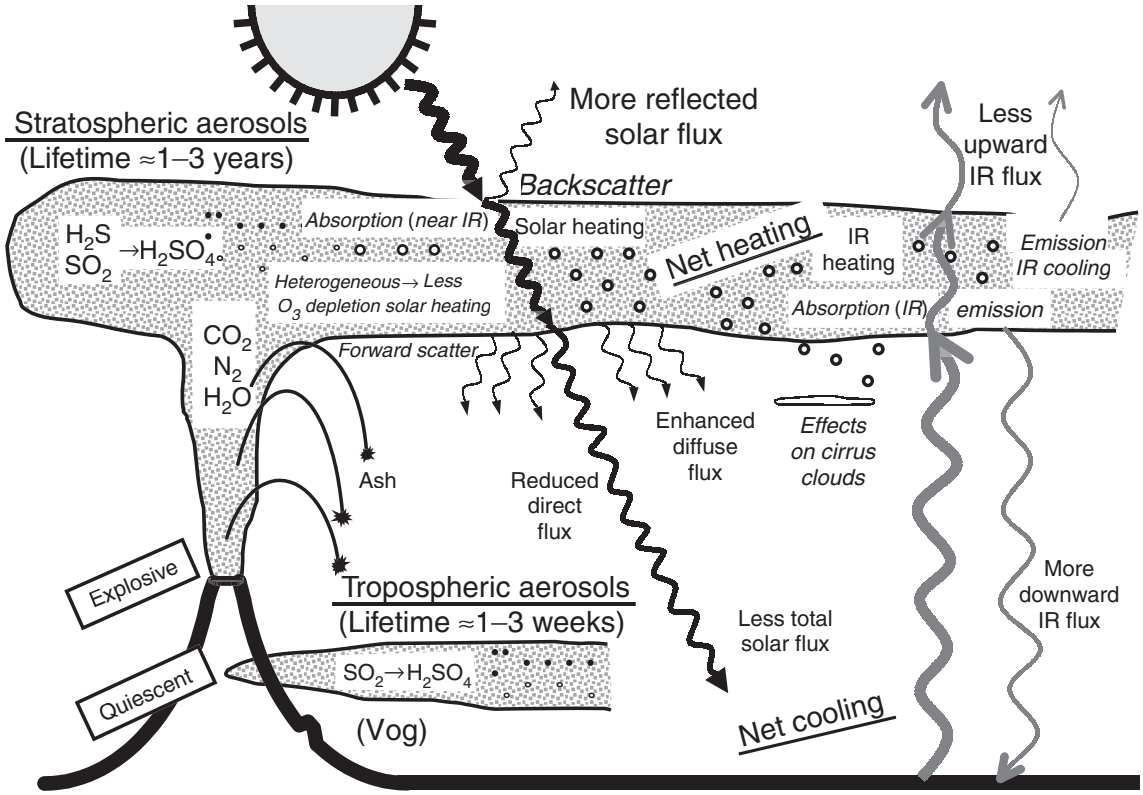

Figure 1.2 – Schematic diagram of volcanic inputs to the atmosphere and their effects. From *Robock* [2000].

in earlier studies. In an assessment of stratospheric aerosol properties [*SPARC*, 2006], studies based on various 2-D and 3-D aerosol models suggested that SO_2 and aerosol particles across the tropopause play a larger role in the lower stratosphere, while OCS is more important above 25 km. However, the relative contributions of sulfur-containing species remained largely uncertain. A recent study of *Brühl et al.* [2012] claims that most of the stratospheric aerosol burden can be explained in terms of OCS. This differs from most previous studies [e.g., *SPARC*, 2006], which indicated that short-lived sulphur gases are also important.

Uncertainties under conditions of large volcanic eruptions. The eruption of Mt. Pinatubo is one of the largest volcanic eruptions in the 20th century. However, the uncertainties in determining the initial total mass and altitude distribution of its emissions remain high. The initial total mass injection into the stratosphere ranges from 13.6 - 28 megatons of SO_2 [*Stowe et al.*, 1992; *Bluth et al.*, 1992; *Krueger et al.*, 1995; *Guo et al.*, 2004]. Also, the altitude distribution of SO_2 emission was not well-known. The only available measurements with vertical resolution of SO_2 in the

stratosphere during the Pinatubo period have been made by the Microwave Limb Sounder (MLS) in September 1991 [*Read et al.*, 1993], which started its mission unfortunately only three months after the eruption. Furthermore, there are remaining uncertainties for the impact of individual processes, such as the aerosol radiative heating, sedimentation scheme, coagulation efficiency, and quasi-biennial oscillation (QBO), on the stratospheric aerosol loading after the eruption of Mt. Pinatubo [e.g., *Timmreck et al.*, 1999a; *Aquila et al.*, 2012; *English et al.*, 2013].

Modeling stratospheric aerosols. Modeling studies are indispensable tools to synthesize our knowledge of stratospheric aerosols. Substantial improvements in current modeling approaches are required to advance our quantitative understanding of the stratospheric aerosol layer and its interaction with atmospheric radiative, dynamical and chemical processes. Earlier studies using one or two-dimensional size-bin resolving aerosol models (also known as sectional/spectral models) [e.g., *Turco et al.*, 1979; *Mills et al.*, 1999; *Weisenstein et al.*, 1997] were in general successful in simulating aerosol microphysics but had difficulties to realistically represent the tropical convection or stratosphere-troposphere exchange. Further progress towards a coupling of an aerosol module into a three-dimensional general circulation model (GCM) or chemistry-climate model (CCM) has been achieved by various studies [*Takigawa et al.*, 2002; *Stier et al.*, 2005; *Rasch et al.*, 2008; *Robock et al.*, 2008; *Timmreck et al.*, 2010; *Aquila et al.*, 2012; *Brühl et al.*, 2012]. The common feature of these models is that they used either a lognormal unimodal distribution ('bulk') or a composite of few lognormal modes ('modal') to prescribe the particles size distribution (i.e. no size bins). However, such a simplification has been found to be often insufficient to accurately reproducing observed stratospheric aerosol size distribution compared to a size-bin resolving aerosol model [*Weisenstein et al.*, 2007]. These problems have been overcome in recent studies [*Hommel et al.*, 2011; *English et al.*, 2011], which have implemented sectional aerosol modules into a GCM/CCM. However, the interaction between the aerosol radiative feedbacks and dynamics remained decoupled in their model. Lacking an explicit treatment of interactive aerosol feedbacks has also been found to be insufficient to accurately predict stratospheric aerosols, particularly after volcanic eruptions [*Aquila et al.*, 2012]. Coagulation reduces number densities very effectively for large volcanic eruptions. *English et al.* [2013] suggested that attractive van der Waals forces, which leads to enhanced coagulation efficiencies in both transition and free molecular regimes, should be taken into account. However, *Narsimhan and Ruckenstein* [1985] investigated the coagulation efficiency using the Lennard-Jones potential (retarded van der Waals forces) and demonstrated that very low coagulation efficiencies in free molecular regimes might prevail. Another important stratospheric aerosol process is sedimentation. [*Benduhn and Lawrence*, 2013] have found that numerical diffusion induced by sedi-

mentation may lead to undesirable transport of the aerosol to the middle and upper stratosphere and an accurate sedimentation scheme with minimizing numerical diffusion should be taken into account.

Motivation and objectives. Simulating stratospheric aerosols challenges models' abilities to properly represent the large-scale transport, chemistry, microphysics, sedimentation, aerosol size distribution, aerosol radiative process and their complex interactions. In response to this challenge, this thesis attempts to provide an accurate assessment of stratospheric aerosols using a coupled aerosol-chemistry-climate model (SOCOL-AER), which includes all the above features. By means of the model simulations under volcanically quiescent and active conditions, the following questions will be addressed:

1. What is the stratospheric aerosol burden under volcanically quiescent conditions and its sensitivity to sulfur emissions?
2. What would be the optimum total mass and altitude distribution for Mt Pinatubo's initial sulfur mass emission?
3. What are roles of aerosol radiative heating, coagulation efficiency, sedimentation and QBO in the evolution of stratospheric aerosols after Pinatubo?

Thesis outlines. This thesis is organized as follows:

Chapter 2: The coupled aerosol-chemistry-climate model SOCOL-AER is validated via detailed comparisons with satellite observations and in-situ measurements, such as aerosol optical properties and particle size distributions. Simulations of the global atmospheric sulfur budget and of the sensitivity with respect to various sulfur emission scenarios are conducted using SOCOL-AER. Relative contributions of natural and anthropogenic sulfur emissions are investigated.

Chapter 3: More than 300 atmospheric simulations of the Pinatubo eruption are performed using the AER 2-D sulfate aerosol model in order to optimize the initial sulfur mass injection such that the resulting aerosol extinctions match satellite and lidar measurements.

Chapter 4: The fully coupled aerosol-chemistry-climate model SOCOL-AER is employed to investigate the impact of the aerosol radiative heating, sedimentation scheme, coagulation efficiency, and quasi-biennial oscillation (QBO) on the stratospheric aerosol loading after the eruption of Mt. Pinatubo.

Chapter 5: Some technical details in the development of SOCOL-AER are provided.

Chapter 6: Conclusions of this work and perspectives on possible future research are presented.

Chapter 2

Global Atmospheric Sulfur Budget under Volcanically Quiescent Conditions and its Sensitivity to Anthropogenic Emissions

Jian-Xiong Sheng[1], Debra K. Weisenstein[2], Bei-Ping Luo[1], Eugene Rozanov[1,3], Andrea Stenke[1], Julien Anet[1], Heinz Bingemer[4] and Thomas Peter[1]

[1] Institute for Atmospheric and Climate Science,ETH Zurich, Zurich, Switzerland
[2] School of Engineering and Applied Science, Harvard University, Cambridge, MA, USA
[3] Physical-Meteorological Observatory/World Radiation Center, Davos, Switzerland
[4] Institute for Atmospheric and Environmental Sciences, Goethe-University, Frankfurt am Main, Germany

Submitted to Journal of Geophysical Research.

Abstract

Simulations of the global atmospheric sulfur budget and its emission dependence have been carried out using the coupled aerosol-chemistry-climate model SOCOL-AER. The aerosol module comprises gaseous and aqueous sulfur chemistry and comprehensive microphysics. The particle distribution is resolved by 40 size bins spanning radii from 0.39 nm to 3.2 μm, including size-dependent particle composition. Radiative properties of the aerosol required by the climate model are calculated online from the aerosol module. The model successfully reproduces main features of stratospheric aerosols under non-volcanic conditions, including aerosol extinctions compared to SAGE II and HALOE, and size distributions compared to in situ particle counter measurements. The calculated stratospheric aerosol burden is 109 gigagram of sulfur, matching the SAGE-II-based burden of 112 Gg. About 56% of this burden are caused by OCS entering the stratosphere, the rest by shorter-lived gases, mainly SO_2. Sensitivity studies with SOCOL-AER reveal that anticipated increases in anthropogenic SO_2 emissions in China and India have a larger influence on stratospheric aerosols than the same increase were it to happen in Western Europe or the US, due to deep convection in the Western Pacific region. However, even a doubling of Chinese and Indian emissions is predicted to contribute only 9% to the stratospheric background aerosol burden. In contrast, small to moderate volcanic eruptions may exert a much more significant influence. A medium-sized volcanic eruption, such as that of Nabro in 2011, may easily double the stratospheric background aerosol burden.

2.1 Introduction

The presence of an aerosol layer in the lower stratosphere was first discovered by *Junge et al.* [1961]. This aerosol layer, mainly composed of binary H_2SO_4/H_2O solution droplets, is important to the Earth's radiative balance and atmospheric chemistry. Stratospheric aerosol particles can scatter solar radiation, absorb the outwelling infrared radiation [*Ramanathan et al.*, 2001] and thus affect atmospheric dynamics [*McCormick et al.*, 1995] and the global climate [*Solomon et al.*, 2011]. They also host heterogeneous chemistry in the stratosphere, which leads to nitrogen deactivation and chlorine activation with implications for subsequent ozone depletion [*Solomon et al.*, 1986; *Solomon*, 1999]. This, in turn, affects the level of UV irradiance at the surface.

The stratospheric aerosol forms via a chain of chemical reactions and microphysical

processes when sulfur-containing gases or preexisting particles enter the stratosphere through the tropical tropopause [e.g., *Hamill et al.*, 1997; *SPARC*, 2006]. The stratospheric aerosol burden is sustained by natural and anthropogenic emissions of sulfur-containing gases at the Earth's surface and sporadic volcanic eruptions, which can release a large amount of sulfur dioxide directly into the stratosphere. Under volcanically quiescent conditions, *Junge* [1974] explained the presence of the stratospheric aerosol layer by penetration of tropospheric sulfur dioxide (SO_2) into the stratosphere, which was later revised by *Crutzen* [1976] and *Turco et al.* [1980] proposing long-lived carbonyl sulfide (OCS) as the dominant source of stratospheric aerosols. *Chin and Davis* [1995] re-evaluated the production of stratospheric aerosols from OCS oxidation to be 2 to 5 times smaller than estimated by *Crutzen* [1976], *Turco et al.* [1980], and *Sze and Ko* [1979, 1980], revealing a possible overestimation of the OCS contribution to the stratospheric background aerosol in earlier studies. In a recent assessment of stratospheric aerosol properties [*SPARC*, 2006], studies based on various 2-D and 3-D aerosol models suggested that the transport of SO_2 and aerosol particles across the tropopause may play a larger role in the lower stratosphere, while OCS is more important above 25 km.

Modeling studies have advanced our quantitative understanding of stratospheric aerosols, albeit constrained by remaining model uncertainties. Simulating stratospheric aerosols challenges our models' ability to resolve the transport, chemistry, microphysics of the aerosol size distribution, and complex interactions between them. One or two-dimensional size-bin resolving aerosol models (also called sectional models or spectral models) [e.g., *Turco et al.*, 1979; *Mills et al.*, 1999; *Weisenstein et al.*, 1997] were generally successful in simulating aerosol microphysics, but are not designed to simulate tropospheric chemistry or dynamics in detail, since topography, tropical convection, surface properties, and localized emissions cannot be included *SPARC* [2006]. Further progress towards a coupling of an aerosol module into a three-dimensional general circulation model (GCM) or chemistry-climate model (CCM) has been achieved by various studies [*Takigawa et al.*, 2002; *Stier et al.*, 2005; *Rasch et al.*, 2008; *Robock et al.*, 2008; *Timmreck et al.*, 2010; *Aquila et al.*, 2012; *Brühl et al.*, 2012]. The common feature of these models is that they use either a lognormal unimodal distribution ('bulk model') or a composite of few lognormal modes ('modal model') to prescribe the particles size distribution (i.e. no size bins). However, such simplifications have been found to be often insufficient to accurately reproduce stratospheric aerosols when compared to a sectional aerosol model [*Weisenstein et al.*, 2007]. Recent studies [*Hommel et al.*, 2011; *English et al.*, 2011] have implemented sectional aerosol modules into a GCM/CCM. However, in these models the aerosol radiative feedbacks, which affect the model dynamics, remained decoupled from the model dynamics. An explicit treatment of interactive

aerosol feedbacks has been identified as essential to properly simulate stratospheric aerosols, in particular after large volcanic eruptions [*Aquila et al.*, 2012].

Significant progress can in principle be achieved when coupling a particle-size resolving aerosol module into a chemistry-climate model, which interactively includes all relevant aerosol microphysics, transport, sedimentation and explicit treatment of the aerosol in the radiation code. However, initially the coupling of complex system modules often increases the model uncertainties, so that a comprehensive validation is required. In this study, we introduce an aerosol-chemistry-climate model, possessing the above features. Applying this model, we analyze the global sulfur budget, and investigate the sensitivity of the stratospheric aerosol burden to SO_2 emissions. We show detailed comparisons of aerosol optical properties and particle size distribution with satellite observations and in-situ measurements. While the main purpose of this paper is to provide a more accurate and comprehensive understanding of stratospheric aerosols under background conditions, the application to strong volcanic eruptions also shows excellent agreement, which will be shown elsewhere (Sheng et al., Size-Resolved Stratospheric Aerosol Distributions after Pinatubo Derived from a Coupled Aerosol-Chemistry-Climate Model, in prep. for Journal of Geophysical Research).

The organization of this paper is as follows: in Section 2, we describe the fully coupled aerosol-chemistry-climate model, including sulfur chemical reactions, aerosol microphysical processes and explicit treatment of the aerosol in the radiation code. We give a detailed description of the experimental setup for different SO_2 emissions used in our simulations. Section 3 presents results of the calculated global sulfur budget under volcanically quiescent conditions and the sensitivity studies of different SO_2 emissions. The results are compared with satellite observations, such as SAGE II, HALOE and CALIOP, and in situ measurements above Laramie, Wyoming, and with other models. Finally, Section 5 provides the conclusions.

2.2 Model description

2.2.1 CCM SOCOL

In this work, we employ an updated version of the chemistry climate model SOCOL [*Stenke et al.*, 2013], coupled to a particle-size resolved sulfate aerosol model. SOCOL is a combination of the global circulation model (GCM) ECHAM5 (the middle atmosphere version) and the chemistry-transport model (CTM) MEZON. ECHAM5 [*Roeckner et al.*, 2003] is a spectral model with adjustable horizontal truncations

(which we are using in T31 or T42) and with a hybrid sigma-pressure coordinate system spanning from the surface to 0.01 hPa (which we are using 39 or 90 vertical levels). The chemistry-transport part MEZON [*Rozanov et al.*, 1999; *Egorova et al.*, 2003] has the same vertical and horizontal resolutions as ECHAM5 and treats 56 chemical species of the oxygen, hydrogen, nitrogen, carbon, chlorine and bromine groups, which interact via more than 160 gas-phase reactions, 58 photolysis reactions and 16 heterogeneous reactions in/on sulfuric acid aerosols, water ice and nitric acid tri-hydrate particles. The chemical reaction rate coefficients are taken from *Sander et al.* [2011]. Photolysis rates are calculated at every chemical time step (2 h) using a look-up-table approach [*Rozanov et al.*, 1999]. The chemical solver is based on the implicit iterative Newton-Raphson scheme [*Ozolin*, 1992; *Stott and Harwood*, 1993]. The chemistry module comprises the full stratospheric chemistry and a reduced set of tropospheric chemical reactions. For carbon-containing species this includes the full methane photochemistry (CH_4, HCHO, CO, and intermediates), but no non-methane hydrocarbons. Dry deposition of O_3, CO, NO, NO_2, HNO_3 and H_2O_2 are taken into account with deposition velocities over land and sea based on *Hauglustaine et al.* [1994]. Furthermore, the tropospheric washout of HNO_3 is described in a simplified manner by a constant removal rate of 4×10^{-6} s^{-1}; i.e., every two hours 2.8% of the tropospheric HNO_3 is removed. SOCOL has also been run with a fully coupled deep ocean module [*Anet et al.*, 2013]. In this study, for computational efficiency the deep ocean module remains decoupled, and the version with the horizontal truncation T31, (i.e., $\sim 3.75^\circ \times 3.75^\circ$ latitude/longitude resolution) and with 39 hybrid vertical levels is employed. Global sea surface temperatures (SSTs) and sea ice coverage (SIC) are prescribed following the HadISST dataset [*Rayner et al.*, 2003]. The quasi-biennial oscillation (QBO) is nudged in terms of a linear relaxation of the simulated zonal winds in the equatorial stratosphere to observed wind profiles. For a more detailed description we refer to *Stenke et al.* [2013] and the references therein.

2.2.2 Aerosol module

The aerosol module is based on the AER two-dimensional model of sulfate aerosols [*Weisenstein et al.*, 1997]. The module includes the sulfate precursor gases dimethyl sulfide (DMS), carbon disulfide (CS_2), hydrogen sulfide (H_2S), methyl sulfonic acid (MSA), carbonyl sulfide (OCS), sulfur dioxide (SO_2), sulfur trioxide (SO_3) and sulfuric acid (H_2SO_4). For the chemical reactions we follow *Weisenstein et al.* [1997], but update the rate coefficients according to *Sander et al.* [2011], see Table 2.1. In comparison to the original AER code, the photolysis rate of H_2SO_4 has been updated to include photodissociation not only in the ultra-violet, but also in the

Table 2.1 – Sulfur Chemical Reactions and Rate Coefficients Included in SOCOL-AER (in units $cm^3\ s^{-1}$, except for photolysis rates in s^{-1}). All gas reaction rates are taken from *Sander et al.* [2011] and the references therein except for the photolysis rate of H_2SO_4 following *Vaida et al.* [2003] and *Miller et al.* [2007]. Short-lived intermediate radicals such as S, SO, and HSO_3 are omitted, and immediately converted to the next more stable intermediate. Balancing oxygen molecules are omitted from the reaction equations. Temperature (T) in Kelvin, pressure (p) and surface pressure (p_{surf}) in hPa. [M], [H_2O] and [O_2] are molecule number densities with units cm^{-3}. Symbols A are in units $cm^3\ s^{-1}$, symbols B are unitless).

Reaction	Rate
$CS_2 + h\nu \longrightarrow OCS + SO_2$	lookup table
$OCS + h\nu \longrightarrow SO_2 + CO$	lookup table
$H_2SO_4 + h\nu \longrightarrow SO_3 + H_2O$	*Vaida et al.* [2003]; *Miller et al.* [2007]
$SO_3 + h\nu \longrightarrow SO_2 + O$	lookup table
$CS_2 + OH \longrightarrow OCS + SO_2$	$\frac{A}{T+B}\left(\frac{p}{p_{\mathrm{surf}}}\right)$
	$A = 1.25 \times 10^{-16} \exp(4550/T)$
	$B = 1.81 \times 10^{-3} \exp(3400/T)$
$CS_2 + O \longrightarrow OCS + SO_2$	$3.2 \times 10^{-11} \exp(-650/T)$
$OCS + OH \longrightarrow SO_2 + CO + H$	$1.1 \times 10^{-13} \exp(-1200/T)$
$OCS + O \longrightarrow SO_2 + CO$	$2.1 \times 10^{-11} \exp(-2200/T)$
$H_2S + OH \longrightarrow SO_2 + H_2O$	$6.1 \times 10^{-12} \exp(-75/T)$
$H_2S + O \longrightarrow SO_2 + OH$	$9.2 \times 10^{-12} \exp(-1800/T)$
$H_2S + Cl \longrightarrow HCl + SO_2$	$3.7 \times 10^{-11} \exp(210/T)$
$H_2S + Br \longrightarrow HBr + SO_2$	$1.4 \times 10^{-11} \exp(-2750/T)$
$DMS + OH \longrightarrow SO_2 + CH_2O + CH_3O_2H$	$1.1 \times 10^{-11} \exp(-240/T)$
$DMS + OH \longrightarrow SO_2 + CH_2O + CH_3O_2H$	$AB/(1+B)$
	$A = 2.8 \times 10^{-12} \exp(350/T)$
	$B = 5.53 \times 10^{-31} \exp(7460/T)[O_2]$
$DMS + OH \longrightarrow MSA + CH_2O$	$AB/(1+B)$
	$A = 7.6 \times 10^{-13} \exp(350/T)$
	$B = 5.53 \times 10^{-31} \exp(7460/T)[O_2]$
$DMS + NO_3 \longrightarrow SO_2 + NO_2 + CH_3O_2 + CH_2O$	$1.9 \times 10^{-13} \exp(500/T)$
$DMS + ClO \longrightarrow SO_2 + HOCl$	$2.1 \times 10^{-15} \exp(340/T)$
$DMS + Br \longrightarrow SO_2 + HBr$	$9.0 \times 10^{-11} \exp(-2390/T)$
$DMS + BrO \longrightarrow SO_2 + HOBr$	$1.4 \times 10^{-14} \exp(950/T)$
$SO_2 + OH \longrightarrow SO_3 + HO_2$	$\frac{A}{1+B} \times 0.6^{[1+(\log B)^2]^{-1}}$
	$A = 3.3 \times 10^{-31}(300/T)^{4.3}[M]$
	$B = A/1.6 \times 10^{-12}$
$SO_2 + O \longrightarrow SO_3$	$\frac{A}{1+B} \times 0.6^{[1+(\log B)^2]^{-1}}$
	$A = 1.8 \times 10^{-33}(300/T)^{-2}[M]$
	$B = A/4.2 \times 10^{-14}(300/T)^{-1.8}$
$SO_2 + O_3 \longrightarrow SO_3 + O_2$	$3.0 \times 10^{-12} \exp(-7000/T)$
$SO_3 + H_2O \longrightarrow H_2SO_4$	$8.5 \times 10^{-41} \exp(6540/T)[H_2O]$
$S(IV) + O_3(aq) \longrightarrow S(VI) + O_2(aq) + H^+$	*Jacob* [1986]
$S(IV) + H_2O_2(aq) + H^+ \longrightarrow S(VI) + 2H^+ + H_2O(aq)$	*Jacob* [1986]

visible based on *Vaida et al.* [2003] with the corrected J value suggested by *Miller et al.* [2007]. Additionally, the aqueous phase reactions of S(IV) with ozone (O_3) and hydrogen peroxide (H_2O_2) in cloud water content [*Jacob*, 1986] have been taken into account. In a simplified approach, we prescribe the vertical distribution of the pH value according to *Walcek and Taylor* [1986]. The oxidants involved in the sulfur chemistry (OH, $O(^1D)$, $O(^3P)$, O_3, H_2O_2) are calculated interactively by MEZON together with all other 56 chemical species.

Detailed descriptions of the coded microphysics are provided by *Weisenstein et al.* [1997, 2007] and the references therein. Here we describe major features of the original model, and improvements implemented in our coupled model. Aerosol particles are resolved into 40 size bins from 0.39 nm to 3.2 μm by volume doubling. Aerosol composition (sulfuric acid weight percent) is calculated from ambient water vapor and temperature [*Tabazadeh et al.*, 1997]. Beyond the original AER code the composition of individual aerosol particles is allowed to be size-dependent such that, for each size bin, the water vapor pressure is corrected by the Kelvin effect [*Thomson*, 1871]. All relevant microphysical processes are implemented in the module. Sulfate particles are created by binary homogeneous nucleation [*Vehkamäki et al.*, 2002]. Particles can also grow/shrink by condensation/evaporation of H_2SO_4 and H_2O vapors, and evaporate completely above $\sim$35 km depending on sulfuric acid equilibrium vapor pressure over binary solution calculated by *Ayers et al.* [1980] including temperature correction provided by *Kulmala and Laaksonen* [1990]. The calculation of activity coefficients of water and sulfuric acid follows *Giauque et al.* [1960]. Coagulation reduces number densities of particles and is solved by a semi-implicit method [*Jacobson and Seinfeld*, 2004], which is another improvement beyond the original AER model code. The coagulation kernel is calculated by the empirical formula of *Fuchs* [1964]. Gravitational settling, which reduces the lifetime primarily of larger stratospheric particles, is treated following *Kasten* [1968]. Sedimentation adopts the numerical scheme of *Walcek* [2000] instead of the simple upwind method used in the original AER code in order to minimize the numerical diffusion [*Benduhn and Lawrence*, 2013]. Sulfate aerosols as well as gaseous H_2SO_4, MSA and SO_2 are removed below the tropopause by wet scavenging and surface deposition following *Weisenstein et al.* [1997], in which total tropospheric wet and dry removal rates were adopted: 2.5 days mean lifetime for SO_2, 5 days mean lifetime for H_2SO_4 and MSA, and 1 cm s^{-1} for deposition velocity.

2.2.3 Coupled SOCOL-AER

The aerosol module is adapted to the 3-D fields using the same vertical and horizontal resolutions as SOCOL. Sulfur chemical reactions (Table 2.1) are integrated into MEZON's chemical solver. The transport of each sulfur gas species and aerosol size bin is implemented in the advection scheme of *Lin and Rood* [1996] in ECHAM5. The SOCOL 6-band shortwave [*Cagnazzo et al.*, 2007] and 16-band longwave [*Mlawer et al.*, 1997] radiation schemes in the stratosphere are driven directly by the aerosol module instead of the off-line aerosol treatment that we used in *Heckendorn et al.* [2009] or data from a record [*Arfeuille et al.*, 2013] or from climatological data. The required extinction coefficients, single scattering albedos and asymmetry factors for each of the 22 wavelength bands are calculated from the particle size distribution in the aerosol module according to Mie theory with the refraction indices following *Biermann et al.* [2000]. Operator splitting approaches are used in the model: transport is calculated every 15 minutes, whereas chemistry, microphysics and radiation are calculated every two hours with 40 substeps (3-minute) for the microphysical processes.

2.3 Experimental setup

The standard model setup for sulfur emissions is given in Table 2.2. Anthropogenic (including shipping) and biomass burning SO_2 emissions account for 53.2 teragram of sulfur per year (Tg S/yr) based on the monthly decadal emission data [*Lamarque et al.*, 2010; *Smith et al.*, 2011] for year-2000 conditions. The SO_2 emission due to continuous volcanic degassing is horizontally distributed according to volcano locations, and set to 12.6 Tg S/yr based on the dataset of *Andres and Kasgnoc* [1998] with suggested corrections [*Graf et al.*, 1998; *Halmer et al.*, 2002; *Textor et al.*, 2004; *Dentener et al.*, 2006]. The volcano elevations are not fully resolved due to the relatively low horizontal resolution T31. OCS is passive in the troposphere and its concentration is set to a constant of 500 pptv at the surface [*Chin and Davis*, 1995; *Kettle et al.*, 2002]. We neglect the OCS annual cycle (which is of the order of 3% peak-to-peak) and interannual variability (less than 10%) [*SPARC*, 2006]. The flux of DMS is obtained from the monthly climatological sea surface DMS concentration fields [*Kettle et al.*, 1999; *Kettle and Andreae*, 2000] using the parametrization of *Nightingale et al.* [2000]. The surface flux of CS_2 is assumed to be 1 Tg S/yr between 52°S and 52°N, and H_2S is specified with a fixed mixing ratio of 30 pptv at the surface following [*Weisenstein et al.*, 1997].

Table 2.2 – Standard Model Setup of Boundary Conditions for Sulfur Source Gases

Species	Source	Boundary Value
SO_2	Anthropogenic (including ship)	51.3 Tg S/yr [a]
	Biomass burning	1.9 Tg S/yr [a]
	Continuous volcanic degassing	12.6 Tg S/yr [b]
OCS	Prescribed surface mixing ratio	500 pptv
DMS	Ocean	online calculated [c]
CS_2	Prescribed surface flux	1 Tg S/yr, 52°S-52°N [d]
H_2S	Prescribed surface mixing ratio	30 pptv [d]

[a] Decadal historic data for the year 2000 [*Lamarque et al.*, 2010; *Smith et al.*, 2011]; mapped to horizontal resolution T31.
[b] Based on *Andres and Kasgnoc* [1998] and scaled according to *Dentener et al.* [2006]; horizontally distributed according to volcano locations.
[c] Based on sea surface DMS concentration fields [*Kettle et al.*, 1999; *Kettle and Andreae*, 2000] using the parametrization of *Nightingale et al.* [2000].
[d] Following *Weisenstein et al.* [1997].

The sensitivity of the atmospheric sulfur budget with respect to sulfur emissions is estimated in both volcanically quiescent and weak to moderate active conditions. We perform calculations for 12 background and 2 volcanically perturbed scenarios, as summarized in Section 2.4.4 (Table 2.4). Each of these 12 background model simulations has been integrated over 10 years, initializing from precalculated aerosol mixing ratios [*Weisenstein et al.*, 1997]. The first 5 years are discarded as a spin-up period, and results are analyzed based on the last 5 years. Volcanic simulations are conducted with the spin-up files of REF for initialization. For volcanically perturbed conditions, we perform Nabro-like eruptions on 13 June of the first simulation year after the spin-up period in the region (13°N, 42°E): VolT injects 0.7 Tg S into the free troposphere (9-14 km) in a single pulse; VolS injects 0.7 Tg S directly into the stratosphere (16-19 km), again single pulse. In contrast to the long-term background cases, the volcanic simulations (VolT and VolS) are averaged over the first 6 months after the eruption, and compared with the long-term averages of the background cases.

2.4 Results and Discussions

2.4.1 Precursor gases

Carbonyl sulfide (OCS) and sulfur dioxide (SO_2) are the primary sources of stratospheric background aerosols. We examine these two precursor gases to validate the modeling of OCS/SO_2 oxidation and aerosol formation in the stratosphere. Here the simulated OCS is compared to measurements from Atmospheric Trace Molecule Spectroscopy (ATMOS) [*Gunson et al.*, 1996; *Rinsland et al.*, 1996] and from JPL MkIV Balloon Interferometer [*Leung et al.*, 2002]. The simulated SO_2 is compared against various model results presented in *SPARC* [2006], MIPAS (Michelson Interferometer for Passive Atmospheric Sounding) measurements operated quasi-continuously from July 2002 until April 2012 [*Höpfner et al.*, 2013] and ATMOS taken in April 1985 [*Rinsland et al.*, 1995].

Carbonyl sulfide (OCS). Figure 2.1 (left) shows the comparison between a calculated profile of OCS and measurements by ATMOS (version 3) at 5-10°N in November. The simulated values are within the range of the measurements at most altitudes (only near 28 km slightly out of the range). The modeled OCS is almost constant in the troposphere, where only the slow reaction with OH leads to OCS loss. In the stratosphere OCS decreases rapidly due to photodissociation and chemical reactions with O and OH. Our model calculation shows that photodissociation accounts for about 80% of loss of OCS in the stratosphere, while O and OH account for 17% and 3%, respectively. The calculated profile of OCS at 65°N compares favorably with MkIV observations as shown in Figure 2.1 (right). There is only a slight overestimation at 19 km. Overall, the agreement of SOCOL-AER with the ATMOS (version 3) and MkIV measurements is better than that for the models participating in the ASAP comparison (see Fig. 6.10 in *SPARC* [2006], where ATMOS version 2 was used). Of course, the tropospheric variability of OCS is absent in the model due to the prescribed 500 pptv surface mixing ratio.

Sulfur Dioxide (SO_2). Figure 2.2 (left) shows the comparison of seasonal SO_2 mixing ratio calculated by SOCOL-AER at 0-20°N with MIPAS measurements [*Höpfner et al.*, 2013]. In the UTLS region, the SOCOL-AER-calculated SO_2 match MIPAS near the tropopause ($\sim$17 km), while the agreement is less satisfactory near 22 km likely due to somewhat too high OH concentration in the model, but nevertheless the simulated SO_2 values are within the natural variability indicated by the measurements. Between 25 and 32 km, the modeled SO_2 is within 20% of MIPAS measurements, reflecting the importance of photodissociation and oxidation of OCS, which are the main sources of SO_2 in this region. Between 32 and 40 km, SOCOL-

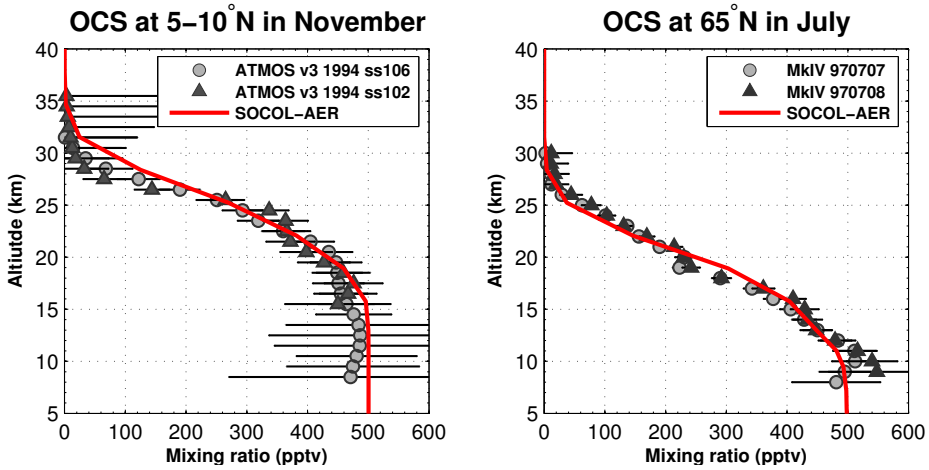

Figure 2.1 – Vertical profiles of OCS mixing ratio calculated by SOCOL-AER at 5°N in November (left) compared to ATMOS observations (version 3) [*Gunson et al.*, 1996; *Rinsland et al.*, 1996] and at 65°N in July (right) compared to MkIV balloon observations [*Leung et al.*, 2002]. Horizontal bars: observed natural variability.

AER underestimates SO_2 compared to MIPAS measurements by factors 2-3. For example, around 32 km, the modeled seasonal SO_2 mixing ratios lie between 12 and 30 pptv, while the measured mean values range from 30 to 60 pptv. One reason could be that the photolysis rate of H_2SO_4 is underestimated. The photolysis of H_2SO_4 via photodissociation of vibrationally excited states of sulfuric acid under atmospheric conditions [*Vaida et al.*, 2003] has been implemented in SOCOL-AER as additional photolysis pathway based on the parametrization by *Miller et al.* [2007] (we use the corrected J-values with quantum yield for collisional overtone de-excitation, i.e. the yellow curve in their Fig. 3). Overall, this implementation improved the agreement of SOCOL-AER with the ATMOS measurements (Figure 2.2, right panel), which is better than that for the models participating in the ASAP comparison (see Fig. 6.11b in *SPARC* [2006]). However, the resulting enhancement appears too weak to obtain good agreement with MIPAS. Near 32 km, the MIPAS mean SO_2 mixing ratios are around 20 pptv larger than those measured by ATMOS, while SOCOL-AER-calculated SO_2 mixing ratios are between these two observations. It is unclear whether this disparity between the measurements is due to measurement errors or natural variability. Between 35 to 45 km, SOCOL-AER shows excellent agreement with ATMOS (within 10%). Above 50 km, SO_2 simulated SOCOL-AER is larger by a factor of 2 compared to ATMOS (MIPAS measurements are available only up to 45 km) possibly owing to the lack of meteoritic material, which is suggested as

a permanent sink for gaseous H_2SO_4 [*SPARC*, 2006], or the lack of SO_2 photolysis [*Farquhar et al.*, 2001] in the model.

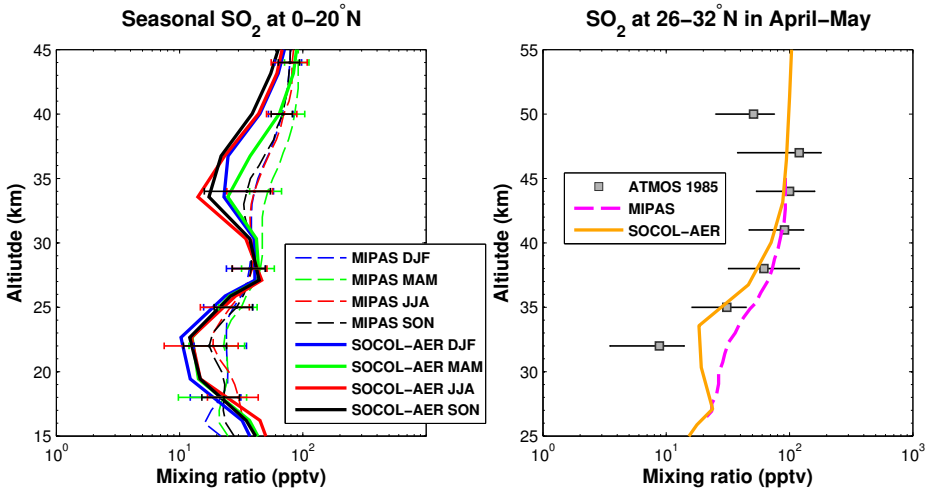

Figure 2.2 – Left panel: Seasonal SO_2 mixing ratio calculated by SOCOL-AER (solid lines) at 0-20°N compared to MIPAS measurements (dashed lines) extracted from Fig. 8 of *Höpfner et al.* [2013]; Right panel: SO_2 mixing ratio calculated by SOCOL-AER (orange line) at 26-32°N compared to ATMOS observations (squares) taken in April-May 1985 [*Rinsland et al.*, 1995] and MIPAS observations (violet line) extracted from Fig. 9 of *Höpfner et al.* [2013]. Horizontal bars: observed natural variability.

2.4.2 Sulfur budget

Figure 2.3 shows a schematic diagram of the global atmospheric sulfur budget. The solid arrows represent surface emissions, net fluxes across the tropopause, wet/dry deposition, or chemical and microphysical transformations, all in units of gigagram of sulfur per year (Gg S/yr). The dash-dotted arrows represent one-way fluxes across the tropopause into the stratosphere. The boxes denote the burden of gas and aerosol in units of gigagram of sulfur (Gg S). Red numbers are simulated by SOCOL-AER. Black numbers are retrieved from the AER 2-D model or (in brackets) from the observations, both as presented in *SPARC* [2006]. Green numbers in the troposphere are based on the GOCART model [*Chin et al.*, 2000]. Orange numbers are taken from *Chin and Davis* [1995].

In the troposphere, OCS accounts for 74% of the tropospheric total sulfur mass

in our model while short-lived SO_2 and sulfate aerosol account for 10% and 14%, respectively. The total SO_2 emission noticeably deviates among the models due to the application of different emission data. In SOCOL-AER, the decadal SO_2 emission data of *Lamarque et al.* [2010] for the year 2000 is employed. This lists about 51 Tg S/yr of anthropogenic SO_2 emissions (including ship emissions), leading to a total of ∼65 Tg S/yr for SO_2 emissions when combined with the emissions from biomass burning and volcanic degassing. Conversely, when the year 1990 chosen as basis [*SPARC*, 2006; *Chin et al.*, 2000], the total SO_2 emissions are about 75-78 Tg S/yr, mainly because the sulfur emissions by Western developed countries were decreasing in this time window. The other primary sulfur species DMS, H_2S and C_2S account for less than 2% of the tropospheric total sulfur burden, but they are an important source for SO_2 in the middle and upper troposphere and contribute about 27 Tg S/yr for SO_2, which is almost one third of the modeled tropospheric SO_2 total source strength of 92 Tg S/yr.

In the troposphere, there are additional major discrepancies between models, e.g. that SO_2 wet and dry deposition amounts to only 53 Tg S/yr in SOCOL-AER (similar to 52 Tg S/yr found by *Chin et al.* [2000]), whereas 2-D AER [*SPARC*, 2006] found 100 Tg S/yr. Furthermore, fluxes from SO_2 to the aerosol phase and aerosol deposition fluxes are comparable between this work and *Chin et al.* [2000], but have been about 5 times lower in 2-D AER. The main reason is that *SPARC* [2006] aimed at optimizing the performance of 2-D AER in the stratosphere, while tropospheric processes were highly simplified. In SOCOL-AER tropospheric performance has been largely improved (e.g., additional aqueous phase reactions of S(IV) with ozone (O_3) and hydrogen peroxide (H_2O_2) in cloud water content with prescribed vertical distribution of the pH value), although simplifications remain (e.g., the crude tropospheric washout scheme). These remaining approximations may be a reason for the discrepancies of detailed wet and dry deposition fluxes between SOCOL-AER and the tropospheric GOCART model results by *Chin et al.* [2000].

The calculated net fluxes across the tropopause (dotted horizontal line in Figure 2.3) are calculated based on mass balance considerations. Our model suggests a total net flux of 103.2 Gg S/yr of sulfur-containing gases into the stratosphere. This flux results in a burden of 109 Gg S, supporting the stratospheric aerosols under non-volcanic conditions. About 40% of the total net flux is in the form of OCS, 50% in the form of SO_2 and 10% from other primary sulfur species. The one-way OCS flux into the stratosphere calculated by SOCOL-AER is about 20% higher than calculated by 2-D AER, while the SOCOL-AER calculated net OCS flux is larger by ∼30% compared to the 2-D AER result, mainly due to differences in transport and loss processes. For SO_2, the net flux provided by SOCOL-AER of 50.9 Gg S/yr differs by more than 70% compared to 28.8 Gg S/yr calculated by 2-D

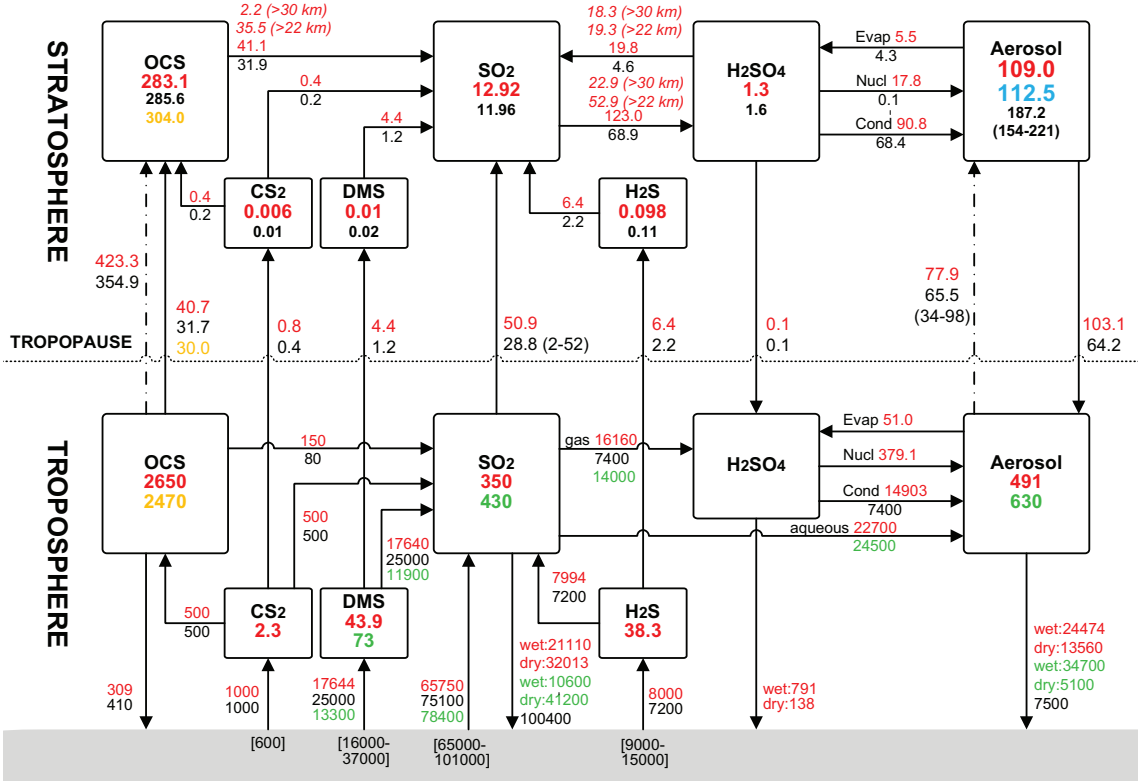

Figure 2.3 – Global atmospheric sulfur budget. Solid arrows: net fluxes of surface emissions, cross-tropopause transport (horizontal dotted line), wet/dry deposition, or chemical and microphysical transformations in Gg S/yr. Arrows point to net direction. Dash-dotted arrows: one-way fluxes across the tropopause into the stratosphere. Boxes: burdens of gases and H_2SO_4 aerosols in Gg S. Red numbers: SOCOL-AER results. Black numbers: AER 2-D results, sensitivity studies (in parentheses) and measured data (in brackets), all from *SPARC* [2006]. Green numbers: tropospheric GOCART model results *Chin et al.* [2000]. Orange numbers: *Chin and Davis* [1995]. Blue number: SAGE-II-derived aerosol mass using the SAGE-4λ method [*Arfeuille et al.*, 2013].

AER in *SPARC* [2006], indicating differences in transport and mixing ratios at the tropopause. In addition, large amounts of OCS and aerosols enter the stratosphere (dash-dotted arrows in Figure 3), but leave it again in the same form, i.e. do not contribute to the net sulfur flux.

In the stratosphere, the calculated oxidation of SO_2 to H_2SO_4 is nearly 70% higher than calculated by the 2-D AER in *SPARC* [2006], revealing a stronger gaseous source through the tropopause in SOCOL-AER. Over 85% of gaseous H_2SO_4 trans-

form to aerosols through condensation. The calculated nucleation rate is roughly two orders of magnitude larger than in 2-D AER, even though the same nucleation parameterization [*Vehkamäki et al.*, 2002] is applied in both models. This difference is to be expected, as the longitudinal temperature inhomogeneity in the 3-D model triggers more effective nucleation in comparison to the zonally averaged temperature in the 2-D model. These differences in nucleation rates are partly compensated by coagulation processes, which readily reduce particle number densities after nucleation bursts. In the upper stratosphere, aerosols evaporate and release gaseous H_2SO_4 which then photolyzes back to SO_2. The higher conversion rate here is due to the enhanced photolysis rate [*Vaida et al.*, 2003; *Miller et al.*, 2007]. The source strength for stratospheric aerosols is 186.5 Gg S/yr (108.6 Gg S/yr in form of gas and 77.9 Gg S/yr in form of aerosols) in SOCOL-AER. The resulting stratospheric aerosol burden in SOCOL-AER is 109.0 Gg S, which is 40% less than 187.2 Gg S simulated by 2-D AER (which has a total source strength 134 Gg S/yr including 68.5 Gg S/yr in form of gas and an upward flux 65.5 from prescribed primary aerosols). This noticeable difference between the two models is likely due to the rate of exchange of air between the troposphere and stratosphere (as an important aerosol removal process), which is generally not well represented by two-dimensional models [*Weisenstein et al.*, 1997], and remains a major uncertainty in the 2-D AER results. These fluxes in Figure 2.3 are hard to validate with measurements [e.g., *SPARC*, 2006], whereas the stratospheric aerosol burden can be verified through satellite and in situ measurements. Detailed model-observation comparisons of this sort are presented in the next subsection.

2.4.3 Comparisons to stratospheric aerosol measurements

In this subsection, the SOCOL-AER-based calculations of aerosol extinctions from visible to IR wavelengths are examined against SAGE II and HALOE. Specifically, the stratospheric aerosol burden is compared with SAGE-4λ data described by *Arfeuille et al.* [2013]. Particle size distributions and volume densities are compared to in situ measurements above Laramie, Wyoming [*Deshler et al.*, 2003; *Deshler*, 2008].

Comparisons with SAGE extinctions. The Stratospheric Aerosol and Gas Experiments (SAGE) provides the best space-time coverage of aerosol extinctions in the stratosphere [*Thomason et al.*, 1997, 2008]. Here we use the two most reliable wavelengths 525 and 1020 nm from SAGE II version 7.0, which is an update of *SPARC* [2006] (version 6.2). Figure 2.4 compares SOCOL-AER's extinctions with 2-D AER in *SPARC* [2006] and with SAGE II v7.0 at the equator for different

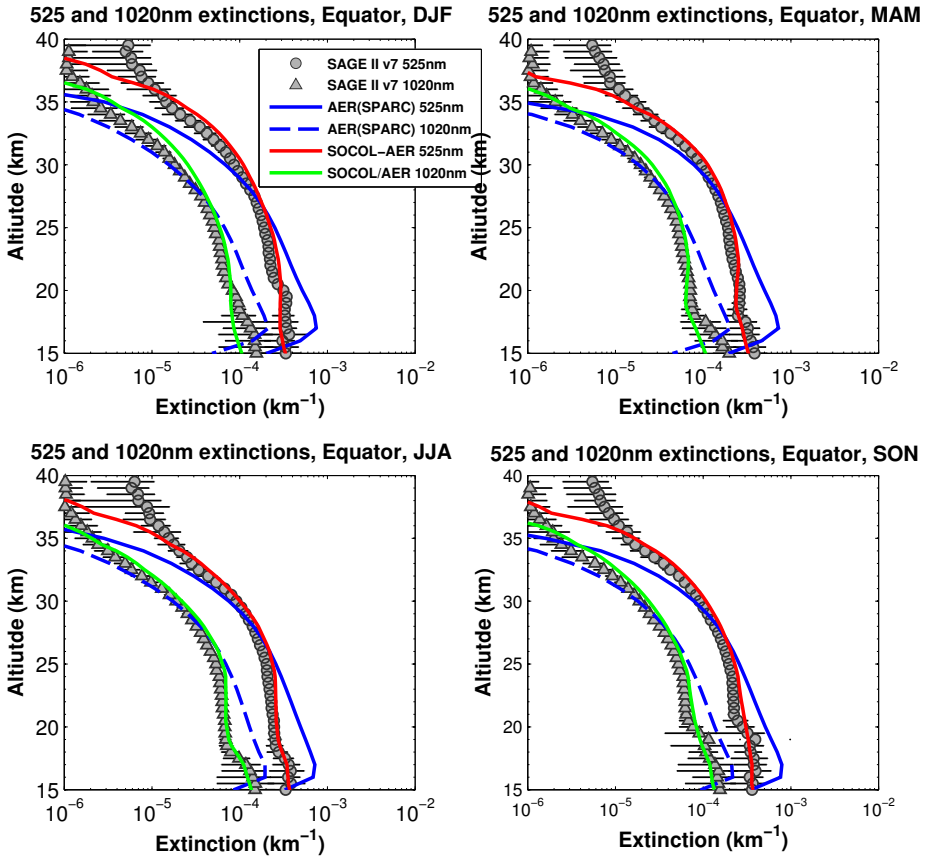

Figure 2.4 – Comparison of SAGE II version 7.0 and SOCOL-AER-calculated zonal mean extinctions at 525 and 1020 nm at the equator. SAGE II data: averaged over five years (2000 to 2004). Horizontal bars: observed natural variability.

seasons. The observations are averaged for five years (2000 to 2004). Model extinctions are calculated according to Mie theory using refractive indices provided by *Yue et al.* [1994]. In the tropical UTLS region and mid-stratosphere, the SOCOL-AER results generally lie in the range of the measurements; horizontal bars in Figure 2.4 indicate measured variability. In addition there is an uncertainty in extinction precision of up to 40%, see Fig. 4.1 in *SPARC* [2006], which is not shown here. Overall this provides an excellent match with the observed extinctions. It successfully reproduces the observed vertical gradients in the extinctions during summer and fall, but somewhat less satisfactorily during spring and winter. At low altitudes deviations are unlikely to be caused by clouds, which are already filtered in SAGE II [*SPARC*, 2006], and more likely caused by the seasonal variabilities in the tro-

pospheric sources and transport. The AER 2-D model fails to capture the seasonal gradients, and largely over-/underestimates the observed extinctions above/below the tropopause due to the inadequacy of the tropical convection and the imposed primary aerosol distribution. Above 35 km, neither of the two models are able to reproduce the observations, possibly because of the absence of meteoritic dust, which is a dominant source of aerosol extinctions in the upper stratosphere [*Neely et al.*, 2011]. The comparison of aerosol extinctions at mid-latitudes (40–45°N) is shown in Figure 2.5. In the lower and middle stratosphere, SOCOL-AER successfully reproduces the observed extinctions in all seasons. However, the modeled extinctions decline rapidly above 30 km, which is likely an indication for the lack of meteoritic dust in the model.

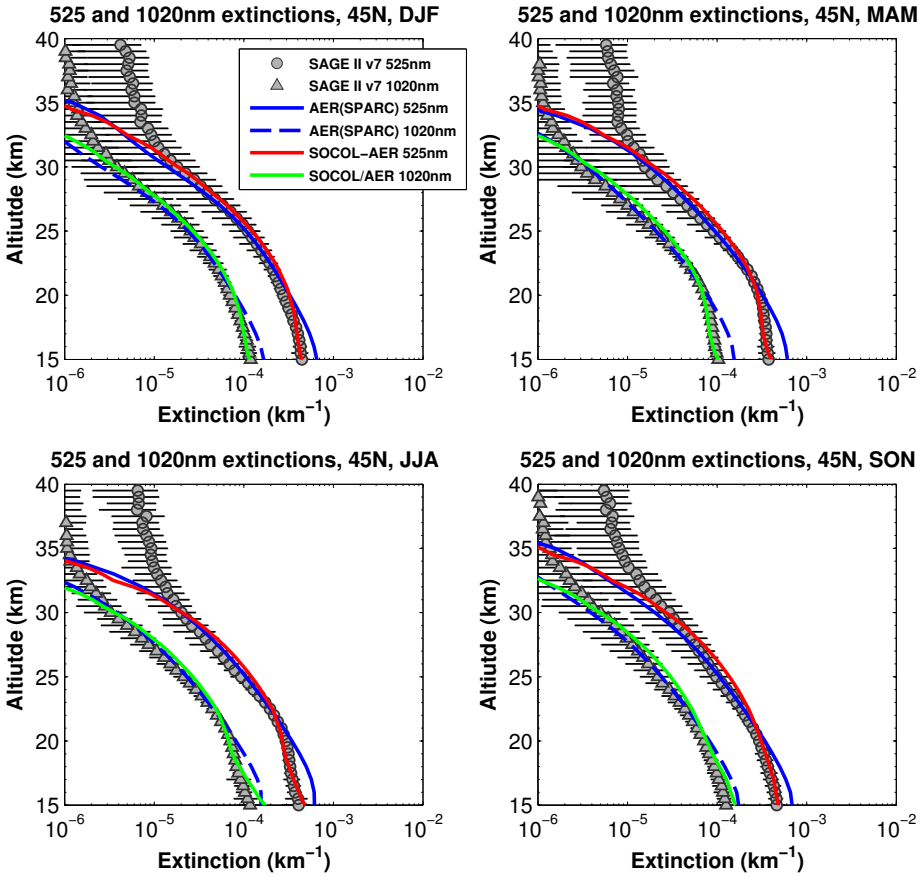

Figure 2.5 – Comparison of SAGE II version 7.0 and SOCOL-AER-calculated zonal mean extinctions for 525 and 1020 nm at 45°N. SAGE II data: averaged over five years (2000 to 2004). Horizontal bars: observed natural variability.

Comparisons with HALOE extinctions. The Halogen Occultation Experiment

(HALOE) provides aerosol extinction coefficients at IR wavelengths (3.46 and 5.26 μm). In contrast to the SAGE wavelengths, for which extinctions are dominated by scattering and roughly proportional to particle surface area density, aerosol extinctions at the HALOE wavelengths are mostly caused by absorption and therefore are representative of the particle volume density. Figure 2.6 shows comparisons of modeled and HALOE extinctions at 3.46 and 5.26 μm (the latter averaged over the period 2000-2004 at the equator). Model extinctions are calculated from Mie theory using refractive indices based on *Tisdale et al.* [1998]. Between 17 and 35 km, SOCOL-AER calculated extinctions at 3.46 μm are in excellent agreement with HALOE, and much improved in comparison with 2-D AER results. However, SOCOL-AER has difficulties representing very large particle sizes as can be judged from the long wavelength measurements: for 5.26 μm, the calculations underestimate observations by a factor 1.5-3 in the stratosphere possibly due to a coarse resolution at the largest size bins. The 2-D AER overestimates the observed extinctions in the UTLS region and decays too fast with altitudes.

Comparisons with SAGE aerosol burden. The aerosol burden can be derived by fitting the SAGE II extinctions to retrieve the particle size distribution and surface area density (SAD). To this end we employ the SAGE-4λ method, which retrieves the aerosol size properties based on the extinctions at all SAGE II wavelengths. The extinctions at 3.46 μm from the particle size distribution fitted by SAGE-4λ [*Arfeuille et al.*, 2013] is within 25% of extinctions observed by HALOE right after the Pinatubo eruption and differ marginally under the non-volcanic conditions. Table 2.3 summarizes the stratospheric aerosol optical depth (AOD) and burden from the model results, SAGE II observations and SAGE-4λ data. The 525 and 1020 nm AOD calculated by SOCOL-AER differ by less than 3% from SAGE II, while the 2-D AER overestimates SAGE II AOD by more than 20% for 525 nm and 10% for 1020 nm. The SAGE-4λ aerosol burden is 112.5 Gg S. Therefore, 109.0 Gg S simulated by SOCOL-AER can be qualified as an excellent representation of the observational data, while 187.2 Gg S provided by the 2-D AER overestimates the observations by over 60%.

Table 2.3 – Comparison of Stratospheric Aerosol Optical Depth (AOD) and Burden.

	AOD 525 nm	AOD 1020 nm	Burden (Gg S)
SAGE II (2000-2004)	3.97×10^{-3}	9.99×10^{-4}	112.5 [a]
SOCOL-AER	3.82×10^{-3}	9.92×10^{-4}	109.0
2-D AER (SPARC)	4.76×10^{-3}	1.12×10^{-3}	187.2

[a] Derived by the algorithm SAGE-4λ [*Arfeuille et al.*, 2013]

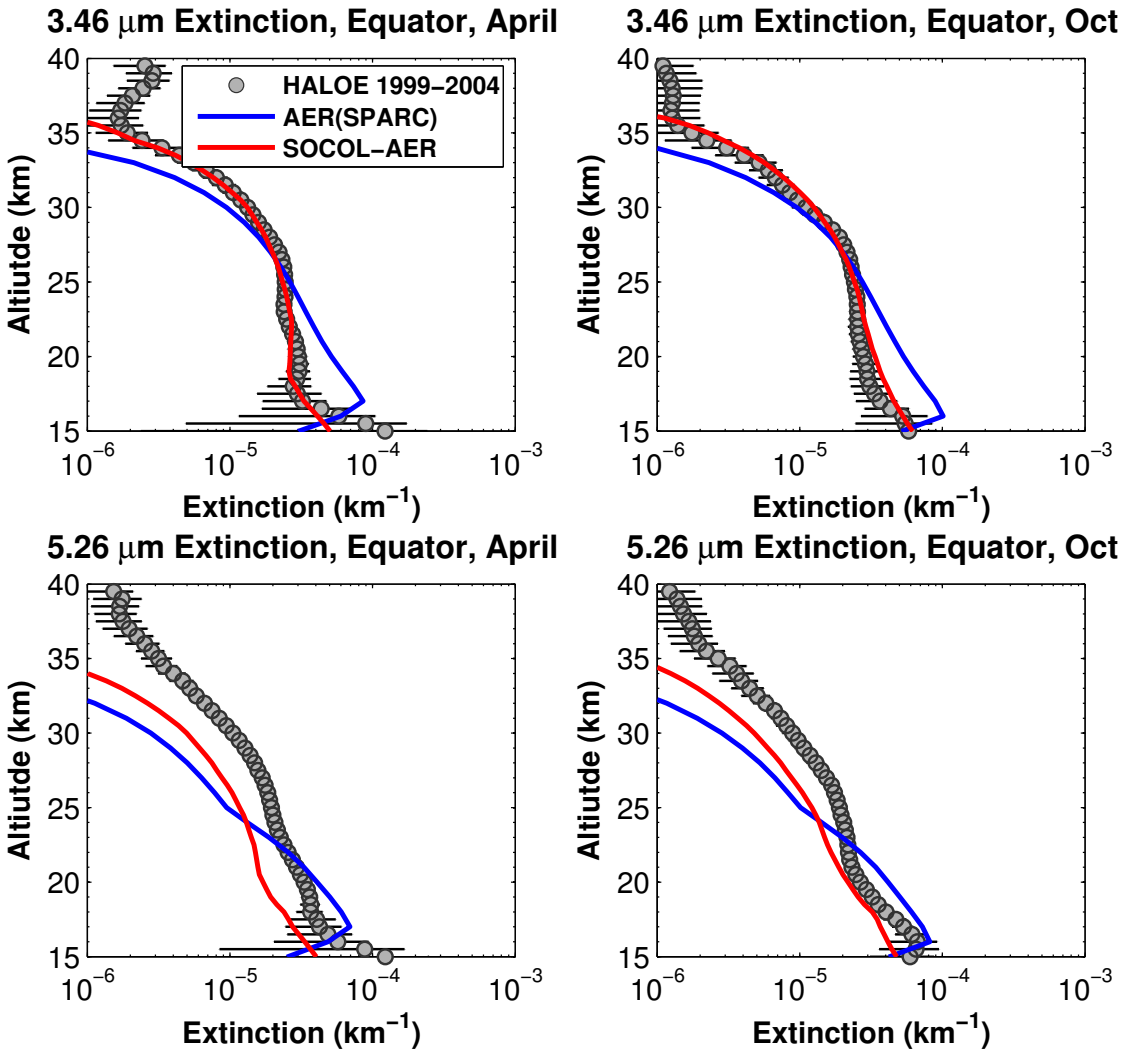

Figure 2.6 – Comparison of HALOE and model-calculated extinctions at 3.46 and 5.26 μm at the equator for April and October. HALOE observations: averaged over five years (2000 to 2004). Horizontal bars: observed natural variability.

Comparisons with OPC size channels. The optical particle counter (OPC) operated at Laramie, Wyoming [*Deshler et al.*, 2003; *Deshler*, 2008], provides a long-term in situ stratospheric aerosol record that started regular (∼monthly) measurements in 1971. Here we use the volcanically quiescent part of the record from 2000 to 2010 to compare with our model results.

Figure 2.7 shows simulated and observed vertical profiles of cumulative particle num-

ber densities for different size channels (particles larger than specified radius). The distribution reflects the observed natural variability and is depicted by standard boxplots (providing minimum outlier, minimum excluding outliers, 25th percentile, median value, 75th percentile, maximum excluding outliers, maximum outlier). Below 25 km, the calculated annual mean values are generally within the range of the measurements (i.e., within the boxes). Above 25 km, the modeled number densities start to deviate from the measurements with concentrations generally too high for particles larger than 0.15 μm and lower for condensation nuclei (particle size 10 nm). The overestimation might be partially due to the numerical diffusion of the applied sedimentation scheme in the model [*Benduhn and Lawrence*, 2013] since our previous simulations using a simple upwind method for sedimentation gave even higher number densities above 20 km. Too fast meridional transport from the tropics to higher latitudes might be another reason for the enhanced number densities in the larger radius channels, which would not provide the aerosol particles enough time to leave the stratosphere via gravitational settling. An underestimation of the stratospheric age-of-air is a common artifact of many CCMs, in particular also the ECHAM-based SOCOL family [*Stenke et al.*, 2013]. The observed increase in number densities of the observed condensation nuclei ($r > 10$ nm) above 25 km could be the result of freshly nucleated particles imported from Arctic regions in air that descended into the Arctic vortex region during winter and spring, termed the "stratospheric condensation nucleus layer" [*Campbell and Deshler*, 2014]. The modeled CN at wintertime (dashed black curve in Figure 2.7) gives some indication of this process, but underestimates its strength.

Comparisons with OPC volume density. A model-observation comparison of particle volume density is shown in Figure 2.8. The simulated volume density is in excellent agreement with the OPC measurements below 25 km, and declines faster above, which could be due to the underestimation of condensation nuclei concentration (black curve in Figure 2.7) or due to the lack of meteoritic material in the model.

Stratospheric aerosol burden. Based on the aerosol extinctions comparisons with SAGE II and HALOE, the 2-D AER model produces too high aerosol extinctions at visible to IR wavelengths compared to SAGE II and HALOE in the UTLS region, and thus higher aerosol optical depths, because aerosols in the lower stratosphere contribute most to volume densities. This overestimation is possibly due to the imposed boundary conditions at the tropopause or the deficit of isentropic mass exchange in the 2-D model. This implies that 187.2 Gg S modeled by the 2-D AER model [*SPARC*, 2006] is very likely an overestimation for the stratospheric aerosol burden (see Figure 2.3). In contrast, SOCOL-AER agrees closely with the SAGE II measurements, properly simulates the extinction profiles in the tropical UTLS

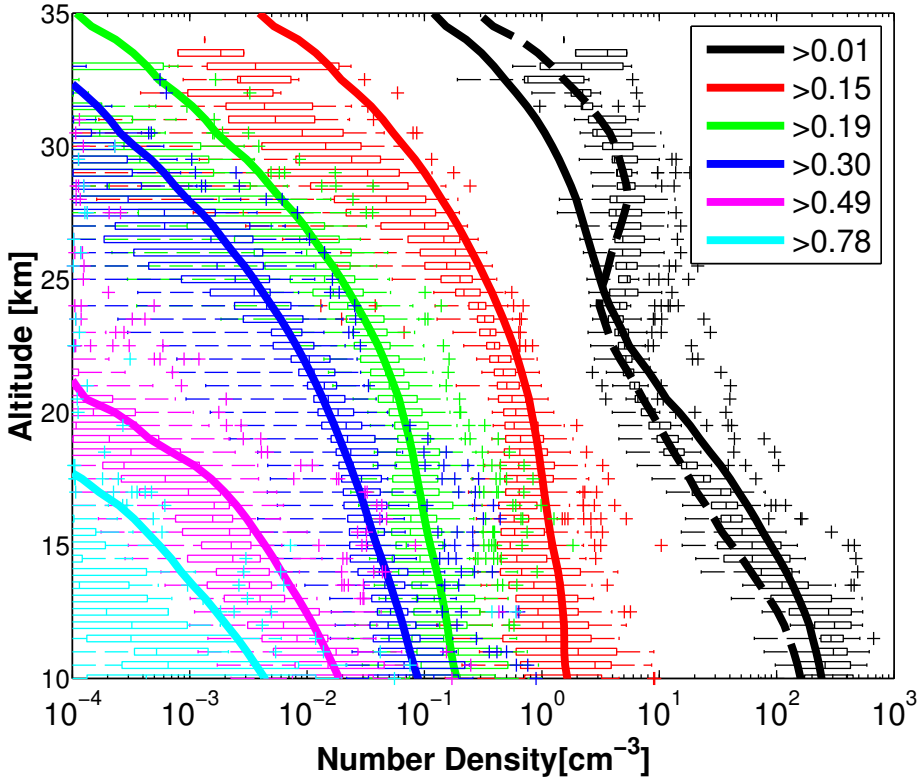

Figure 2.7 – Cumulative number densities (for radii larger than stated radius in μm) calculated by SOCOL-AER (solid lines) compared to in situ stratospheric aerosol measurements over the period 2000-2010 at Laramie, Wyoming [*Deshler et al.*, 2003; *Deshler*, 2008]. Measurements: represented as standard boxplots. Colors: different wet particle radii (H_2SO_4/H_2O, in μm). Solid curves: model results, zonal mean annual average at 42°N. Dashed curve: model results, zonal mean wintertime at 42°N.

region and reasonably reproduces the tropospheric sources and dynamics. The resulting stratospheric background aerosol burden is 109.0 Gg S, which differs by ∼3% from 112.5 Gg S derived from the SAGE II using the SAGE-4λ method. Further comparisons with in situ stratospheric aerosol measurements support our confidence in the simulated particle size distribution and volume density.

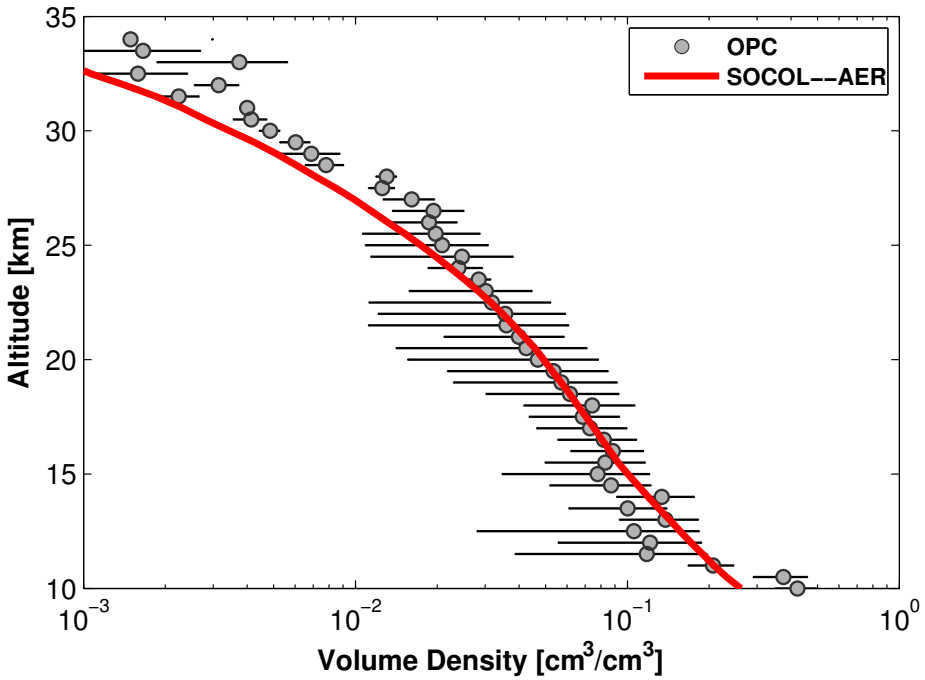

Figure 2.8 – Particle volume density calculated by SOCOL-AER (solid red line) compared to in situ stratospheric aerosol measurements averaged over the period 2000-2010 at Laramie, Wyoming [Deshler et al., 2003; Deshler, 2008]. Horizontal bars: natural variability captured by the measurements. Red curve: zonal mean annual average at 42°N.

2.4.4 Sensitivity of sulfur emissions

Relative contributions of OCS versus shorter-lived gases. The impact of various emissions scenarios on the stratospheric aerosol burden is summarized in Table 2.4. The scenario without SO_2 transport across the tropopause (noSO_2/TP) predicts 74% of the stratospheric background aerosol burden, while the scenario with no OCS across the tropopause (noOCS/TP) predicts only 47%, even though its net tropopause-crossing gaseous sulfur flux is stronger by 20% than that in noSO_2/TP. This may be explained by the fact that OCS is degrading, converting sulfur to SO_2 and later aerosol, mainly above 22 km, see fluxes above 22 km specified at upper margin of Figure 2.3. There the mean age-of-air and the residence time of sedimenting aerosol are greater than in the lower stratosphere. Conversely, the transport of SO_2 and aerosols across the tropopause remains relatively shallow due to the short chemical lifetime of SO_2 and impact of sedimentation. Sedimentation redistributes sulfur mass from the middle stratosphere to the lower stratosphere, where subse-

Table 2.4 – Impact of various emission scenarios (columns 1) on total net tropopause-crossing gaseous sulfur fluxes into the global stratosphere (column 3), stratospheric aerosol burden (sulfur burden above tropopause, column 4), and percentage change in burden (relative to REF, column 5).Values in volcanic simulations (VolT and VolS) are averaged over the first 6 months after the eruption.

Scenario	Characteristic	Flux Gg S/yr	Burden Gg S	Fraction %
REF	Reference (standard model setup)	103	109	100
noSED	No gravitational sedimentation	103	210	193
noSO_2/TP	No SO_2 across tropopause	52	81	74
noOCS/TP	No OCS across tropopause	62	51	47
noShLived/TP	No DMS, H_2S and C_2S across tropopause	92	106	97
noSO_2_DMS_H_2S	No SO_2, DMS and H_2S emissions	42	61	56
noASO_2	No anthropogenic SO_2 emissions	77	91	84
noDMS_H_2S	No DMS and H_2S emissions	79	95	87
noVolc	No volcanic SO_2 degassing	87	99	91
2Volc	Double volcanic SO_2 degassing	117	120	110
CH/IN	Double anthropogenic SO_2 emissions in China and India (+13.4 Tg S/yr)	112	118	109
US/EU	USA and Europe + 13.4 Tg S/yr	106	112	103
VolT	REF + 0.7 Tg S, single pulse at 9-14 km	113	116	106
VolS	REF + 0.7 Tg S, single pulse at 16-19 km	335	225	206

quent transport of aerosols into the troposphere leads to removal [*SPARC*, 2006]. Figure 6.5 of *SPARC* [2006] shows a reduction of roughly 12% in the stratospheric aerosol burden in the equatorial region due to sedimentation. In extra-tropical regions an even stronger reduction may be expected. Indeed, the calculated stratospheric aerosol burden without sedimentation (noSED) is about 210 Gg S, which is 93% higher than the 109 Gg S calculated for the reference run.

The scenario noShLived/TP predicts 97% of the stratospheric background aerosol burden, revealing that the transport of short lived species DMS, H_2S and CS_2 across the tropopause are relatively insignificant in the stratosphere. The scenario noSO_2_DMS_H_2S, which has no SO_2, DMS and H_2S emissions, implies virtually no SO_2 and aerosol particles entering the stratosphere through the tropical tropopause (except a very small amount through CS_2) , thus reflecting only the OCS contribution, which accounts for 56% of the stratospheric background aerosol burden. Interestingly, this result is consistent with the EMAC-modeled non-organic results of *Brühl et al.* [2012] as shown in Figure 2.9. However, *Brühl et al.* [2012] sug-

gested that OCS contributes over 70% of the stratospheric sulfate aerosol burden under non-volcanic conditions when organic aerosols in the EMAC model are taken into account. Uncertainties of the organic contribution to the stratospheric aerosols remain high and further measurements may be required to confirm the validity of organic contributions in lower stratospheric aerosols. However, existing single particle measurements show that the fraction of organic aerosols decreases from more than 50% in the upper tropical troposphere to 10-20% just 1-2 km above the tropical tropopause [*Murphy et al.*, 1998]. Also our results do not support the 70% burden due to OCS as suggested by *Brühl et al.* [2012], but rather only 56% and the rest due to short-lived sulfur-containing species.

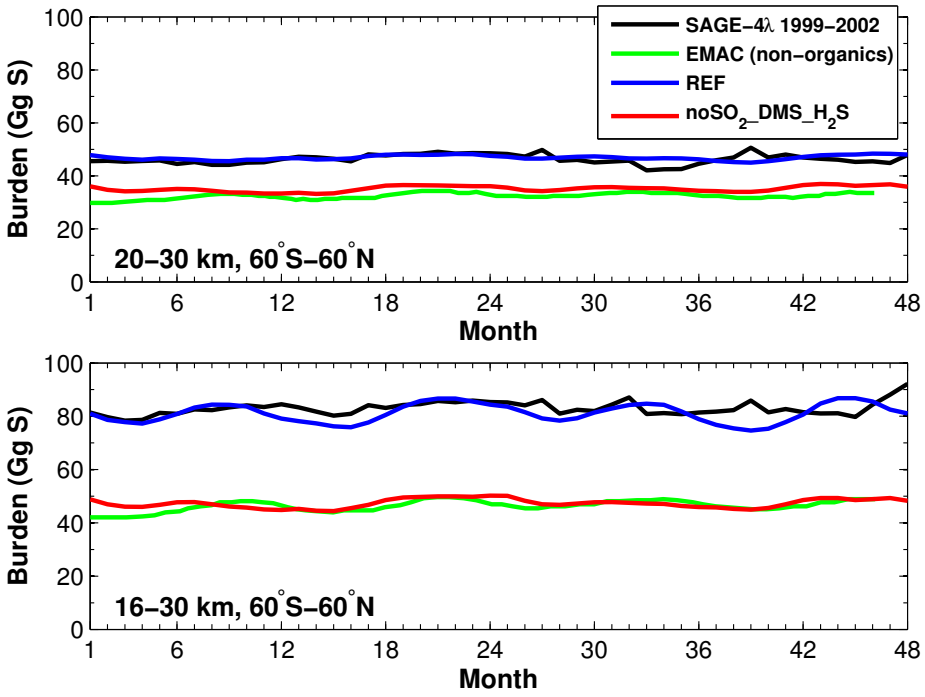

Figure 2.9 – Stratospheric aerosol burdens integrated between 60°S and 60°N, and in 20-30 km (upper panel) and 16-30 km (lower panel). Black: SAGE-II-derived burden using SAGE-4λ method [*Arfeuille et al.*, 2013]. Blue: SOCOL-AER model results from REF. Red: SOCOL-AER model results from the scenario noSO$_2$_DMS_H$_2$S. Green: EMAC model results without organic aerosols taken from the supplement of *Brühl et al.* [2012].

The scenario without anthropogenic SO_2 emissions produces 84% of the stratospheric background burden, which is similar to the scenario without DMS and H_2S emissions (noDMS_H$_2$S). This is not surprising because these short lived species contribute roughly one third of the tropospheric SO_2 total source strength (see the

budget analysis in Figure 2.3) and they are transported by convection into the tropical middle and upper troposphere [*Chatfield and Crutzen*, 1984], serving as more efficient source gases for SO_2 compared to anthropogenic emissions at the surface (which accounts for more than half of the tropospheric SO_2 total source strength). Sensitivity studies related to volcanic degassing (noVolc and 2Volc) show roughly 10% of the stratospheric aerosol burden from volcanic degassing, which is comparable to the impact of anthropogenic emissions, albeit their relatively small emission fluxes. This is mainly due to the geographical distribution and height of volcanic degassing sources [*Graf et al.*, 1998].

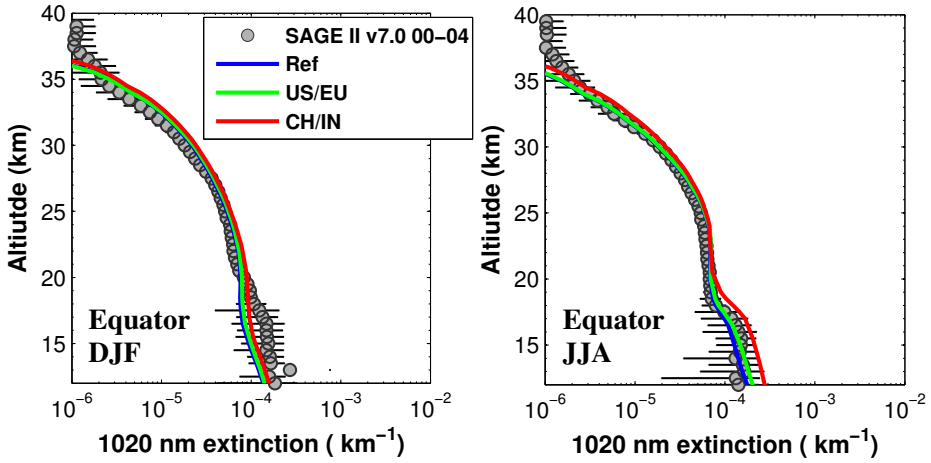

Figure 2.10 – Comparison of seasonal zonal mean 1020 nm extinctions for sensitivity experiments of anthropogenic SO_2 emissions at the equator. Black symbols: SAGE II data averaged over five years (2000-2004). Colored lines: SOCOL-AER results.

Geographical dependence of anthropogenic SO_2 emissions. Doubling the emission in China and India (CH/IN), i.e. +13.4 Tg S/yr, leads to roughly 9% more stratospheric aerosol burden compared to the reference simulation (see Table 2.4). When the same additional flux of SO_2 (+13.4 Tg S/yr) is superimposed on the emissions of the USA and Europe (scenario US/EU), this leads to an increase of the stratospheric aerosol burden of only 3% (see Table 2.4). This weaker response is due to deep convection in the Western Pacific region amplifying the impact of sulfur emissions there, particularly during the summertime, and transporting SO_2 into the middle and upper troposphere, from where it is more readily available for transport into the stratosphere [*Thornton et al.*, 1997; *Notholt et al.*, 2005]. Figure 2.10 compares the aerosol extinction at 1020 nm wavelength for the CH/IN and US/EU scenarios. The aerosol extinction for CH/IN scenario is about 10-20% higher between 17 and 20 km during the summertime and much less pronounced during

other seasons, which are less convective over India or China. Conversely, the US/EU scenario almost overlaps with the reference simulation.

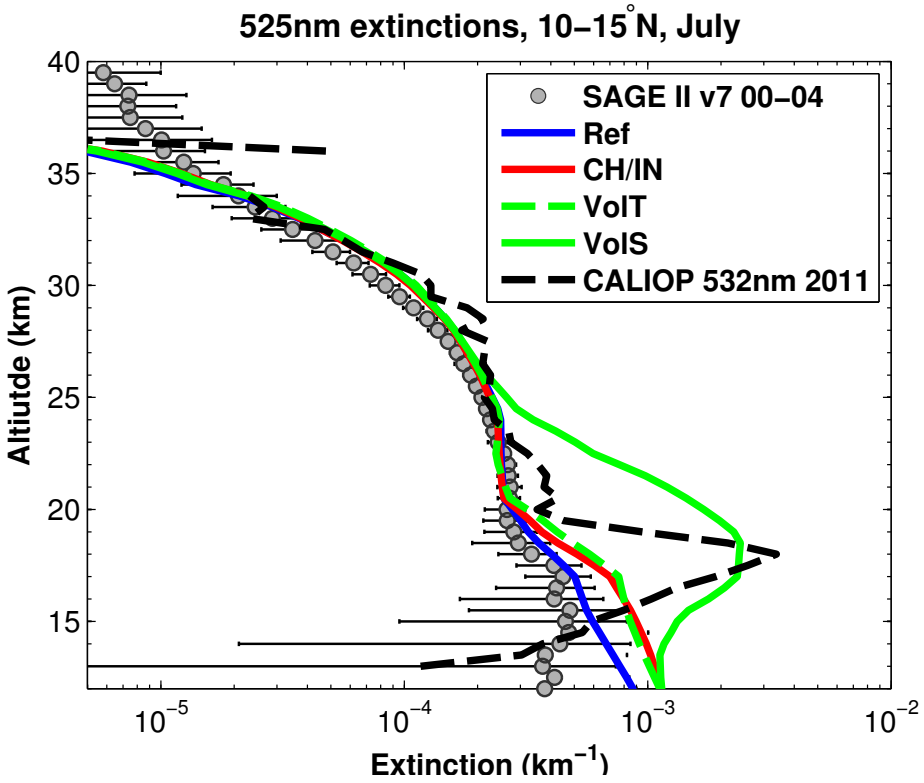

Figure 2.11 – Comparison of 525 nm extinctions for sensitivity experiments of SO_2 in July at 10-15°N. Gray circles: SAGE II data in July averaged over five years (2000-2004). Horizontal bars: natural variability observed by SAGE II. Colored lines: SOCOL-AER results for different scenarios. Black dashed line: CALIOP data, mean of July 2011, the month after the Nabro eruption.

Altitude dependence of volcanic SO_2. Two simulations (VolT and VolS) of a Nabro-like eruption have been conducted, where VolT injects sulfur into the free troposphere (9-14 km), and VolS into the stratosphere (16-19 km). As shown in Table 2.4, VolS doubles the background stratospheric background aerosol burden during the first 6 months after eruption, while VolT contributes only about 6%, similar to the anthropogenic scenario CH/IN. Figure 2.11 shows profiles of aerosol extinctions at 10-15°N in July 2011, one month after the eruption. VolT basically remains at background levels and is close to the results of CH/IN, while VolS results in a massive increase of extinction in the lower stratosphere. VolS reaches maximum extinction of about 2×10^{-3} km^{-1} at 18 km, which is comparable to the Cloud-Aerosol Li-

dar with Orthogonal Polarization (CALIOP) onboard the CALIPSO satellite. The calculated aerosol extinctions are elevated across a larger altitude range than observed by CALIOP. This might be caused by the insufficient vertical resolution of the model or by an imperfect initial SO_2 distribution in the volcanic injection plume. Our model results show that the simulation VolT fails to affect stratospheric aerosols. In contrast, *Bourassa et al.* [2012] indicated, based on the Optical Spectrograph and IR Imaging System (OSIRIS) observations, that Nabro injected SO_2 into 9 to 14 km and suggested a significant increase in the stratospheric AOD because of deep convection associated with the Asian summer monsoon. This discrepancy might be due to the resolution of convection in SOCOL-AER. However, a recent analysis of the CALIPSO lidar data by *Vernier et al.* [2013] has suggested that Nabro volcanic plume was injected directly into the lower stratosphere, which agrees with our model results. The calculated stratospheric AOD is compared with CALIOP observations as shown in Figure 2.12. SOCOL-AER simulates the evolution of the observed aerosol optical depth reasonably well, and peaks at 0.01, which is roughly 4 times the background conditions.

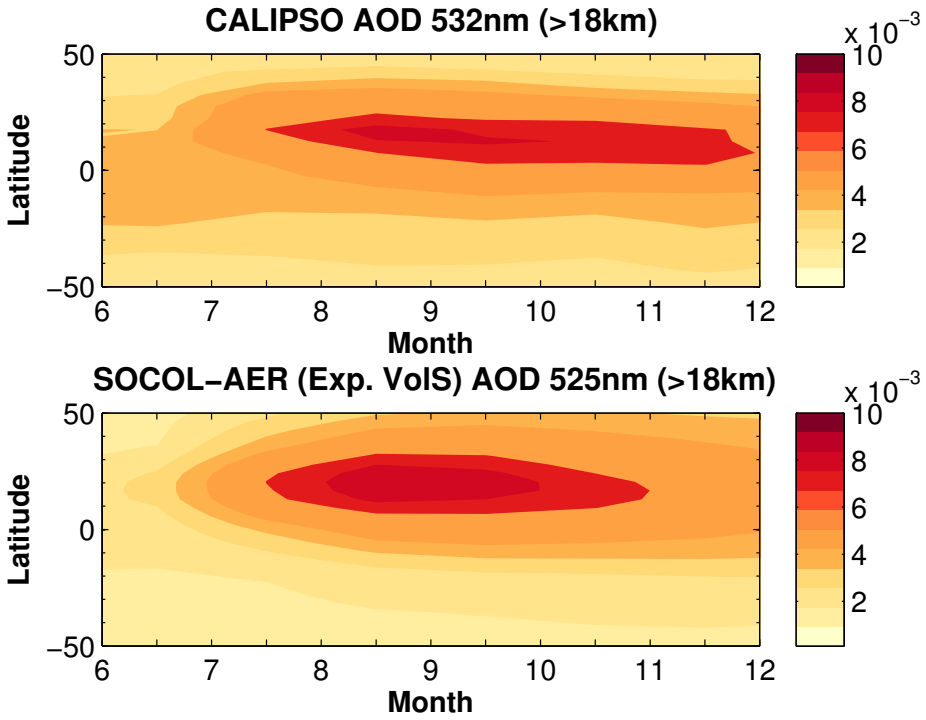

Figure 2.12 – Comparison of the time-space evolutions of CALIOP AOD (>18 km) at 532 nm and SOCOL-AER AOD (>18 km) at 525 nm after the Nabro eruption on 13 June 2011.

2.5 Summary and Conclusions

We have developed the aerosol-chemistry-climate model SOCOL-AER which includes prognostic transport, chemistry, particle-size resolving aerosol microphysics, sedimentation and interactive aerosol radiative feedbacks. SOCOL-AER accurately reproduces the characteristic features of stratospheric aerosols under non-volcanic conditions. It is also doing a fine job under conditions with strong volcanic perturbations, as will be shown elsewhere (Sheng et al., in prep. for Journal of Geophysical Research).

Modeled OCS mixing ratios are mostly within the range of ATMOS and MkIV measurements. Modeled SO_2 mixing ratios are consistent with the ATMOS and MIPAS measurements throughout the atmosphere. At altitudes above 30 km, agreement can only be achieved by including an enhanced photolytic conversion of gaseous H_2SO_4 into SO_2 [*Vaida et al.*, 2003]. The model sulfur budget indicates that a net sulfur flux of approximately 103 Gg S/yr through the tropopause enters the stratosphere, in which 40% are in the form of OCS, 50% in the form of SO_2, and 10% in the form of CS_2, DMS and H_2S. In addition, large amounts of OCS and aerosols enter the stratosphere, but leave it again in the same form, i.e. do not contribute to the net sulfur flux. The modeled stratospheric aerosol burden is 109 Gg S, providing excellent agreement with the burden (102.5 Gg S) derived from SAGE II (by means of the retrieval algorithm SAGE-4λ). This corrects the modeled 187.2 Gg S stratospheric aerosol burden in the previous study [*SPARC*, 2006]. SOCOL-AER successfully reproduces aerosol extinctions from visible to IR wavelengths (within $\pm$30%, and mostly better than $\pm$10%) compared to SAGE II and HALOE observations in the lower and middle stratosphere (with the exception of the extinction at 5.6 μm, which is underestimated by 30-60% for unknown reasons). Above $\sim$35 km, close to the upper edge of the Junge layer, SOCOL-AER is not able to match observations due to the lack of meteoritic dust in the model. Model comparisons with in situ measurements by optical particle counters above Wyoming [*Deshler et al.*, 2003] verify that the model successfully represents the particle size distribution and particle volume density in the lower and middle stratosphere. Measurements in the UTLS region are necessary for model validation, i.e. to validate our knowledge of sulfur fluxes into the stratosphere in the form of SO_2 and aerosols under volcanically quiescent conditions.

Sensitivity studies indicate that OCS contributes about 56% of the background stratospheric aerosol burden, whereas the transport of SO_2 across the tropopause contributes about 26%. The model results also suggest that anthropogenic SO_2 emissions in East Asia and India contribute generally more to the lower stratospheric

aerosols than emissions in Europe and USA, in particular during the summertime. This may be explained by the importance of deep convection and the proximity of the Western Pacific region. The model results further suggest that emissions of DMS, H_2S and volcanic degassing contribute comparably to the stratospheric aerosol burden as do anthropogenic SO_2 emissions, and must be taken into account in modeling studies. However, even more important in terms of sulfur input into the stratosphere are small and medium-size volcanic eruptions. Simulations of Nabro-like eruptions demonstrate that even a modest volcanic eruption can dramatically perturb the stratospheric aerosol layer and dominate anthropogenic SO_2 emissions over months-long timescales, but only if the volcanic plume reaches the lower stratosphere.

Acknowledgments

This work was stimulated by the "Assessment of Stratospheric Aerosol Properties (ASAP)", a previous activity of SPARC (Stratosphere-troposphere Processes and their Role in Climate) [*SPARC*, 2006]. The authors are grateful to Larry Thomason, one of the co-editors of the ASAP report, for continuing support over the past 10 years. We would like to thank Holger Tost and Marc von Hobe for useful discussions on our work. We are particularly grateful to Mian Chin for valuable comments which helped to improve the manuscript. The work was supported by the Swiss National Science Foundation under the grant 200021-130478(IASSA).

Chapter 3

Parametric Modeling of Mt Pinatubo's Initial Sulfur Mass Emission

Jian-Xiong Sheng[1], Debra K. Weisenstein[2], Bei-Ping Luo[1], Eugene Rozanov[1,3], Florian Arfeuille[1,4] and Thomas Peter[1]

[1] Institute for Atmospheric and Climate Science,ETH Zurich, Zurich, Switzerland
[2] School of Engineering and Applied Science, Harvard University, Cambridge, MA, USA
[3] Physical-Meteorological Observatory/World Radiation Center, Davos, Switzerland
[4] Oeschger Centre for Climate Change Research and Institute of Geography, University of Bern, Bern, Switzerland

In preparation for Atmos. Chem. Phys.

Abstract

We have performed more than 300 atmospheric simulations of the Pinatubo eruption using the AER 2-D sulfate aerosol model to optimize the initial sulfur mass injection as function of altitude, which in previous modeling studies has often been chosen in an ad hoc manner (e.g., by applying a rectangular-shaped emission profile). Our simulations are generated by variations of a 4-parameter vertical mass distribution, determined by a total injection mass and a skew-normal distribution function. Our results suggest that (a) the initial mass loading is ∼14 Mt of SO_2; (b) the injection vertical distribution extends from the tropical tropopause to 30 km; (c) has a strong skewness toward the lower stratosphere, leading to a peak mass injection at ∼20 km. The optimized distribution largely corrects the previously found overestimation in modeled extinctions (light scattering and absorption) when comparing to SAGE II solar occultation measurements.

3.1 Introduction

The eruption of Mt Pinatubo on 15 June 1991 injected large amounts of sulfur dioxide into the stratosphere. It perturbed the radiative, dynamical and chemical processes in the Earth atmosphere [*McCormick et al.*, 1995] and caused a global surface cooling of approximately 0.5 K [*Dutton and Christy*, 1992]. The Pinatubo eruption has also served as an important analogue for suggested geoengineering measures by injection of sulfur containing gases into the stratosphere [*Crutzen*, 2006; *Robock et al.*, 2013]. Modeling studies of volcanic eruptions can advance our knowledge of their impact on weather and climate.

However, the uncertainties in determining the initial total mass and altitude distribution of SO_2 released by Pinatubo remain high. *Stowe et al.* [1992] deduced a mass of 13.6 megatons of SO_2 based on the aerosol optical thickness observed by AVHRR. By analysis of SO_2 absorption measurements using the Total Ozone Mapping Spectrometer (TOMS) satellite instrument, *Bluth et al.* [1992] estimated an initial mass loading of approximately 20 Mt of SO_2. This study was later reevaluated by *Krueger et al.* [1995], pointing to the large retrieval uncertainties and specifying a range of 14-28 Mt emitted by Pinatubo. Later, *Guo et al.* [2004] constrained this to 14-22 Mt of SO_2. Besides the total emitted mass also the altitude distribution of the SO_2 emission is not well constrained. The only available measurements with vertical resolution of SO_2 in the stratosphere during the Pinatubo period have been made by the Microwave Limb Sounder (MLS) in September 1991 [*Read et al.*, 1993], which

started its mission unfortunately only three months after the eruption. Owing to these circumstances, modeling studies of Pinatubo [e.g., *Timmreck et al.*, 1999b; *Heckendorn et al.*, 2009; *Niemeier et al.*, 2009; *Aquila et al.*, 2012; *English et al.*, 2013] have employed very different mass loadings, emission altitudes and vertical mass distributions, which leads to biases in the local heating and consequently in the dynamical responses and time evolution of the stratospheric aerosol burden. These uncertainties result in difficulties to accurately simulate the Pinatubo eruption in addition to model-specific artifacts.

In this study, we use a 2-D size-bin resolving (also called sectional or spectral) sulfate aerosol model. This model has been among the stratospheric aerosol models with best performance in a recent international aerosol assessment [*SPARC*, 2006]. The present study conducts more than 300 atmospheric simulations of the Pinatubo eruption based on different combinations of four emission parameters, namely the total SO_2 mass and a 3-parameter skew-normal distribution of SO_2 as function of altitude. We calculate aerosol extinctions from all these simulations and compare with SAGE II (Stratospheric Aerosol and Gas Experiment II) measurements. Such a head-on approach is generally impossible for global 3-D models due to computational expenses. The purpose of this work is to provide a universal emission scenario for global 3-D simulations. To this end we optimize the emission parameters such that the resulting SO_2 plume, aerosol burdens and extinctions match satellite and lidar measurements (including the most heavily perturbed regions in which occultation measurements are unavailable due to instrument saturation). In Section 2 we describe the 2-D model and the experimental design of our Pinatubo simulations. Section 3 shows comparisons of the Pinatubo simulations to satellite observations, and conclusions are provided in Section 4.

3.2 Method

3.2.1 AER 2-D sulfate aerosol model

The AER 2-D sulfate aerosol model was one of the stratospheric aerosol models participating in a recent international aerosol assessment [*SPARC*, 2006]. There the model has been compared with satellite, ground lidar and balloon measurements, as well as with other 2-D and 3-D aerosol models, qualifying the AER model to be one of the best existing stratospheric aerosol models. The model represents sulfuric acid aerosols (H_2SO_4/H_2O) on the global domain from the surface to about 60 km with approximately 9.5° horizontal and 1.2 km vertical resolution. Model

dynamics (wind fields and temperature) are prescribed as a record and allowed to vary year by year, and are based on observed ozone, water vapor, zonal wind, temperature, planetary waves and QBO [*Fleming et al.*, 1999]. The model transport was found to be in good agreement with observations. The model is optimally suited to simulate stratospheric and upper tropospheric processes. It is not designed to capture tropospheric dynamics although it utilizes a parameterization of convection [*Dvortsov et al.*, 1998] in the troposphere. The model chemistry includes the sulfate precursor gases carbonyl sulfide (OCS), sulfur dioxide (SO_2), sulfur trioxide (SO_3), sulfuric acid (H_2SO_4), dimethyl sulfide (DMS), carbon disulfide (CS_2), hydrogen sulfide (H_2S) and methyl sulfonic acid (MSA). The model uses pre-calculated values of OH and other oxidants from [*Weisenstein et al.*, 1996]. The photodissociation and chemical reactions are listed in *Weisenstein et al.* [1997] and their rates are updated to *Sander et al.* [2011]. The particle size is resolved by 40 size bins spanning from 0.39 nm to 3.2 μm with volume doubling. Such a sectional approach was proven to be more accurate in representing aerosol size distribution compared to prescribed unimodal or multimodal lognormal distributions [*Weisenstein et al.*, 2007]. The sulfuric acid aerosols are treated as liquid binary solution droplets. Their exact composition is directly derived from the surrounding temperature and humidity according to *Tabazadeh et al.* [1997]. Microphysical processes in the model include homogeneous nucleation, condensation/evaporation, coagulation, sedimentation, as well as tropospheric rainout/washout. These processes determine the evolution of the aerosol concentration in each size bin, thus the entire particle size distribution. Operator splitting methods are used in the model with a time step of one hour for transport, chemistry, and microphysics, and 3-minute substeps for the microphysical processes that exchange gas-phase H_2SO_4 with condensed phase, and 15-minute substeps for the coagulation process. For more detailed descriptions of chemistry and microphysics in the model we refer to *Weisenstein et al.* [1997, 2007].

3.2.2 Experiments

We have simulated the Pinatubo eruption by injecting SO_2 directly into the stratosphere. The emission takes place into the latitude band 5°S–14°N. In the 2-D model the injection is immediately mixed zonally, which is an approximation to the observed rapid zonal transport of the SO_2 cloud derived from satellite measurements [*Bluth et al.*, 1992; *Guo et al.*, 2004]. The lack of zonal resolution is clearly a deficiency of our approach, but since SO_2 removal/conversion rate (e-folding time) is sufficiently slow ($\tau \sim 25$ days) and the zonal transport around the globe sufficiently fast ($\tau \sim 20$ days) [*Guo et al.*, 2004], a zonal mean description is a reasonable approximation. Also, the spaceborne aerosol data are typically provided as zonal

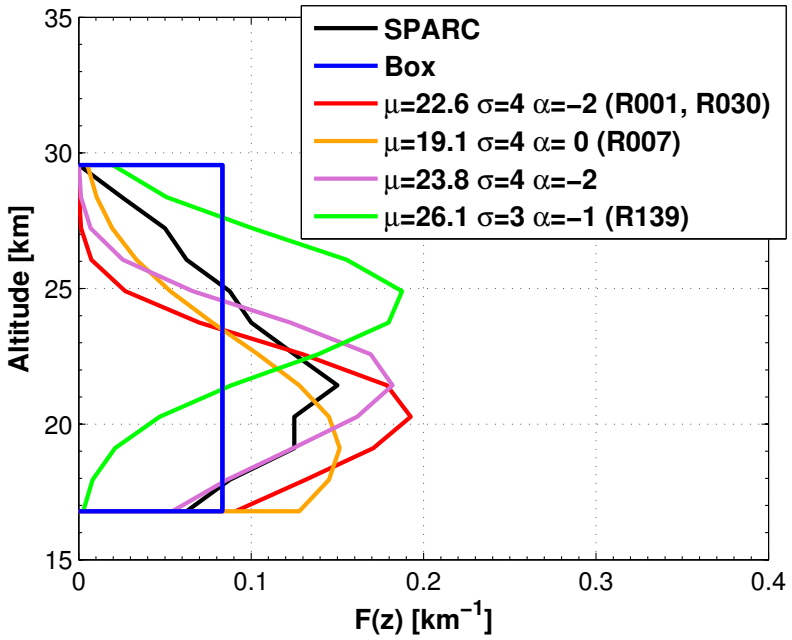

Figure 3.1 – Vertical distribution function $F(z)$. Black line: used in *SPARC* [2006] Blue line: uniform (box) profile that distributes SO_2 homogeneously with altitudes. Each of these curves encloses a unit area.

averages. We examined three cases of total mass, namely 14, 17 and 20 Mt of SO_2. The injection height extends from near the tropical tropopause (17 km) to 30 km. The vertical mass distribution is then represented by $M_{tot}F(z)$ where M_{tot} is the SO_2 mass magnitude in unit of megaton (Mt) and $F(z) = f(z)/\int_{z_{\min}=17}^{z_{\max}=30} f(x)\,\mathrm{d}x$ (in km^{-1}) is a function of altitude $z \in [17\text{ km},\ 30\text{ km}]$ with a skew-normal distribution $f(z)$ given by [*Azzalini*, 2005]

$$f(z) = \frac{2}{\sqrt{2\pi}\sigma} e^{-\frac{(z-\mu)^2}{2\sigma^2}} \int_{-\infty}^{\alpha\frac{z-\mu}{\sigma}} \frac{1}{\sqrt{2\pi}} e^{-\frac{x^2}{2}}\,\mathrm{d}x$$

Figure 3.1 shows a few examples of $F(z)$. The location parameter μ depends on available model levels and determines the altitude near which the maximum of the emitted SO_2 cloud is located. The scale parameter σ indicates how much dispersion takes place near the maximum, , i.e. it determines the width or standard deviation of the asymmetric bell-shaped curve. The skewness or asymmetry of the curve increases when $|\alpha|$ increases and vanishes when $\alpha = 0$ (normal distribution). A negative α drives the location of the maximum SO_2 emission to lower altitudes, while a positive α to higher altitudes.

The four parameters M_{tot}, μ, σ and α allow to represent a substantial space of SO_2 distributions, whose evolution is computed forward in time including the transport and comprehensive chemical and microphysical processes, in order to compare with the satellite extinction data. In detail, we simulate the following cases:

$$M_{tot} \in \{14 \text{ Mt}, 17 \text{ Mt}, 20 \text{ Mt}\},$$

$$\mu \in \{16.79 \text{ km} + n \times 1.16 \text{ km}, n = 0 \dots 11\},$$

$$\sigma \in \{2 \text{ km}, 3 \text{ km}, 4 \text{ km}\}$$

$$\alpha \in \{-2, -1, 0\}$$

which results in 324 different scenarios. The choice of the boundaries of this set of scenarios is itself already based on exploratory simulations. For example, based on the results of our 2-D model, it does not make sense to consider total masses $M_{tot} > 20$ Mt, since no choice of the other three parameters would allow to reconcile the model results with the observations. Similarly, skewness $\alpha > 0$ cannot lead to agreement, because the skew towards higher altitudes cannot be compensated by lower M_{tot}. In addition to the above 324 simulations, we consider another two scenarios, which are often adopted in modeling studies of Pinatubo: (1) Box14Mt has a uniform ('Box') profile (shown in Figure 3.1) and distributes the SO_2 mass homogeneously along altitudes; (2) SPARC20Mt is the reproduction of the Pinatubo simulation conducted in *SPARC* [2006], which injects 20 Mt of SO_2 and has a vertical profile 'SPARC' shown in Figure 3.1.

3.3 Results and Discussions

We compare our results with SO_2 vertical profiles measured by the Microwave Limb Sounder (MLS) onboard the Upper Atmosphere Research Satellite (UARS) between 10°S-0° in September 1991 [*Read et al.*, 1993], the global aerosol burden derived from the High-resolution Infrared Radiation Sounder [*Baran and Foot*, 1994] and from Stratospheric Aerosol and Gas Experiment II (SAGE II) [*Arfeuille et al.*, 2013], as well as aerosol extinctions measured by SAGE II [*Thomason et al.*, 2008].

To determine an optimal set of the emission parameters, we define three metrics based on these three measurements, and all the simulations are ranked according to a weighted score (ScoreWt) of the three metrics (see Table 3.1). This overall score is weighted as follows: 20% of the SO_2 score (ScoreSO_2), 40% of the global burden score (ScoreBurden), and 40% of the aerosol extinction score (ScoreExt). All scores are calculated as relative 2-norm errors with respect to the measurements.

Table 3.1 – Overall ranking of 326 atmospheric simulations of the Pinatubo eruption sorted according the weighted rank ("RankWt").

Mass (Mt SO_2)	Location μ (km)	Scale σ (km)	Skewness α	Score SO_2	Score Burden	Score Ext	Score Avg	Rank Wt	Rank SO_2	Rank Burden	Rank Ext	Rank Avg	Rank Wt	Scenario Name
14	22.59	4	-2	0.22	0.16	0.25	0.21	0.21	20	7	11	2	1	R001
14	22.59	3	-2	0.11	0.19	0.28	0.20	0.21	4	14	28	1	2	
14	21.43	4	-1	0.35	0.14	0.23	0.24	0.22	52	2	4	8	3	
14	20.27	2	0	0.19	0.19	0.27	0.22	0.22	14	11	24	3	4	
14	21.43	3	-1	0.28	0.17	0.26	0.23	0.22	29	8	12	6	5	
14	20.27	3	0	0.31	0.17	0.24	0.24	0.23	42	9	6	7	6	
14	19.11	4	0	0.41	0.14	0.22	0.26	0.23	68	3	1	15	7	R007
14	17.95	4	0	0.44	0.13	0.23	0.27	0.23	72	1	2	17	8	
14	19.11	3	0	0.38	0.15	0.24	0.25	0.23	57	4	7	12	9	
14	22.59	3	-1	0.22	0.21	0.26	0.23	0.23	18	20	18	4	10	
14	22.59	4	-1	0.34	0.19	0.24	0.26	0.24	51	13	5	13	11	
14	21.43	2	-1	0.19	0.21	0.30	0.23	0.24	13	19	43	5	12	
14	23.75	4	-2	0.29	0.22	0.26	0.26	0.25	36	24	15	14	13	
14	20.27	4	-1	0.45	0.16	0.25	0.29	0.26	77	6	10	30	14	
14	16.79	4	0	0.50	0.15	0.24	0.30	0.26	88	5	8	32	15	
...	...	...	...	...	...	...	...	...	...	...	...	...	...	
14	23.75	3	-2	0.28	0.27	0.29	0.28	0.28	35	40	40	22	29	
17	22.59	4	-2	0.07	0.31	0.36	0.25	0.28	3	63	108	9	30	R030
14	21.43	3	0	0.39	0.26	0.26	0.30	0.28	60	39	14	34	31	
...	...	...	...	...	...	...	...	...	...	...	...	...	...	
14	/	/	/	0.70	0.31	0.27	0.43	0.37	133	66	20	96	79	Box14Mt
...	...	...	...	...	...	...	...	...	...	...	...	...	...	
14	26.07	3	-1	0.94	0.43	0.32	0.56	0.49	104	141	74	155	139	R139
...	...	...	...	...	...	...	...	...	...	...	...	...	...	
20	/	/	/	0.47	0.67	0.61	0.58	0.61	79	249	245	163	211	SPARC20Mt
...	...	...	...	...	...	...	...	...	...	...	...	...	...	
20	29.55	3	-1	1.46	0.92	0.95	1.11	1.04	307	313	322	319	321	
20	29.55	3	0	1.52	0.91	0.96	1.13	1.05	317	306	326	320	322	
20	28.39	2	0	1.60	0.89	0.95	1.15	1.06	320	298	323	322	323	
20	29.55	2	-2	1.68	0.87	0.94	1.16	1.06	322	295	315	323	324	
20	29.55	2	0	1.68	0.86	0.94	1.16	1.06	323	291	319	324	325	
20	29.55	2	-1	1.67	0.88	0.95	1.16	1.06	321	297	321	325	326	

MLS onboard of UARS detected residual SO_2 in the stratosphere after about 100 days after the eruption. The uncertainty of ScoreSO_2 is likely larger than ScoreBurden and ScoreExt due to short lifetime of SO_2 and uncertain OH fields. Assuming an uncertainty in OH fields of 10% [e.g., *Prinn et al.*, 2005] translates into an uncertainty of 30% in SO_2 at ∼90 days after the eruption. In contrast, SAGE II, as an occultation instrument, becomes very reliable when the stratosphere starts to be sufficiently transparent. The measurement uncertainty is generally better than ∼20% for 525 nm wavelength and ∼10% for 1020 nm (see Fig. 4.1 in *SPARC* [2006]). Therefore, ScoreExt is weighted as one third for 525 nm and two thirds for 1020 nm. Finally, ScoreBurden uses the HIRS-derived data up to month 18 and the SAGE-derived data afterwards. During the first year after the Pinatubo eruption, the SAGE II instrument was largely saturated in the tropical region [*Russell et al.*, 1996; *Thomason et al.*, 1997; *SPARC*, 2006; *Arfeuille et al.*, 2013], and therefore the aerosol mass retrieved from SAGE II during this period very likely underestimates the initial loading significantly. The SAGE-4λ data set corrects for this deficiency by filling observational gaps by means of Lidar data. However, it probably remains being a lower limit in the first year after the eruption. Conversely, HIRS measurements are more reliable in this time period since it measures the entire aerosol column including the troposphere. This explains the remarkable difference between SAGE II and HIRS during the first year after Pinatubo (see Figure 3.3 below). After this period, HIRS tends to be noisy due to its lack of sensitivity at high latitudes where there is a contribution from errors in the background signal [*Baran and Foot*, 1994]. By contrast, SAGE II, as an occultation instrument, becomes more reliable when the stratosphere starts to be sufficiently transparent. Therefore, ScoreBurden uses the HIRS-derived data up to month 18 and the SAGE-derived data afterwards, with an overall uncertainty of 20%.

Table 3.1 shows the scores of selected scenarios, sorted according the weighted rank ("RankWt" in the second but last column). The best scenarios (RankWt ≤15) reveal that the total injection mass (M_{tot}) is 14 Mt of SO_2, 70-80% of which is below 23 km, and its maximum is likely located near 19-21 km with 3-4 km width (scale parameter σ). Location parameters μ larger than 21 km have generally a skewness towards a lower altitude (negative α). This sort of vertical profiles (e.g. the scenarios R001 and R007 marked in Table 3.1) are demonstrated in Figure 3.1. The worst scenarios (RankWt ≥321) in Table 3.1 are those with 20 Mt SO_2 injection mass and highest location parameters (μ = 29.55 km). The scenarios such as Box14Mt and R139 rank much worse than the optimal scenarios, though their injection mass is the same, because their vertical profiles (shown in Figure 3.1) inject over 50% mass above 23-24 km. The scenario R030 has the same vertical profile as R001, but more emitted mass (17 Mt SO_2), leading to worse ranks in the aerosol burden

and extinctions. The scenario SPARC20Mt ranks at 211 in Table 3.1, although its vertical profile is close the optimal profiles (about 10-20% more mass above 23 km). This implies that emitting 17 or 20 Mt SO_2 is very likely an overestimation.

We choose five scenarios (R001, R030, R139, Box14Mt and SPARC20Mt) to be discussed in detail. R001 represents the optimal scenario. In comparison, R030, R139 and Box14Mt are in the center span of the ranking field: R030 has the same vertical profile as R001, but injects larger sulfur mass (17 Mt SO_2); R139 and Box14Mt (with Rank 79) inject the same sulfur mass as in R001, but use different vertical profiles. SPARC20Mt (with Rank 211) turns out to be a bad presentation, which reproduces the previous simulation conducted in *SPARC* [2006].

In addition to the AER 2-D sulfate aerosol model runs we also performed the scenario R001 and R139 using the 3-D aerosol-chemistry-climate model SOCOL-AER (Sheng et al., submitted to Journal of Geophysical Research) in order to verify the consistency between 2-D and 3-D free-running models.

Figure 3.2 shows the comparison of modeled SO_2 with MLS measurements three months after the eruption. The scenario R001 captures the measured SO_2 profile, and only underestimates by about 20% the measured maximum SO_2 mixing ratio near 26 km. SO_2 modeled by R030 show excellent agreement (within 7%) with MLS measurement. Box14Mt and R139 fail to match the observed profile, and SPARC20Mt shows better agreement with the observations under 28 km, but nevertheless largely overestimates the observations above. The common feature of R139, Box14Mt and SPARC20Mt is that their initial vertical distributions release much more SO_2 above 24 km compared to R001, which is skewed to lower altitudes keeping over 90% of emitted SO_2 below 24 km (Figure 3.1). SO_2 simulated by the two 3-D simulations (dashed curves in Figure 3.2) are similar to the corresponding AER 2-D simulations, though SOCOL-AER predicts a lower maximum value and distributes SO_2 more widely, reflecting differences in OH and transport in the models.

Figure 3.3 shows the evolution of simulated stratospheric aerosol burden (integrated above tropopause) in units of teragram of H_2SO_4/H_2O droplet total mass compared to the aerosol mass derived from HIRS [*Baran and Foot*, 1994], and SAGE II using the 4λ method [*Arfeuille et al.*, 2013]. In Figure 3.3, R001 matches the HIRS-derived maximum aerosol burden after the first few months of the eruption, and then agree with SAGE-derived burden (mostly within 20%) after month 18. SPARC20Mt reaches its maximum burden 32 Mt of H_2SO_4/H_2O, and $\sim$50% more than 21 Mt derived from HIRS. R030 emits 17 Mt of SO_2 using the same vertical profile as R001, and peaks at 25 Mt, about $\sim$30% more than HIRS, whereas the uncertainty of HIRS is about 10% [*Baran and Foot*, 1994]. This means that the initial mass loading of

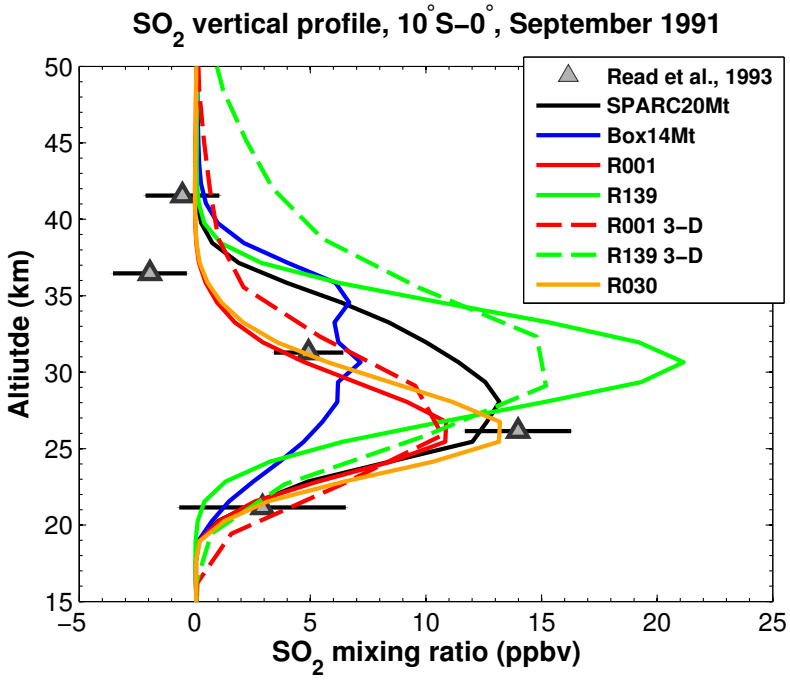

Figure 3.2 – Vertical profiles of monthly zonal mean SO_2 mixing ratio at 10°S-0°N in September 1991. Simulations are represented in different colors. Observations (triangles) are taken from Microwave Limb Sounder (MLS) measurements [*Read et al.*, 1993].

17 or 20 Mt of SO_2 into the stratosphere is apparently too high. Different vertical profiles using 14 Mt of SO_2 show a high sensitivity in the evolution of the aerosol burden. R139 and Box14Mt inject about 60% and 40% of their sulfur mass above 24 km, respectively, and lead to a greater maximum aerosol burden than R001. R139 has even a slightly larger maximum aerosol burden than R030, though R030 has larger initial SO_2 mass loading. This is mainly due to the fact that above 24 km the mean age-of-air and the residence time of sedimenting aerosol are greater than in the lower stratosphere, where most sulfur mass of R001 and R030 is located. The results of "R001 3-D" using the coupled aerosol-chemistry-climate model SOCOL-AER is very consistent (mostly within 10%) with the 2-D AER simulation R001. In contrast, the consistency for R139 and "R139 3-D" is less satisfactory. The maximum aerosol burden simulated by "R139 3-D" is within 10% of R139, but the e-folding time of the aerosol burden in the 3-D simulation ("R139 3-D") is visibly faster (about 2 months) than in the 2-D simulation (R139), indicating in addition to the initial mass loading and microphysics, model dynamics also plays an important role in the decay of the volcanic aerosols. This difference between R139 (AER) and

"R139 3-D" (SOCOL-AER) is possibly due to not well-represented rate of exchange of air between the troposphere and stratosphere in the 2-D AER [*Weisenstein et al.*, 1997] or a faster Brewer-Dobson circulation in the middle stratosphere using the free-running 3-D SOCOL-AER.

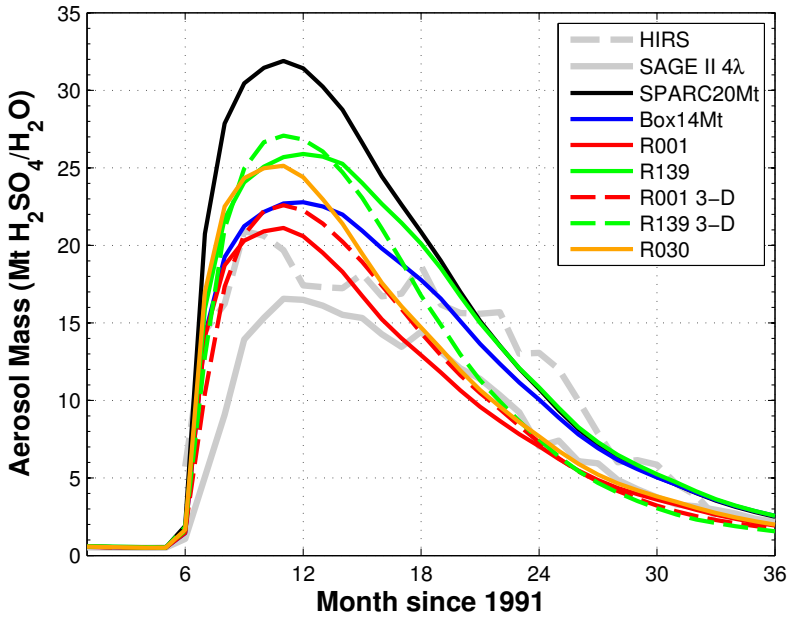

Figure 3.3 – Evolution of simulated global stratospheric aerosol burden (Mt H_2SO_4/H_2O) compared to the HIRS and SAGE II-derived data. HIRS-derived data include both tropospheric and stratospheric aerosols [*Baran and Foot*, 1994]. SAGE II aerosol data is derived from the retrieval algorithm SAGE 4λ by *Arfeuille et al.* [2013], and include only stratospheric aerosols.

We compare our modeled 1020 nm extinctions with the gap-filled SAGE II version 7.0 (Figure 3.4). SAGE II data points with horizontal bars are actual SAGE II measurements and denote natural variabilities, while data points without bars are gap-filled from lidar ground stations [*SPARC*, 2006]. The gap-filled points have a higher uncertainty and likely represent lower limits of the actual optical depth. Figure 3.4 shows comparisons in January (upper panel) and July (lower pannel) 1992 for five latitude bands from left to right: 50-40°S, 30-20°S, 5°S-5°N, 20-30°N and 40-50°N.

In January 1992, all the simulations reproduce reasonably near 20 km (mostly within 50% of observed extinctions). The calculations with R001 agrees better with observed aerosol extinctions compared to other 2-D simulations, particularly above 24 km. R030 is generally 10-20% larger than R001 due to its higher initial mass load-

ing, although it has the same vertical profile as R001. SPARC20Mt has even larger values than R030 due to a 20 Mt of SO_2 mass loading. Box14Mt and R139 largely overestimate the observed extinctions above 24 km. The 3-D simulation "R001 3-D" is superior to all the 2-D simulations, while "R139 3-D" performs worse than the 2-D simulations R001 and R030. Likewise, in June 1992, R001 also does a better job than other 2-D simulations. The two 3-D simulations "R001 3-D" and "R139 3-D" are now both superior to all 2-D model results, although the differences between them start to shrink as the their aerosol burdens are now within 10% difference. Overall, the calculations of SPARC20Mt, Box14Mt, R030 and R139 display a common deficiency, as they tends to overestimate aerosol extinctions in high altitudes above 24 km. Excessive initial mass loading (as in SPARC20Mt or R030) is one of the reasons. However, the shape of the initial mass vertical profiles appears to be at least as important as the initial mass loading. Box14Mt has 30% less total mass loading than SPARC20Mt, but it shows even higher extinctions in high altitudes because it has 40% of its mass injected above 24 km, while SPARC20Mt has only about 20% there.

3.4 Conclusions

We have conducted over 300 Pinatubo-like simulations based on the combinations of parameters of initial total SO_2 mass and altitude distribution. These parameters predominantly control the temporal and spacial evolution of stratospheric aerosols in the first 18 months after the Pinatubo eruption. The magnitude of the initial SO_2 mass released into the stratosphere is approximately 14 Mt based on HIRS and SAGE II observations. The altitude distribution of SO_2 injection is represented by a skew-normal distribution. Model results suggest that about 80% of emitted sulfur mass is distributed below 24 km with the maximum located between 19-21 km. This corrects the previously found overestimation in *SPARC* [2006] in modeled extinctions at high altitudes when comparing to SAGE II gap-filled measurement, and realistically simulates aerosol extinctions in the lower stratosphere. This defines an optimal set of the emission parameters such that the resulting SO_2 plume, aerosol burdens and extinctions match satellite and lidar measurements, and reduce the uncertainties in modeling initial mass loading of Pinatubo.

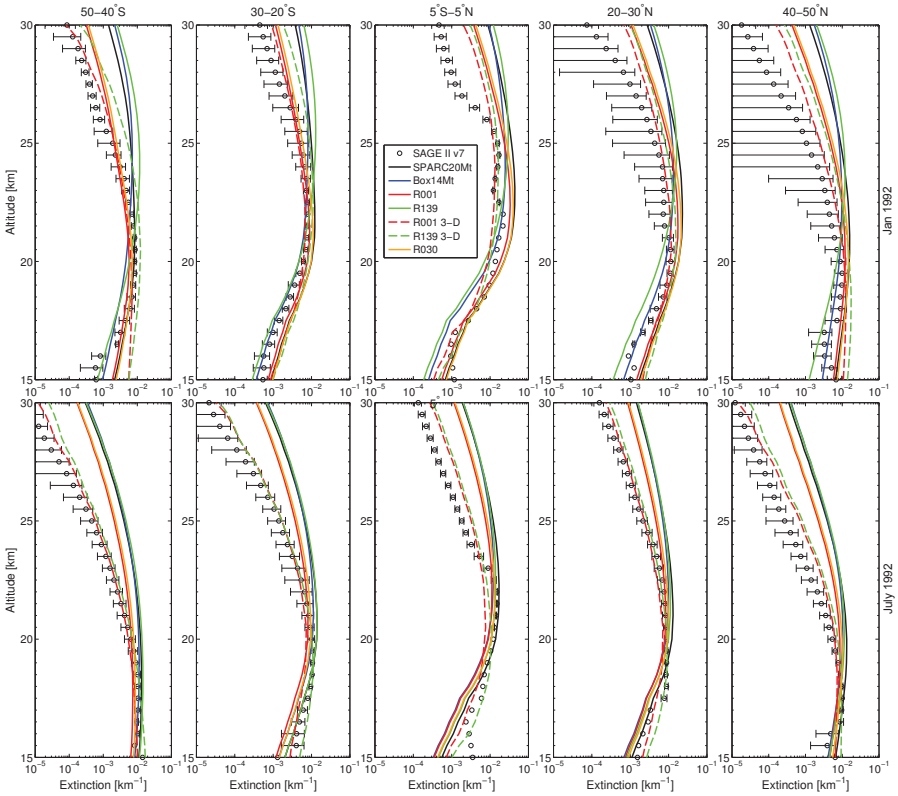

Figure 3.4 – Aerosol 1020 nm extinction comparisons of SAGE II (version 7.0) and model simulations at five latitude bands 50-40°S, 30-20°S, 5°S-5°N, 20-30°N and 40-50°N for January 1991 (upper panel) and July 1992 (lower panel). Solid curves: 2-D AER model results. Dashed curves: 3-D SOCOL-AER model results.

Acknowledgements

This work was stimulated by the "Assessment of Stratospheric Aerosol Properties (ASAP)", a previous activity of SPARC (Stratosphere-troposphere Processes and their Role in Climate). This work was supported by the Swiss National Science Foundation under the grant 200021-130478(IASSA). We would like to thank Jason English and Anthony Baran for helpful discussion on HIRS measurements. Also thanks to Andrew Gettelman for useful suggestions on our work. We are particularly grateful to Mian Chin for valuable comments which helped to improve the manuscript.

Chapter 4

Size-Resolved Stratospheric Aerosol Distributions after Pinatubo Derived from a Coupled Aerosol-Chemistry-Climate Model

Jian-Xiong Sheng[1], Debra K. Weisenstein[2], Bei-Ping Luo[1], Eugene Rozanov[1,3] and Thomas Peter[1]

[1] Institute for Atmospheric and Climate Science,ETH Zurich, Zurich, Switzerland
[2] School of Engineering and Applied Science, Harvard University, Cambridge, MA, USA
[3] Physical-Meteorological Observatory/World Radiation Center, Davos, Switzerland

In preparation for Journal of Geophysical Research.

Abstract

We employ the coupled aerosol-chemistry-climate model SOCOL-AER to investigate the impact of the aerosol radiative heating, sedimentation scheme, coagulation efficiency, and quasi-biennial oscillation (QBO) on the stratospheric aerosol loading after the eruption of Mt. Pinatubo. The aerosol module includes comprehensive sulfur chemistry and microphysics, in which the particles are size-resolved by 40 size bins spanning radii from 0.39 nm to 3.2 μm. Radiative forcing is calculated online from the aerosol module according to Mie theory. The simulation shows excellent agreement with the Stratospheric Aerosol and Gas Experiment II (SAGE II) measurements, the High-Resolution Infrared Radiation Sounder (HIRS), and in situ measurements by optical particle counters above Laramie, Wyoming. An accurate sedimentation scheme is essential in order to prevent particles diffusing too rapidly to high latitudes. The use of a sophisticated particle coagulation scheme plays a lesser role. The aerosol radiative feedback and the QBO help to sustain the aerosol in the tropical reservoir and affect the maximum of stratospheric aerosol burden, improving the agreement with observed distributions, but do not per se influence the decay rate of the aerosol burden. Overall, the results demonstrate the necessity of the combination of detailed resolution of individual processes and comprehensive coupling in order to achieve a proper prediction of atmospheric and climate effects following large volcanic eruptions or sulfur injections related to geoengineering.

4.1 Introduction

The eruption of Mt. Pinatubo in June 1991 emitted 7-11 megatons (Mt) of sulfur into the stratosphere and significantly affected the global climate. It disturbed the Earth's radiative balance, resulting in a top-of-the-atmosphere global mean radiative forcing approximately -3 W m^{-2} [*Minnis et al.*, 1993], a global surface cooling of $\sim$0.5 C$^\circ$ [*Dutton and Christy*, 1992] and a temperature increase of $\sim$3 K in the tropical lower stratosphere [*Labitzke and McCormick*, 1992; *Randel et al.*, 2009]. The increasing equator-pole temperature gradient further altered the global atmospheric circulation [e.g., *Kodera*, 1994; *Graf et al.*, 2007]. Moreover, the enhanced stratospheric aerosol surface area density facilitated heterogeneous reactions, leading to stratospheric ozone depletion [*Solomon*, 1999].

Modeling studies of Mt. Pinatubo eruption can synthesize our knowledge of its impact on the climate system. However, there are large remaining uncertainties in current modeling approaches of the Pinatubo eruption due to the lack of a com-

plete representation of all the relevant processes such as chemical, microphysical and radiative processes, large-scale transport and gravitational sedimentation, as well as their interactions. Modeling studies of the Pinatubo eruption using three-dimensional general circulation models (GCM) or chemistry-climate models (CCM) with prescribed particle size distribution (bulk or modal approaches) [e.g., *Timmreck et al.*, 1999a,b; *Aquila et al.*, 2012] represented successfully the dynamical responses, and demonstrated the importance of including the quasi-biennial oscillation (QBO) and radiative heating of volcanic aerosols in the models, but they were often less satisfactory at reproducing volcanic aerosol size distributions. *Weisenstein et al.* [2007] have shown that size-bin resolving (or sectional) aerosol models are superior to modal models in accurate representing aerosol size distribution after large volcanic eruptions. Further progress using a CCM coupled with a size-bin resolving microphysical aerosol module to simulate Pinatubo-like eruptions has been achieved by *English et al.* [2013]. However, the decline of the simulated aerosol burden was too fast compared to observations, which they attributed to the lack of aerosol heating as interactive aerosol feedbacks remained decoupled in their model. Furthermore, they also suggested that attractive van der Waals forces, which leads to enhanced coagulation efficiencies in both transition and free molecular regimes, should be taken into account, although this leads to a faster decay in their simulated global aerosol burden. However, *Narsimhan and Ruckenstein* [1985] investigated the coagulation efficiency using the Lennard-Jones potential (retarded van der Waals forces) and demonstrated that very low coagulation efficiencies in free molecular regimes might prevail due to the fact that the coagulation efficiency decrease rapidly with increasing Knudsen number as particles without energy dissipation of a third collision partner (here an air molecule) are likely to escape from the interactive potential well. Another important stratospheric aerosol process is sedimentation. A recent study found that numerical diffusion induced by sedimentation may lead to undesirable transport of the aerosol to the middle and upper stratosphere and an accurate sedimentation scheme with minimizing numerical diffusion should be taken into account [*Benduhn and Lawrence*, 2013].

In this study, we attempt to clarify the roles of the aerosol radiative heating, sedimentation scheme, coagulation efficiency, and quasi-biennial oscillation (QBO) in the evolution of stratospheric aerosol loading after Pinatubo, which have not been resolved in previous modeling studies. To address these questions, we utilize a coupled 3-D aerosol-chemistry-climate model (SOCOL-AER), including all essential features, such as relevant prognostic transport, quasi-biennial oscillation, chemistry, particle-size resolving aerosol microphysics, sedimentation scheme with minimizing numerical diffusion and explicit treatment of the aerosol in the radiation code. We examine our results against satellite observations and in-situ measurements, and

Table 4.1 – List of Experiments

Name	QBO nudged	Aerosol feedbacks	Sedimentation scheme	Coagulation Efficiency α
REF	Yes	Yes	Walcek	$\alpha = 1$ everywhere
REF_UPWIND	Yes	Yes	Upwind	$\alpha = 1$ everywhere
RAD/OFF	Yes	No	Walcek	$\alpha = 1$ everywhere
QBO/OFF	No	Yes	Walcek	$\alpha = 1$ everywhere
RQ/OFF	No	No	Walcek	$\alpha = 1$ everywhere
$COAG_{1,2,2}$	Yes	Yes	Walcek	$\alpha = 1$ for continuum regime; $\alpha = 2$ for transition and free molecular regimes
$COAG_{LJ}$	Yes	Yes	Walcek	α based on Lennard-Jones potential, enhanced in transition regime, and reduced in free molecular regime [*Narsimhan and Ruckenstein*, 1985]

analyze in detail the evolution of aerosol burdens, aerosol optical properties and particle size distributions after the Pinatubo eruption.

4.2 Method

We simulate the Pinatubo eruption using a coupled aerosol-hemistry-climate model SOCOL-AER [Sheng et al., Global Atmospheric Sulfur Budget under Volcanically Quiescent Conditions and its Sensitivity to Anthropogenic Emissions, submitted to Journal of Geophysical Research]. SOCOL-AER includes comprehensive sulfur chemistry and microphysics, in which the particles are size-resolved by 40 size bins spanning radii from 0.39 nm to 3.2 μm, and interactive aerosol radiative feedbacks that the radiative fluxes required by the CCM SOCOL are calculated online from the aerosol microphysical properties using Mie theory. In this study, the model spatial resolution of SOCOL-AER is set to be T31 horizontal truncations and 39 vertical hybrid sigma-pressure levels from surface to 0.01 hPa. The quasi-biennial oscillation (QBO) in the model is nudged according to observed wind profiles. The monthly mean sea surface temperatures (SSTs) and sea ice coverage (SIC) are prescribed. Comprehensive sulfur surface emissions are also fully taken into account.

Simulations of the Pinatubo eruption are modeled by an injection of 14 Mt SO_2 in the region 97-112°E. and 1.8°S-12°N according to observations [*Guo et al.*, 2004]. SO_2 is released continuously from 14 to 15 June 1991 and spread from 16 to 30 km with an optimized vertical mass distribution [Sheng et al., Parametric Modeling of Mt Pinatubo's Initial Sulfur Mass Emission, in prep. for Atmos. Chem. Phys.], which guarantees a realistic initial mass loading of the eruption. All the experiments are summarized in Table 4.1. The reference run (REF) with the standard setup of SOCOL-AER includes nudged QBO, interactive aerosol radiative feedbacks, and coagulation efficiency equals to one. In the experiment RAD/OFF, the interactive aerosol radiation scheme in the model is decoupled and the radiative fluxes are calculated using SAGE 4λ dataset [*Arfeuille et al.*, 2013] averaged over the periods 2000-2004, which eliminates the radiative effects of volcanic aerosols. The experiment QBO/OFF is carried out without the QBO nudging scheme in the model, resulting in a weak easterly zonal wind in the tropical stratosphere. Both the QBO nudging and interactive radiation schemes are switched off in the experiment RQ/OFF. These three experiments allow to identify the impact of QBO and radiative heating of volcanic aerosols on the evolution of the stratospheric aerosol burden after Pinatubo. We also consider two exploratory experiments concerning the coagulation efficiency. The experiment $COAG_{1,2,2}$ doubles the coagulation efficiency in transition and free molecular regimes as a simplification of attractive Van der Waals forces. $COAG_{LJ}$ represents the coagulation efficiency as a smooth function of the Knudsen number retrieved from the results in Figure 3 of [*Narsimhan and Ruckenstein*, 1985] with a Hamaker constant 5×10^{-19} erg. It enhances the coagulation efficiency in the transition regime (maximum enhancement larger than 2) but decreases it rapidly (less than 1) as the Knudsen number increases in the free molecular regime. The experiments REF_UPWIND employs an upwind method as the sedimentation scheme, while all other simulations use the Walcek method with only little numerical diffusion [*Walcek*, 2000]. This is sufficient to clarify the impact of difference sedimentation schemes, though a recent work by *Benduhn and Lawrence* [2013] presented a modified Waleck method, which further improves the Walcek method.

4.3 Results and Discussions

4.3.1 Aerosol burden

The evolution of observation-derived and model-calculated aerosol burdens in units of teragram (Tg) of aerosol mass (H_2SO_4/H_2O) are shown in Figure 4.1. The High-

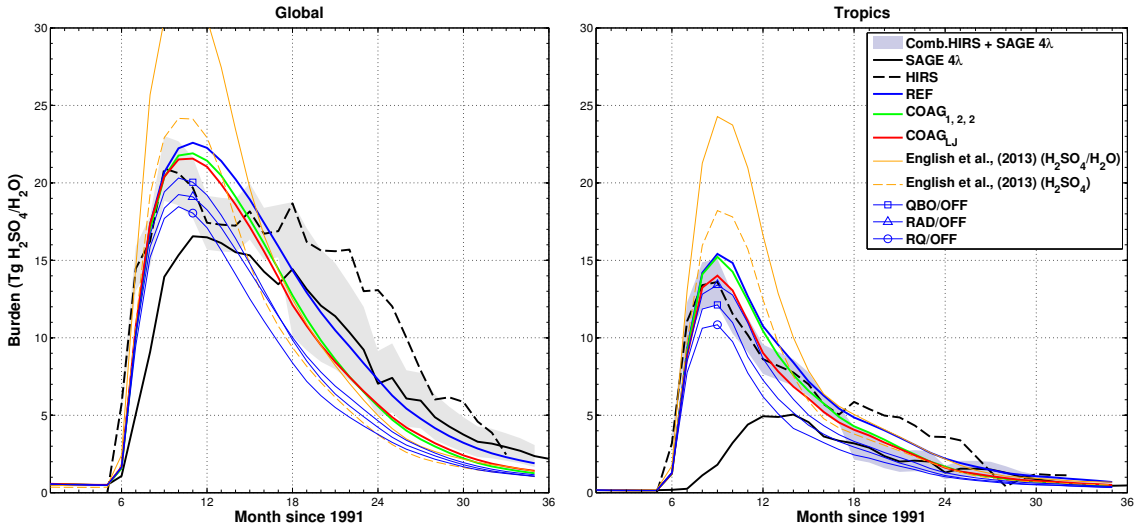

Figure 4.1 – Evolution of model-calculated global (left) and tropical (right) stratospheric aerosol burden (Tg H_2SO_4/H_2O) compared to the HIRS and SAGE II-derived data. HIRS aerosol mass includes both tropospheric and stratospheric aerosols [*Baran and Foot*, 1994]. SAGE II aerosol mass includes stratospheric aerosols derived from the SAGE 4λ method [*Arfeuille et al.*, 2013]. Grey region: uncertainties of HIRS (months 6-18) and SAGE 4λ (month 19 and afterwards).

Resolution Infrared Radiation Sounder (HIRS) measured the aerosol vertical column and the derived mass with about 10% uncertainties includes tropospheric and stratospheric aerosols [*Baran and Foot*, 1994]. The SAGE II-derived mass is retrieved by the SAGE 4λ method using all SAGE wavelengths [*Arfeuille et al.*, 2013] with about 30% uncertainties for non-gap-filled data ($\sim$20% from measured extinctions and $\sim$20% from size distribution, temperature and composition of aerosols). During the first year after Pinatubo, the SAGE II-derived mass is noticeably lower than HIRS due to the saturation of SAGE II, as a limb-occultation instrument, during this period [*Russell et al.*, 1996]. After this period, SAGE II measurements should provide more accurate aerosol extinctions once the atmosphere becomes sufficiently transparent. In contrast, HIRS presents noises owing to its lack of sensitivity at high latitudes where background signal errors contribute [*Baran and Foot*, 1994]. Overall, we are inclined to believe the HIRS data up to June 1992 (month 18) and the SAGE data afterwards. The grey area in Figure 4.1 represents a composite of uncertainties of HIRS and SAGE II-derived data.

The global stratospheric aerosol burden calculated by REF in Figure 4.1 is mostly in the observed range except for month 11-14. The agreement is less satisfactory

in the tropics, where REF is above the upper bound of the SAGE-II derived data (month 18 and afterwards) The calculated burden from REF_UPWIND is almost identical to REF, hence not shown here. The results of the sensitivity runs (namely QBO/OFF, RAD/OFF and RQ/OFF) are also presented in Figure 4.1. Their peak values of the aerosol burden differ by 3-4 Tg less than REF, and QBO/OFF and RAD/OFF predict about 2 Tg higher than RQ/OFF that has no nudged QBO and aerosol radiative heating. The difference in the peak value is mainly due to the difference in the tropical burden as the global difference is small when subtracting the difference from the tropics. During the first few months after the Pinatubo eruption, the initial aerosol mass loading in the tropical reservoir was maintained by the balance between sedimentation and enhanced tropical upwelling due to radiative heating of the volcanic aerosols and the QBO at a strong descending easterly phase [*Trepte and Hitchman*, 1992; *Trepte et al.*, 1993]. Moreover, the aerosol burden decay rates of QBO/OFF, RAD/OFF and RQ/OFF show only minor differences because the gravitational sedimentation becomes a dominant removal process when particles grow sufficiently large after the Pinatubo eruption and their effective radii can reach 0.5 μm or more [*Russell et al.*, 1996], and therefore these particles sediment more effectively.

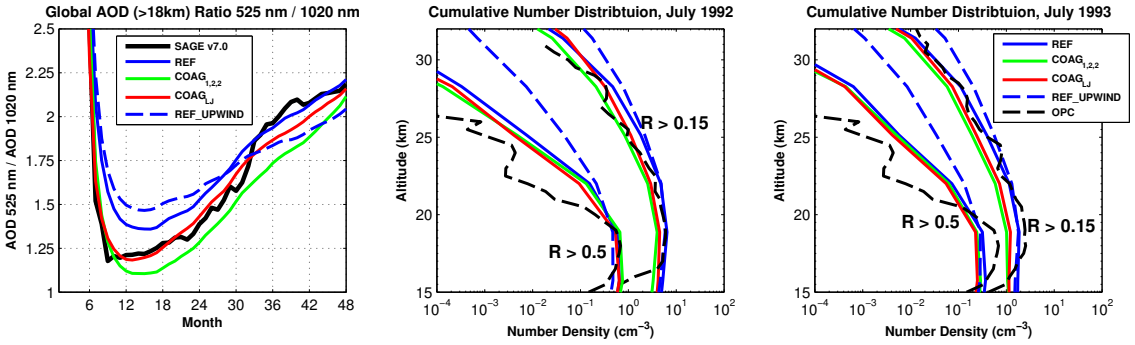

Figure 4.2 – Model-observation Comparison of SAGE II AOD ratio, OPC in situ measurement above Lamarie, Wynoming and the SOCOL-AER simulations. Left Panel: SAGE II and modeled global AOD (> 18 km) ratios 525 nm / 1020 nm. Middle and Right Panels: OPC measurements and modeled cumulative number distribution for two size channels $R > 0.15$ and > 0.5 μm in July 1991 (month 19) and July 1992 (month 31).

The global aerosol burdens calculated by $\mathrm{COAG}_{1,2,2}$ and COAG_{LJ} related to coagulation efficiency in Figure 4.1 are close to the lower bound of the SAGE 4λ-derived mass (month 18 and afterwards), and show a more rapid decay rate of the global volcanic aerosol burden compared to REF. In the tropical region both $\mathrm{COAG}_{1,2,2}$ and COAG_{LJ} improve the agreement with the HIRS and SAGE-derived aerosol bur-

den. This is expected because the overall enhanced coagulation in $COAG_{1,2,2}$ and $COAG_{LJ}$ leads to a faster growth of particle size and thus more rapid sedimentation. Furthermore, the reduced coagulation in the free molecular regimes tends to maintain the number density for the small particles and prevents their aggregation, leading to a slightly slower aerosol decay rate in $COAG_{LJ}$ compared to $COAG_{1,2,2}$. *English et al.* [2013] simulated the Pinatubo eruption by assuming an injection of 10 Mt sulfur into the stratosphere with the explicit treatment of van der Waals forces in coagulation. There is an error in their Figure 6, in which the calculated burden is in the unit of Tg H_4SO_2 while HIRS is Tg H_2SO_4/H_2O. By assuming 75% weight percent, the adapted results (orange lines) are shown in Figure 4.1. These results strongly overestimate the global and tropical aerosol burdens most possibly due to the excess mass loading (10 Mt sulfur) in their simulations. A linear scaling to the injection of 7 Mt sulfur would lead to a comparable result to SOCOL-AER.

4.3.2 Aerosol size distribution

The left panel of Figure 4.2 shows the modeled and SAGE II global AOD (>18 km) ratios 525 nm / 1020 nm, which are inversely related to the particle size: smaller ratio corresponds larger particles. In the early phase of the Pinatubo eruption, a large number of small particles is formed and they coalesce very quickly as shown in the SAGE II ratio, which presents a very sharp drop, falling below 1.25. Afterwards, the small SAGE II ratio keeps nearly constant value for about one year, and around month 22 restores larger values because the large particles sediment out of stratosphere and small tropospheric aerosols are transported into the stratosphere. REF predicts smaller particles than SAGE II in the early phase, and only after month 30 agrees well with SAGE II. In contrast, $COAG_{1,2,2}$ and $COAG_{LJ}$ produce larger particles (smaller ratios) than REF, and show better agreement with SAGE II in the first few months after Pinatubo. However, $COAG_{1,2,2}$ overestimates the particle size as its ratio is generally smaller than SAGE II all the time after Pinatubo, while $COAG_{LJ}$ tends to converge to REF after month 18 and matches the SAGE II ratios over the entire range. REF_UPWIND initially underestimates the particle size (large AOD ratios) and after month 30 starts to overestimates it, and fails to capture the observed particle size evolution.

The middle and right panels of Figure 4.2 show comparisons of the optical particle counter (OPC) measurements operated above Laramie, Wyoming [*Deshler et al.*, 2003; *Deshler*, 2008] and model-calculated cumulative number distributions for two size channels ($R > 0.15$ μm and $R > 0.5$ μm) in July 1992 (month 19) and July 1993 (month 31). REF_UPWIND has more large particles in the middle and upper

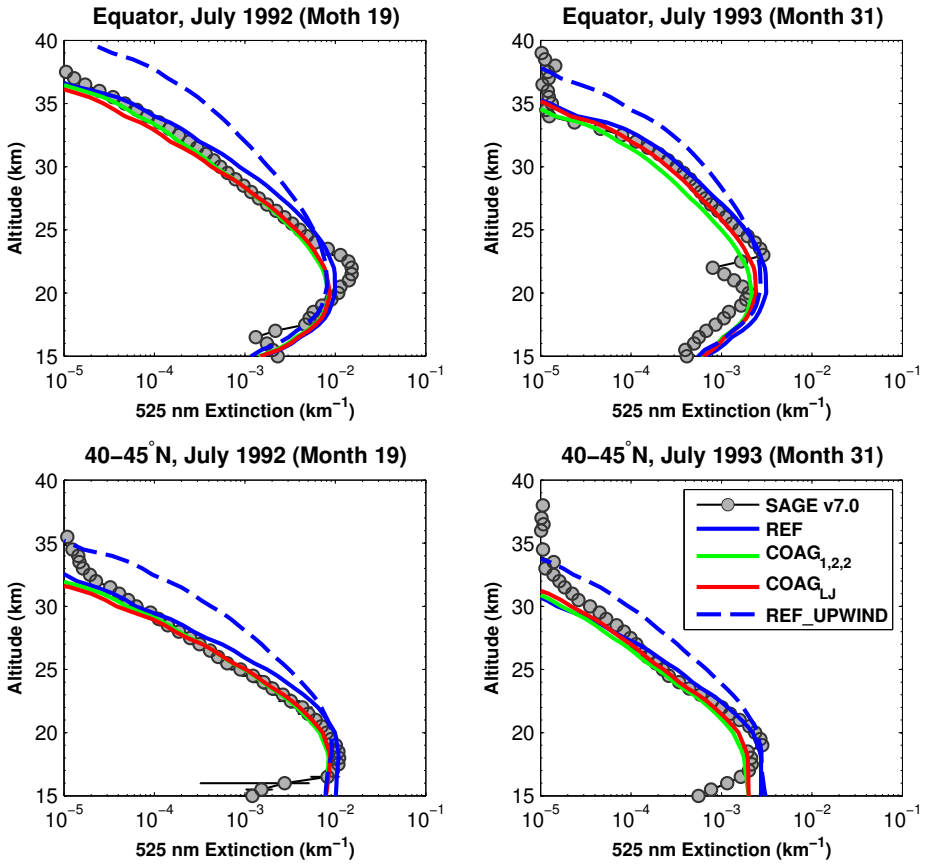

Figure 4.3 – Comparisons of SAGE II version 7.0 and extinctions simulated by SOCOL-AER at 525 nm in July 1992 (month 19) and 1993 (month 31) at the equator 5°N (upper panels) and $40 - 45$°N (lower panels).

stratosphere compared to the OPC measurements. This is because the numerical diffusion of the simple upwind method used in REF_UPWIND leads to artificial slower removal at higher levels of large particles and at the same time artificial faster transport downwards. Consequently, particles simulated by REF_UPWIND have too high number densities at high altitudes (> 22 km), in particular for the large particles. The cumulative number densities simulated by REF, COAG$_{1,2,2}$ and COAG$_{LJ}$ in Figure 4.2 are in good agreement with the OPC measurements. Differences due to coagulation efficiency between these simulations are minor.

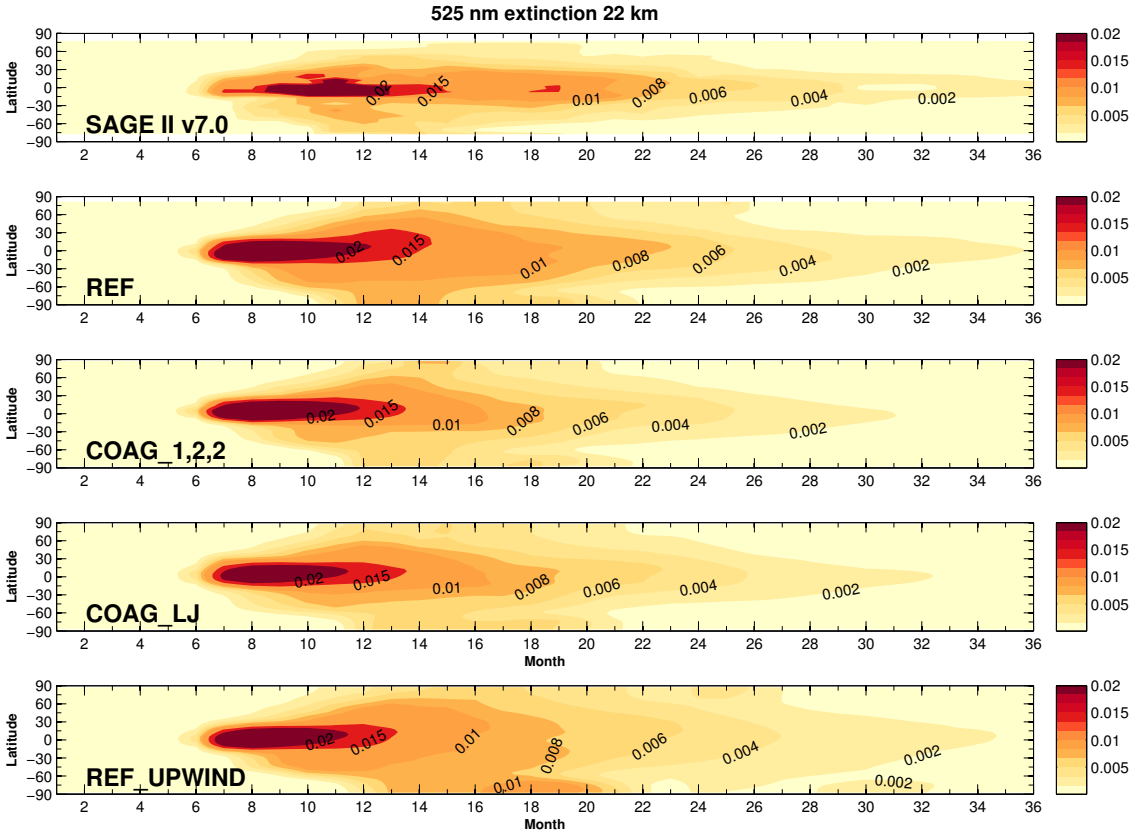

Figure 4.4 – Comparison of the SAGE II v7.0 aerosol extinction for 525 nm at 22 km and the simulations REF, $\text{COAG}_{1,2,2}$, COAG_{LJ} and REF_UPWIND.

4.3.3 Aerosol extinction

Figure 4.3 compares vertical profiles of SAGE II version 7.0 and modeled 525 nm extinction coefficients at the equator and 40-45°N in July 1992 (month 19) and July 1993 (month 31). REF_UPWIND largely overestimates the extinctions in the middle and upper stratosphere, reflecting its too abundant particles there. At the equator, REF slightly overestimates (∼25%) the SAGE II measurements between 25-30 km one year after Pinatubo (month 19), and matches the SAGE II at these altitudes two years after Pinatubo (month 31). $\text{COAG}_{1,2,2}$ improves the agreement between 25 and 30 km in the month 19 compared to REF, but slightly underestimates the extinctions in the month 31 due to the increased coagulation efficiency in the transition and free molecular regions. COAG_{LJ} improves the agreement in the both periods. However, at the equator near 22 km, none of these simulations is able to match the gap-filled SAGE II extinctions, and differs by 30% - 50%. This dis-

crepancy is possibly due to the insufficient vertical levels or too fast Brewer-Dobson circulation in the model. Similarly, in the mid-latitudes (the lower panels in Figure 4.3), $COAG_{1,2,2}$ and $COAG_{LJ}$ show better agreement with SAGE II, and correct the slightly overestimated extinctions from REF, particularly one year after Pinatubo.

Figure 4.4 shows latitude-time cross-sections of SAGE II 525 nm aerosol extinctions at 22 km and the model simulations. All modeled extinctions are higher than SAGE II in the first few months after Pinatubo when SAGE II largely underestimated due to that limb-occultation instruments became opaque in the lower stratosphere [*Russell et al.*, 1996] as discussed earlier in the text. Therefore, here we tend to focus on the periods after month 12. SAGE II shows persistent tropical extinctions (above the contour level of 0.008 km^{-1}) until month 23, and REF successfully reproduces such a persistence albeit less compact meridionally. $COAG_{1,2,2}$ and $COAG_{LJ}$ improve the calculated extinctions in meridional direction and generates a more narrow extinction band in the tropics compared to REF due to the enhanced coagulation. However, the temporal development of the extinction in the tropics is slightly less satisfactory compared to SAGE II as their extinction contour levels of 0.008 km^{-1} cease at month 18 for $COAG_{1,2,2}$ and month 19 for $COAG_{LJ}$. The tropical extinction band of $COAG_{LJ}$ is maintained one month longer than $COAG_{1,2,2}$ due to its retarded coagulation efficiency in the free molecular regime. It appears that the reduced coagulation efficiency in the free molecular regime could be insufficient and should be further reduced or the enhancement in the transition regime might be too high. Extinctions calculated by REF_UPWIND are more spread than the other simulations in meridional directions. REF_UPWIND produces more artificial small particles in the middle and high stratosphere due to numerical diffusion of the sedimentation scheme in the model. These artificial particles are more favorable to transport to high latitudes as high extinction values ($\sim$0.01 km^{-1}) are predicted by REF_UPWIND in the Antarctic region around month 18.

4.3.4 Temperature and ozone responses

In Figure 4.5, tropical and global temperature anomalies in the lower stratosphere after the Pinatubo eruption calculated by the SOCOL-AER scenarios (REF, $COAG_{1,2,2}$, $COAG_{LJ}$ and REF_UPWIND) are compared with the ERA-interim reanalysis and to values from SOCOL using SAGE-4λ [*Arfeuille et al.*, 2013] and feeded by offline 2-D AER aerosol forcing [*Heckendorn et al.*, 2009], different GCM/CCMs presented in *Lanzante and Free* [2008], *Eyring et al.* [2006] and *CCMVal* [2010].

All SOCOL-AER scenarios do not differ significantly, though the scenarios with enhanced coagulation efficiency ($COAG_{1,2,2}$, $COAG_{LJ}$) tend to have slightly higher

temperature in the first few months after the eruption due to larger particles. At 100 hPa in the tropics, the calculations from SOCOL-AER qualitatively match ERA-Interim data. However, in the month 9 -15, the stratospheric warming after the eruption from SOCOL-AER calculations is overestimated at 50 and 70 hPa. In November 1991 (month 11), SOCOL-AER shows a bias between 2-4 K in the tropical region at 50 hPa compared to ERA-Interim data, and globally 1.5-2 K at 50 and 70 hPa. This is possibly due to the overestimated aerosol burden (see Figure 4.1) in this period or deficiencies in microphysics, dynamics and radiation codes in the model. After month 15, SOCOL-AER simulations are generally better or consistent with the simulation using SAGE-4λ data [*Arfeuille et al.*, 2013], and improve massively compared to SOCOL using the offline AER treatment [*Heckendorn et al.*, 2009]. SOCOL-AER is in the upper range of temperature anomalies calculated by GCMs and CCMs at 50 and 70 hPa. However, the range of temperature anomalies could be highly biased since the GCM/CCMs used outdated data that largely underestimated longwave extinctions compared to SAGE-4λ data [*Arfeuille et al.*, 2013].

Figure 4.6 compares the monthly mean zonal mean total ozone column averaged from 60°S to 60°N between New Zealand National Institute of Water and Atmospheric Research (NIWA) observational total ozone data set [*Bodeker et al.*, 2005] and SOCOL-AER model calculations. The total ozone columns calculated by the different SOCOL-AER scenarios are very similar, and generally match the observed ozone column by NIWA. The results from SOCOL-AER are also consistent with the previous study using SOCOL v2 with the offline AER aerosol module [*Heckendorn et al.*, 2009].

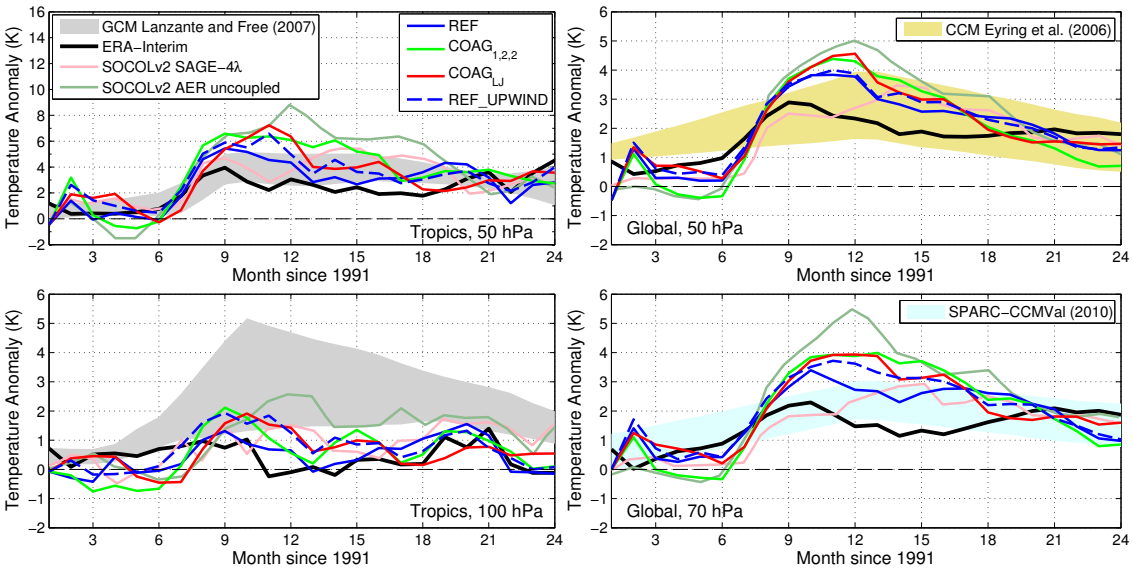

Figure 4.5 – Zonal mean temperature anomalies from SOCOL-AER for tropics (20S20N) at 50 hPa (upper left) and 100 hPa (lower left), global mean anomalies at 50 hPa (upper right) and 70 hPa (lower right). Scenarios anomalies (REF, $COAG_{1,2,2}$, $COAG_{LJ}$ and REF_UPWIND) are computed with respect to an unperturbed simulation. Black line: ERA-interim temperature anomalies with respect to 1995-1998. Light pink line: SOCOL v2 simulated temperature anomalies using SAGE-4λ dataset presented in *Arfeuille et al.* [2013]. Dark green line: SOCOL v2 simulated temperature anomalies using offline 2-D AER aerosol forcing (7 Mt S Pinatubo-like eruption) [*Heckendorn et al.*, 2009]. Grey area: anomaly ranges calculated by GCMs in *Lanzante and Free* [2008]. Yellow area: anomaly ranges calculated by CCMs in *Eyring et al.* [2006]. Cyan area: anomaly ranges calculated by CCMs in *CCMVal* [2010].

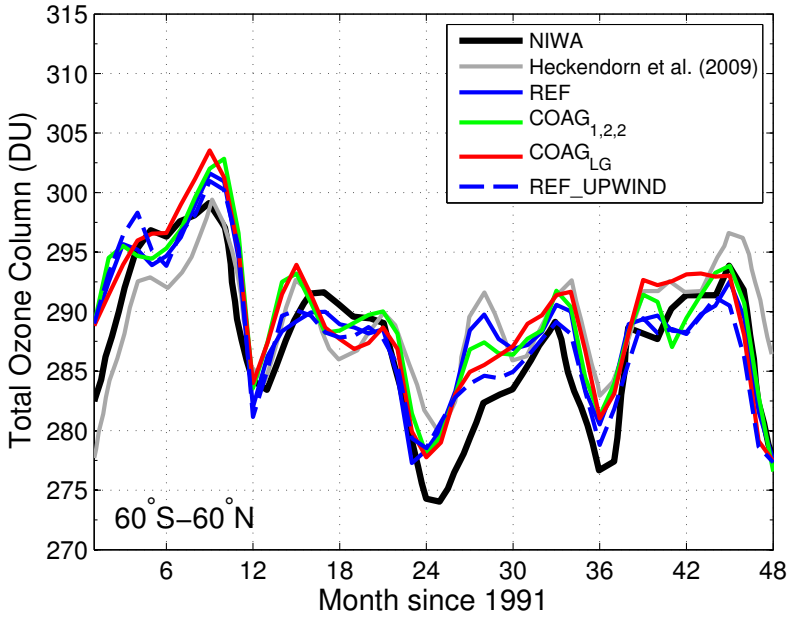

Figure 4.6 – Zonal mean monthly mean total ozone column average from 60°S to 60°N from January 1991 to December 1994. Black line: NIWA observational total ozone data set compiled by *Bodeker et al.* [2005]. Grey line: SOCOL v2 simulation using offline 2-D AER aerosol forcing (7 Mt S Pinatubo-like eruption) [*Heckendorn et al.*, 2009]. Colored lines: SOCOL-AER simulations.

4.4 Conclusions

We have successfully simulated the time-space development of stratospheric aerosols after Pinatubo, as well as temperature and ozone responses, using the free-running 3-D global chemistry-climate model coupled with a particle-size resolving aerosol module (SOCOL-AER). The simulations explore the role of the QBO, aerosol radiative heating, sedimentation scheme and coagulation efficiency in the evolution of the stratospheric aerosol after Pinatubo. The results show that QBO and interactive aerosol radiative heating play a significant role in maintaining the tropical stratospheric aerosols in the first six months after Pinatubo, but do not significantly affect the decay rate of the aerosol burden. Furthermore, the results suggest that an accurate sedimentation scheme helps significantly improve the model's ability to reproduce the stratospheric aerosol. Numerical diffusive methods, such as a simple upwind method, must be avoided in modeling studies of large volcanic eruptions in order to prevent too abundant artificial particles at high altitudes. Based on an accurate sedimentation scheme, Knudson number dependent coagulation coefficients further improve the description the evolution of the stratospheric aerosol after Pinatubo eruption. Stratospheric warming is realistically simulated, and consistent the simulations using SAGE-4λ data, showing massive improvements compared to the previous study [*Heckendorn et al.*, 2009].

Acknowledgments

This work was supported by the Swiss National Science Foundation under the grant 200021-130478(IASSA). We would like to thank Jason English and Anthony Baran for fruitful discussions. Also thanks to Mian Chin for valuable comments.

Chapter 5

Technical Notes

This chapter provides some technical details about the development of SOCOL-AER.

5.1 Size-dependent Composition

In the original AER 2-D model [*Weisenstein et al.*, 1997], aerosol composition (sulfuric acid weight percent) is calculated from ambient water vapor (P_{H_2O}), and temperature (T) following the parameterization [*Tabazadeh et al.*, 1997]. However, this leads to an underestimation of water vapor over small particles size bins because the vapor pressure over a curved surface is greater than over a flat surface. Such an effect is called the Kelvin (or curvature) effect [*Thomson*, 1871]. In this study, we correct the water vapor by the Kelvin effect for each particle size bin:

$$P_{H_2O,i} = P_{H_2O} \Big/ \exp\left(\frac{2\sigma_i \mathbb{V}_{H_2O}}{r_i RT}\right) \tag{5.1}$$

where $P_{H_2O,i}$ is the corrected vapor pressure of water over a curved surface for the size bin i with the radius r_i, σ_i is the surface tension for the size bin i, $\mathbb{V}_{H_2O}$ is the water molar volume, R is the universal gas constant and T is the temperature. Applying each $P_{H_2O,i}$ to the parameterization [*Tabazadeh et al.*, 1997] we obtained the size-dependent composition for sulfuric acid droplet. Figure 5.1 shows the calculated size-dependent weight percent (with Kelvin effect) compared to the original calculation (without Kelvin effect) under a typical stratospheric condition (near 30 km), where evaporation may occurs. The calculated size-dependent weight percent increases

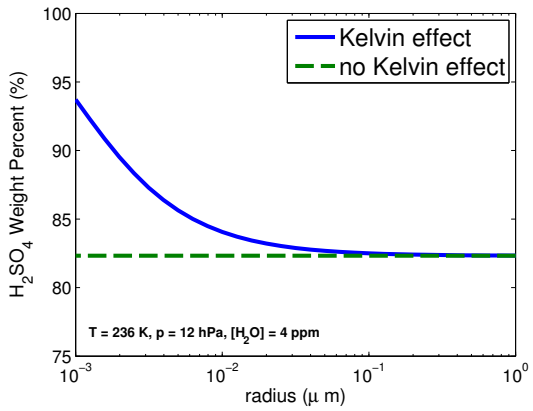

Figure 5.1 – Calculated weight percent with and without the Kelvin effect.

exponentially as the particle size decreases. At the size $r = 0.001$ μm, the size-dependent weight percent reaches about 94%, while the original calculation without Kelvin effect is only near 82%. This difference is significant because the resulting vapor pressure of sulfuric acid differ by two orders of magnitude, as shown in Figure 5.2. Consequently, condensation (evaporation) in the model with the size-dependent composition is less (more) effective for the particle size less than $\sim$0.01 μm.

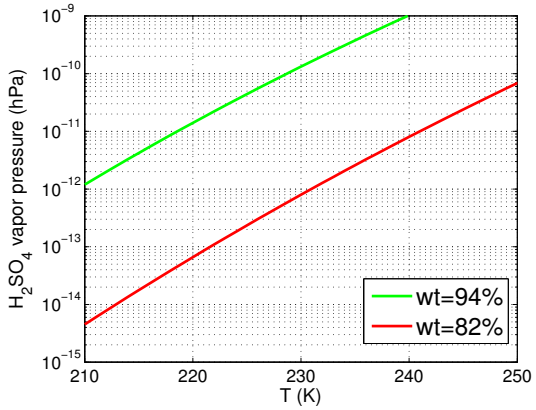

Figure 5.2 – Vapor pressure of sulfuric acid droplet as a function of temperature at two different weight percents (wt=94% and wt=82%).

5.2 Aqueous-Phase Chemistry S(IV)-S(VI)

The initial total concentration of sulfur dioxide [SO_2] (mole L^{-1}, mole per volume of air) can be expressed as

$$[SO_2] = \frac{p^0_{SO_2}}{RT} \tag{5.2}$$

where $p^0_{SO_2}$ is the partial pressure of SO_2 (atm) and R is molar gas constant (atm L mol^{-1} K^{-1}) and T is temperature (K). In clouds, SO_2 is distributed into the gas and aqueous phases:

$$[SO_2] = \frac{p_{SO_2}}{RT} + [S(IV)]w_L \tag{5.3}$$

where p_{SO_2} is the partial pressure of SO_2 after the dissolution of SO_2 in the cloud water, and w_L the cloud water content (volume of water per volume of air). The total dissolved sulfur dioxide [S(IV)] (mole per volume of water) is:

$$[S(IV)]=[SO_2(aq)] + [HSO_3^-] + [SO_3^{2-}]. \tag{5.4}$$

Combine the following sulfur dioxide/water equilibrium reactions:

$$H_{SO_2}: \quad SO_2(g) + H_2O \rightleftharpoons SO_2(aq) \tag{5.5}$$
$$K_{s1}: \quad SO_2(aq) \rightleftharpoons H^+ + HSO_3^- \tag{5.6}$$
$$K_{s2}: \quad HSO_3^- \rightleftharpoons H^+ + SO_3^{2-} \tag{5.7}$$

with the mass balance equation (5.3) and (5.4) and we obtain

$$[SO_2(aq)] = H_{SO_2} p_{SO_2} \tag{5.8}$$
$$[HSO_3^-] = \frac{K_{s1}[SO_2(aq)]}{[H^+]} \tag{5.9}$$
$$[SO_3^2-] = \frac{K_{s2}[SO_2(aq)]}{[H^+]} \tag{5.10}$$
$$[S(IV)] = H^*_{SO_2} p_{SO_2} \tag{5.11}$$

where $H^*_{SO_2} = H_{SO_2}\left(1 + K_{s1}/[H^+] + K_{s1}K_{s2}/[H^+]^2\right)$ the effective Henry's law coefficient for SO_2. Now the fraction of SO_2 that exist in the gas and the mole fractions

of the three S(IV) species can be calculated straightforwardly:

$$\chi_{\mathrm{SO_2(g)}} = \left(1 + H^*_{\mathrm{SO_2}} RT w_L\right)^{-1} \tag{5.12}$$

$$\chi_{\mathrm{SO_2(aq)}} = \frac{[\mathrm{SO_2(aq)}]}{[\mathrm{S(IV)}]} = \left(1 + K_{s1}/[\mathrm{H^+}] + K_{s1}K_{s2}/[\mathrm{H^+}]^2\right)^{-1} \tag{5.13}$$

$$\chi_{\mathrm{HSO_3^-}} = \frac{[\mathrm{HSO_3^-}]}{[\mathrm{S(IV)}]} = \left(1 + [\mathrm{H^+}]/K_{s1} + K_{s2}/[\mathrm{H^+}]^2\right)^{-1} \tag{5.14}$$

$$\chi_{\mathrm{SO_3^{2-}}} = \frac{[\mathrm{SO_3^2-}]}{[\mathrm{S(IV)}]} = \left(1 + [\mathrm{H^+}]/K_{s2} + [\mathrm{H^+}]^2/(K_{s1}K_{s2})\right)^{-1} \tag{5.15}$$

where $[\mathrm{H^+}]$ is the hydrogen ion $[\mathrm{H^+}]$ (or equivalently $\mathrm{pH} = -\log_{10}[\mathrm{H^+}]$). For simplification, we prescribe the pH value ($[\mathrm{H^+}]$) according to the precalculated vertical profile from *Walcek and Taylor* [1986].

The oxidation of S(IV) by ozone (O_3) and hydrogen peroxide (H_2O_2) have been implemented in SOCOL-AER. Their reactions are expressed as follows [*Hoffmann and Calvert*, 1985]:

$$\mathrm{S(IV) + O_3(aq) \longrightarrow S(VI) + O_2(aq) + H^+} \tag{5.16}$$

$$\mathrm{S(IV) + H_2O_2(aq) + H^+ \longrightarrow S(VI) + 2\,H^+ + H_2O(aq)} \tag{5.17}$$

and their rates are given by:

$$\frac{d[\mathrm{S(VI)}]}{dt} = -\frac{d[\mathrm{S(IV)}]}{dt} = (k_0[\mathrm{SO_2(aq)}] + k_1[\mathrm{HSO_3^-}] + k_2[\mathrm{SO_3^{2-}}])[\mathrm{O_3(aq)}] \tag{5.18}$$

$$\frac{d[\mathrm{S(VI)}]}{dt} = -\frac{d[\mathrm{S(IV)}]}{dt} = \frac{k_3[\mathrm{H^+}][\mathrm{H_2O_2(aq)}][\mathrm{HSO_3^-}]}{1 + K_4[\mathrm{H^+}]} \simeq k_3 H_{\mathrm{SO_2}} K_{s1} p_{\mathrm{SO_2}} [\mathrm{H_2O_2(aq)}]. \tag{5.19}$$

The approximation in Eq.(5.19) follows $[\mathrm{H^+}][\mathrm{HSO_3}-] = H_{\mathrm{SO_2}} K_{s1} p_{\mathrm{SO_2}}$ and $1 + K_4[\mathrm{H^+}] \simeq 1$ for pH> 2. This indicates that the reaction with $[\mathrm{H_2O_2(aq)}]$ is practically pH independent over the pH range of atmospheric interest [*Seinfeld and Pandis*, 2006]. $[\mathrm{O_3(aq)}]$ and $[\mathrm{H_2O_2(aq)}]$ can be obtained through Henry's law equilibrium, similarly as $[\mathrm{SO_2(aq)}]$. Therefore, combining (5.9)-(5.15), the reactions (5.18) and (5.19) can be rewritten as

$$\frac{d[\mathrm{S(VI)}]}{dt} = (k_0\chi_{\mathrm{SO_2(aq)}} + k_1\chi_{\mathrm{HSO_3^-}} + k_2\chi_{\mathrm{SO_3^{2-}}}) H^*_{\mathrm{SO_2}} \chi_{\mathrm{SO_2}} H_{\mathrm{O_3}} \chi_{\mathrm{O_3}} p^0_{\mathrm{SO_2}} p^0_{\mathrm{O_3}} \tag{5.20}$$

$$\frac{d[\mathrm{S(VI)}]}{dt} = k_3 K_{s1} H_{\mathrm{SO_2}} H_{\mathrm{H_2O_2}} \chi_{\mathrm{SO_2}} \chi_{\mathrm{H_2O_2}} p^0_{\mathrm{SO_2}} p^0_{\mathrm{H_2O_2}} \tag{5.21}$$

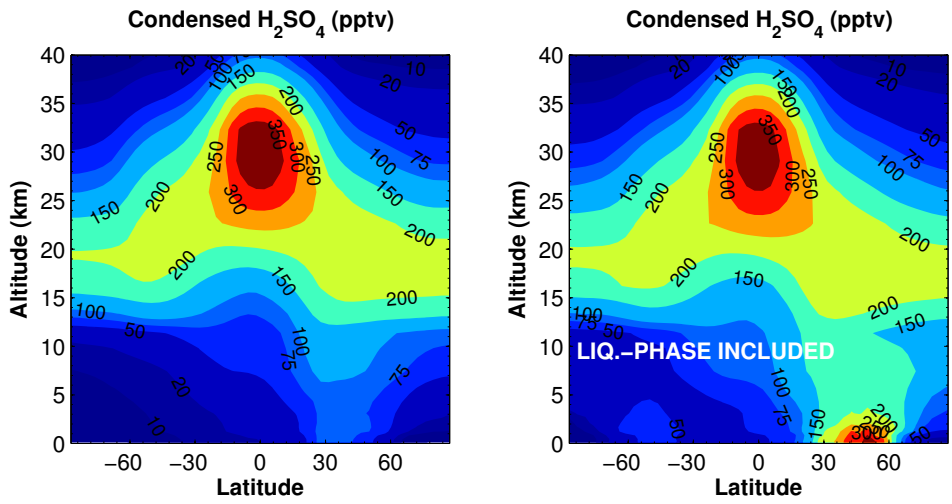

Figure 5.3 – Comparison of SOCOL-AER simulated annual zonal mean condensed H_2SO_4 mixing ratios without liquid-phase reaction (left) and with liquid-phase reaction (right).

where the fractions of O_3 and H_2O_2 can be obtained by the same procedure applied in SO_2. The equations (5.20) and (5.21) are in the form of the second-order-reaction and ready to be solved. The Henry's law and reaction coefficients are taken from *Jacob* [1986]. Figure 5.3 demonstrates the SOCOL-AER simulated annual zonal mean condensed H_2SO_4 mixing ratios with and without sulfur aqueous chemistry.

5.3 Sedimentation Scheme

Gravitational sedimentation is an important removal process for stratospheric aerosols, and particularly dominates the lifetime of the aerosol in large volcanic eruptions. An accurate sedimentation scheme with minimized numerical diffusion is required to properly simulate stratospheric aerosols and prevent artificial upward transport of smaller aerosol particles to the middle or upper stratosphere [*Benduhn and Lawrence*, 2013].

Simple upwind scheme. For a simple upwind scheme, the outgoing flux F_i^{out} due to sedimentation for the i-th grid box per time step Δt is given by

$$F_i^{\text{out}} = M_i u_i \frac{\Delta t}{\Delta z_i} \frac{\Delta p_i}{g} \tag{5.22}$$

where M_i denotes the aerosol mass mixing ratio at the ith grid box with $i = 1$ at the top of the atmosphere, u_i is the sedimentation velocity (m/s), g the gravitational acceleration (m/s^2), and Δz_i and Δp_i are the vertical thickness of the i-th grid box in units of m and Pa, respectively. The incoming flux F_i^{in} for the grid box i is equal to the outgoing flux F_{i-1}^{out} of the grid box $(i-1)$ above. Therefore, the change of the aerosol mass mixing ratio due to sedimentation for the grid box i per time step Δt is

$$\begin{aligned} \Delta M_i &= (F_i^{\text{in}} - F_i^{\text{out}}) \times \frac{g}{\Delta p_i} \\ &= M_{i-1} u_{i-1} \frac{\Delta t}{\Delta z_i} \frac{\Delta p_{i-1}}{\Delta p_i} - M_i u_i \frac{\Delta t}{\Delta z_i} \end{aligned} \tag{5.23}$$

Waleck scheme. For the Walcek scheme [*Walcek*, 2000], the incoming/outgoing fluxes are calculated on staggered grid boxes such that Eq. (5.23) is rewritten as (assuming the downward sedimentation velocity being positive)

$$\begin{aligned} \Delta M_i &= (F_{i-\frac{1}{2}}^{\text{in}} - F_{i+\frac{1}{2}}^{\text{out}}) \times \frac{g}{\Delta p_i} \\ &= M_{i-\frac{1}{2}} u_{i-\frac{1}{2}} \frac{\Delta t}{\Delta z_i} \frac{\Delta p_{i-1}}{\Delta p_i} - M_{i+\frac{1}{2}} u_{i+\frac{1}{2}} \frac{\Delta t}{\Delta z_i} \end{aligned} \tag{5.24}$$

where the aerosol massing mixing ratio $M_{i+\frac{1}{2}}$ at a staggered grid is given by

$$M_{i+\frac{1}{2}} = M_i + \frac{(M_{i+1} - M_{i-1})(1-c)}{4} \alpha \tag{5.25}$$

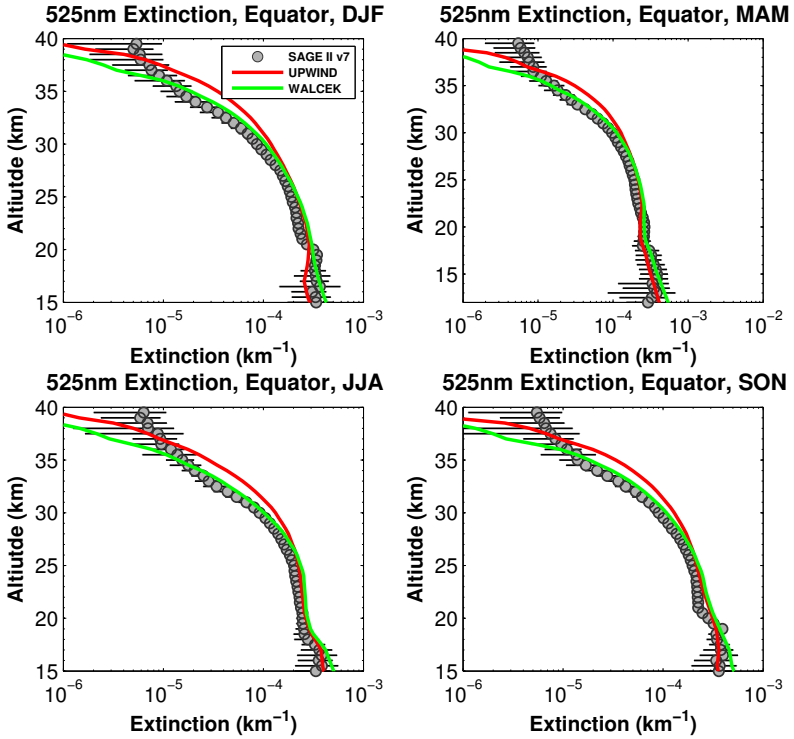

Figure 5.4 – Comparison of SAGE II version 7.0 and SOCOL-AER-calculated zonal mean extinctions at 525 nm at the equator using the upwind (red) and Walcek (green) schemes. The SAGE II data are averaged over the years 2000 to 2004 with horizontal bars being the observed natural variability.

with $c = u_{i+\frac{1}{2}} \frac{\Delta t}{\Delta z_i}$ being the Courant number and $\alpha = 1$ the adjustment factor except for local extremes. It was found that numerical diffusion is significantly reduced when $\alpha = 1.75 - 0.45c$ at the edge downwind of the local extreme combined with $\alpha = \max\{1.5, 1.2 + 0.6c\}$ at the edge upwind of the local extreme (see *Walcek* [2000] for details). Applying the Walcek scheme into the coupled SOCOL-AER, we find significant improvements in simulated aerosol extinctions and particle size distributions. Figure 5.4 shows SOCOL-AER-calculated zonal mean seasonal extinctions at 525 nm at the equator using the upwind (red) and Walcek (green) schemes compared to SAGE II version 7.0. The calculation using the Walcek scheme are in excellent agreement with SAGE II observations, whereas the simple upwind scheme predicts too high extinctions above 25 km. Figure 5.5 shows comparison of cumulative particle number densities for different size channels (particles larger than specified radius). The distribution of the measurement reflects the natural variability and is depicted by standard boxplots. The model calculation using the

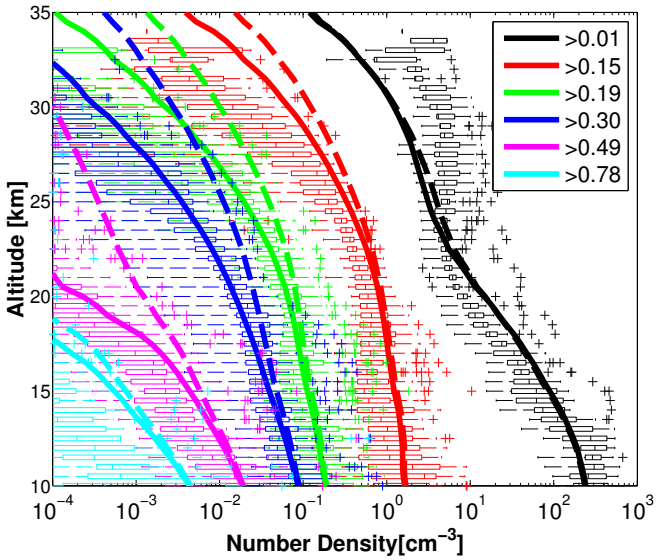

Figure 5.5 – Cumulative number densities above Laramie, Wyoming, for the period 2000-2010. Different colors: (wet) particle radii in μm (particles larger than specified radius). Solid lines: calculated by SOCOL/AER using the Walcek scheme (zonal mean annual average at 42N), Dashed lines: calculated by SOCOL/AER using the simple upwind scheme (zonal mean annual average at 42N). Standard boxplots: distribution of in situ stratospheric aerosol measurements at Laramie, Wyoming [*Deshler et al.*, 2003; *Deshler*, 2008]).

Walcek scheme (solid lines) are generally within the range of the measurements, although at the altitudes above 25 km, the modeled number densities start to deviate from the measurements with densities slightly higher for particles larger than 0.15 μm and lower for condensation nuclei. In contrast, the calculation using the simple upwind scheme (dashed lines) largely overestimate the measured values above 20 km, revealing too abundant particles in the middle and upper stratosphere due to numerical diffusion.

5.4 Time Step for Microphysics

Operator splitting approaches are used in SOCOL-AER in wihch transport is calculated every 15 minutes, whereas chemistry, microphysics and radiation are calculated every two hours. However, the timescale of microphysical processes may vary substantially, particularly under conditions of large volcanic eruptions. Therefore, it is important to identify a proper sub-time step for microphysics.

Several simulations of a Pinatubo-like eruption have been performed using different time steps (from 120 to 1.5 minutes) for microphysics. A convergence test based on the simulated global stratospheric aerosol burdens is shown in Figure 5.6. The calculation with the 120-minute time step (black line) fails to simulate properly the evolution of the stratospheric aerosol burden, which is substantially lower than the other calculations. The simulated burdens with smaller time steps tend to converge to the one with the finest time step (1.5 minutes) as the time step decreases.

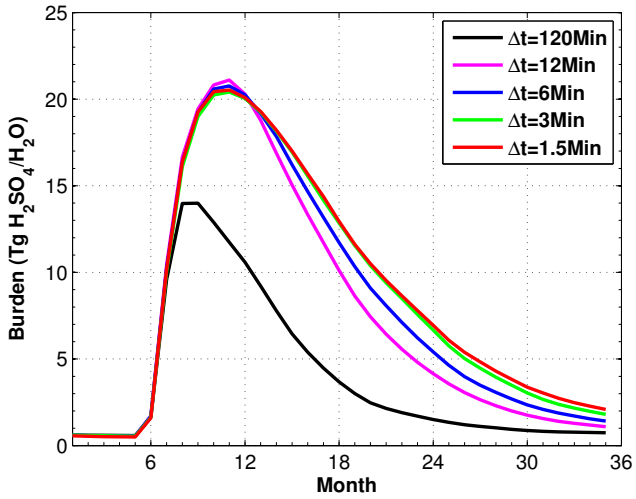

Figure 5.6 – Comparison of SOCOL-AER simulated global stratospheric aerosol burden after the Pinatubo eruption for different time steps Δt of microphysics.

Chapter 6

Conclusions and Perspectives

6.1 Conclusions

The chemistry-climate model SOCOL has been coupled to the particle size-resolving sulfate aerosol model AER. The novel aerosol-chemistry-climate model SOCOL-AER includes prognostic transport, chemistry, particle-size resolving aerosol microphysics, sedimentation and interactively aerosol radiative feedbacks. SOCOL-AER successfully reproduces the characteristic features of stratospheric aerosols under both non-volcanic and volcanic conditions.

Model validation and atmospheric sulfur budget

Modeled OCS mixing ratios are mostly within the range of ATMOS and MkIV measurements. Modeled SO_2 mixing ratios are consistent with the ATMOS and MIPAS measurements throughout the atmosphere. At altitudes above 30 km, agreement can only be achieved by including an enhanced photolytic conversion of gaseous H_2SO_4 into SO_2 [*Vaida et al.*, 2003]. The model sulfur budget indicates that a net sulfur flux of approximately 103 Gg S/yr through the tropopause enters the stratosphere, in which 40% are in the form of OCS, 50% in the form of SO_2, and 10% in the form of CS_2, DMS and H_2S. In addition, large amounts of OCS and aerosols enter the stratosphere, but leave it again in the same form, i.e. do not contribute to the net sulfur flux. The modeled stratospheric aerosol burden is 109 Gg S, providing excellent agreement with the burden (102.5 Gg S) derived from SAGE II (by means of the retrieval algorithm SAGE-4λ). This corrects the modeled 187.2 Gg S stratospheric aerosol burden in the previous study [*SPARC*, 2006]. SOCOL-AER

successfully reproduces aerosol extinctions from visible to IR wavelengths (within ±30%, and mostly better than ±10%) compared to SAGE II and HALOE observations in the lower and middle stratosphere (with the exception of the extinction at 5.6 μm, which is underestimated by 30-60% for unknown reasons). Above ∼35 km, close to the upper edge of the Junge layer, SOCOL-AER is not able to match observations due to the lack of meteoritic dust in the model. Model comparisons with in situ measurements by optical particle counters above Wyoming [*Deshler et al.*, 2003] verify that the model successfully represents the particle size distribution and particle volume density in the lower and middle stratosphere. Measurements in the UTLS region are necessary for model validation, i.e. to validate our knowledge of sulfur fluxes into the stratosphere in the form of SO_2 and aerosols under volcanically quiescent conditions.

Sensitivity of stratospheric aerosol to sulfur emissions

Sensitivity studies indicate that OCS contributes about 56% of the background stratospheric aerosol burden, whereas the transport of SO_2 across the tropopause contributes about 26%. The model results also suggest that anthropogenic SO_2 emissions in East Asia and India contribute generally more to the lower stratospheric aerosols than emissions in Europe and USA, in particular during the summertime. This may be explained by the importance of deep convection and the proximity of the Western Pacific region. The model results further suggest that emissions of DMS, H_2S and volcanic degassing contribute comparably to the stratospheric aerosol burden as do anthropogenic SO_2 emissions, and must be taken into account in modeling studies. However, even more important in terms of sulfur input into the stratosphere are small and medium-size volcanic eruptions. Simulations of Nabro-like eruptions demonstrate that even a modest volcanic eruption can dramatically perturb the stratospheric aerosol layer and dominate anthropogenic SO_2 emissions over months-long timescales, but only if the volcanic plume reaches the lower stratosphere.

Mt Pinatubo's initial sulfur mass emission

Over 300 Pinatubo-like simulations have been conducted based on the combinations of parameters of initial total SO_2 mass and altitude distribution. These parameters predominantly control the temporal and spacial evolution of stratospheric aerosols in the first 18 months after the Pinatubo eruption. The magnitude of the initial SO_2 mass released into the stratosphere is approximately 14 Mt based on HIRS

and SAGE II observations. The altitude distribution of SO_2 injection is represented by a skew-normal distribution. Model results suggest that about 80% of emitted sulfur mass is distributed below 24 km with the maximum located between 19-21 km. This corrects the previously found overestimation in *SPARC* [2006] in modeled extinctions at high altitudes when comparing to SAGE II gap-filled measurement, and realistically simulates aerosol extinctions in the lower stratosphere. This defines an optimal set of the emission parameters such that the resulting SO_2 plume, aerosol burdens and extinctions match satellite and lidar measurements, and reduce the uncertainties in modeling initial mass loading of Pinatubo.

Size-Resolved Stratospheric Aerosol Distributions after Pinatubo

The coupled aerosol-chemistry-climate model SOCOL-AER has successfully simulated the time-space development of stratospheric aerosols after Pinatubo, as well as temperature and ozone responses. The simulations explore the role of the QBO, aerosol radiative heating, sedimentation scheme and coagulation efficiency in the evolution of the stratospheric aerosol after Pinatubo. The results show that QBO and interactive aerosol radiative heating play a significant role in maintaining the tropical stratospheric aerosols in the first six months after Pinatubo, but do not significantly affect the decay rate of the aerosol burden. Furthermore, the results suggest that an accurate sedimentation scheme helps significantly improve the model's ability to reproduce the stratospheric aerosol. Numerical diffusive methods, such as a simple upwind method, must be avoided in modeling studies of large volcanic eruptions in order to prevent too abundant artificial particles at high altitudes. Based on an accurate sedimentation scheme, Knudson number dependent coagulation coefficients further improve the description the evolution of the stratospheric aerosol after Pinatubo eruption. Stratospheric warming is realistically simulated, and consistent with SAGE-4λ data, showing massive improvements compared to the previous study [*Heckendorn et al.*, 2009]. Overall, the results demonstrate the necessity of the combination of detailed resolution of individual processes and comprehensive coupling in order to achieve a proper prediction of atmospheric and climate effects following large volcanic eruptions or sulfur injections related to geoengineering.

6.2 Future Perspectives.

An important task of present climate research is to estimate benefits and negative side effects of different geoengineering measures, which could potentially be adopted

as emergency actions to slow overshooting greenhouse warming. However, so far only a few attempts to address this issue have been made, and the uncertainty of the available estimates remains very high. Therefore, the various suggestions for geoengineering actions are still largely unexplored ideas that require scrutiny before they might become geoengineering options. Substantial improvements in understanding of geoengineering will be required to reduce uncertainties in current modeling approaches. SOCOL-AER shows excellent performance in representing the stratospheric sulfate aerosol under background and strong volcanic conditions. The application of this advanced model is expected to provide a much improved, objective scientific basis from which the geoengineering scenarios can be assessed. Further endeavor may involve establishing a more reliable assessment of the potential benefits and negative side-effects of geoengineering by injection of sulfur containing gases, and quantifying the role of interactive dynamic ocean in the future climate and ozone development assuming different geoengineering scenarios.

List of Figures

Bibliography

Andres, R. J., and A. D. Kasgnoc (1998), A time-averaged inventory of subaerial volcanic sulfur emissions, *Journal of Geophysical Research: Atmospheres*, *103*(D19), 25,25125,261, doi:10.1029/98JD02091.

Anet, J. G., et al. (2013), Forcing of stratospheric chemistry and dynamics during the dalton minimum, *Atmospheric Chemistry and Physics Discussions*, *13*(6), 15,061–15,104, doi:10.5194/acpd-13-15061-2013.

Aquila, V., L. D. Oman, R. S. Stolarski, P. R. Colarco, and P. A. Newman (2012), Dispersion of the volcanic sulfate cloud from a mount pinatubolike eruption, *Journal of Geophysical Research: Atmospheres*, *117*(D6), n/an/a, doi:10.1029/2011JD016968.

Arfeuille, F., et al. (2013), Modeling the stratospheric warming following the mt. pinatubo eruption: uncertainties in aerosol extinctions, *Atmos. Chem. Phys.*, *13*(22), 11,221–11,234, doi:10.5194/acp-13-11221-2013.

Ayers, G. P., R. W. Gillett, and J. L. Gras (1980), On the vapor pressure of sulfuric acid, *Geophysical Research Letters*, *7*(6), 433436, doi:10.1029/GL007i006p00433.

Azzalini, A. (2005), The skew-normal distribution and related multivariate families, *Scandinavian Journal of Statistics*, *32*(2), 159188, doi:10.1111/j.1467-9469.2005.00426.x.

Baran, A. J., and J. S. Foot (1994), New application of the operational sounder HIRS in determining a climatology of sulphuric acid aerosol from the pinatubo eruption, *Journal of Geophysical Research: Atmospheres*, *99*(D12), 25,67325,679, doi:10.1029/94JD02044.

Benduhn, F., and M. G. Lawrence (2013), An investigation of the role of sedimentation for stratospheric solar radiation management, *Journal of Geophysical Research: Atmospheres*, *118*(14), 79057921, doi:10.1002/jgrd.50622.

Biermann, U. M., B. P. Luo, and T. Peter (2000), Absorption spectra and optical constants of binary and ternary solutions of H_2SO_4, HNO_3, and H_2O in the mid infrared at atmospheric temperatures, *The Journal of Physical Chemistry A*, *104*(4), 783–793, doi:10.1021/jp992349i.

Bluth, G. J. S., S. D. Doiron, C. C. Schnetzler, A. J. Krueger, and L. S. Walter (1992), Global tracking of the SO_2 clouds from the june, 1991 mount pinatubo eruptions, *Geophysical Research Letters*, *19*(2), 151154, doi:10.1029/91GL02792.

Bodeker, G. E., H. Shiona, and H. Eskes (2005), Indicators of antarctic ozone depletion, *Atmos. Chem. Phys.*, *5*(10), 2603–2615, doi:10.5194/acp-5-2603-2005.

Bourassa, A. E., A. Robock, W. J. Randel, T. Deshler, L. A. Rieger, N. D. Lloyd, E. J. T. Llewellyn, and D. A. Degenstein (2012), Large volcanic aerosol load in the stratosphere linked to asian monsoon transport, *Science*, *337*(6090), 78–81, doi:10.1126/science.1219371, PMID: 22767926.

Brühl, C., J. Lelieveld, P. J. Crutzen, and H. Tost (2012), The role of carbonyl sulphide as a source of stratospheric sulphate aerosol and its impact on climate, *Atmos. Chem. Phys.*, *12*(3), 1239–1253, doi:10.5194/acp-12-1239-2012.

Cagnazzo, C., E. Manzini, M. A. Giorgetta, P. M. D. F. Forster, and J. J. Morcrette (2007), Impact of an improved shortwave radiation scheme in the MAECHAM5 general circulation model, *Atmos. Chem. Phys.*, *7*(10), 2503–2515, doi:10.5194/acp-7-2503-2007.

Campbell, P., and T. Deshler (2014), Condensation nuclei measurements in the midlatitude (19822012) and antarctic (19862010) stratosphere between 20 and 35km, *Journal of Geophysical Research: Atmospheres*, *119*(1), 2013JD019,710, doi:10.1002/2013JD019710.

CCMVal (2010), Report on the evaluation of chemistry-climate models, edited by: Eyring, v., shepherd, TG, and waugh, DW, *Tech. rep.*, SPARC Report No. 5.

Chagnon, C. W., and C. E. Junge (1961), THE VERTICAL DISTRIBUTION OF SUB-MICRON PARTICLES IN THE STRATOSPHERE, *Journal of Meteorology*, *18*(6), 746–752, doi:10.1175/1520-0469(1961)018⟨0746:TVDOSM⟩2.0.CO;2.

Chatfield, R. B., and P. J. Crutzen (1984), Sulfur dioxide in remote oceanic air: Cloud transport of reactive precursors, *Journal of Geophysical Research: Atmospheres*, *89*(D5), 71117132, doi:10.1029/JD089iD05p07111.

Chin, M., and D. D. Davis (1995), A reanalysis of carbonyl sulfide as a source of stratospheric background sulfur aerosol, *Journal of Geophysical Research: Atmospheres*, *100*(D5), 89939005, doi:10.1029/95JD00275.

Chin, M., R. B. Rood, S.-J. Lin, J.-F. Mller, and A. M. Thompson (2000), Atmospheric sulfur cycle simulated in the global model GOCART: model description and global properties, *Journal of Geophysical Research: Atmospheres*, *105*(D20), 24,67124,687, doi:10.1029/2000JD900384.

Crutzen, P. J. (1976), The possible importance of CSO for the sulfate layer of the stratosphere, *Geophysical Research Letters*, *3*(2), 7376, doi:10.1029/GL003i002p00073.

Crutzen, P. J. (2006), Albedo enhancement by stratospheric sulfur injections: A contribution to resolve a policy dilemma?, *Climatic Change*, *77*(3-4), 211–220, doi:10.1007/s10584-006-9101-y.

Dentener, F., et al. (2006), Emissions of primary aerosol and precursor gases in the years 2000 and 1750 prescribed data-sets for AeroCom, *Atmos. Chem. Phys.*, *6*(12), 4321–4344, doi:10.5194/acp-6-4321-2006.

Deshler, T. (2008), A review of global stratospheric aerosol: Measurements, importance, life cycle, and local stratospheric aerosol, *Atmospheric Research*, *90*(24), 223–232, doi:10.1016/j.atmosres.2008.03.016.

Deshler, T., M. E. Hervig, D. J. Hofmann, J. M. Rosen, and J. B. Liley (2003), Thirty years of in situ stratospheric aerosol size distribution measurements from laramie, wyoming (41N), using balloon-borne instruments, *Journal of Geophysical Research: Atmospheres*, *108*(D5), n/an/a, doi:10.1029/2002JD002514.

Dutton, E. G., and J. R. Christy (1992), Solar radiative forcing at selected locations and evidence for global lower tropospheric cooling following the eruptions of el chichn and pinatubo, *Geophysical Research Letters*, *19*(23), 23132316, doi:10.1029/92GL02495.

Dvortsov, V. L., M. A. Geller, V. A. Yudin, and S. P. Smyshlyaev (1998), Parameterization of the convective transport in a two-dimensional chemistry-transport model and its validation with radon 222 and other tracer simulations, *Journal of Geophysical Research: Atmospheres*, *103*(D17), 22,04722,062, doi:10.1029/98JD02084.

Egorova, T., E. Rozanov, V. Zubov, and I. Karol (2003), Model for investigating ozone trends (MEZON), *Izvestiya Atmospheric and Oceanic Physics*, *39*(3), 277292.

English, J. M., O. B. Toon, M. J. Mills, and F. Yu (2011), Microphysical simulations of new particle formation in the upper troposphere and lower stratosphere, *Atmos. Chem. Phys.*, *11*(17), 9303–9322, doi:10.5194/acp-11-9303-2011.

English, J. M., O. B. Toon, and M. J. Mills (2013), Microphysical simulations of large volcanic eruptions: Pinatubo and toba, *Journal of Geophysical Research: Atmospheres*, *118*(4), 18801895, doi:10.1002/jgrd.50196.

Eyring, V., et al. (2006), Assessment of temperature, trace species, and ozone in chemistry-climate model simulations of the recent past, *Journal of Geophysical Research: Atmospheres*, *111*(D22), D22,308, doi:10.1029/2006JD007327.

Farquhar, J., J. Savarino, S. Airieau, and M. H. Thiemens (2001), Observation of wavelength-sensitive mass-independent sulfur isotope effects during SO_2 photolysis: Implications for the early atmosphere, *Journal of Geophysical Research: Planets*, *106*(E12), 32,82932,839, doi:10.1029/2000JE001437.

Fleming, E. L., C. H. Jackman, R. S. Stolarski, and D. B. Considine (1999), Simulation of stratospheric tracers using an improved empirically based two-dimensional model transport formulation, *Journal of Geophysical Research: Atmospheres*, *104*(D19), 23,91123,934, doi:10.1029/1999JD900332.

Fuchs, N. A. (1964), *The mechanics of aerosols*, Pergamon Press, Oxford.

Giauque, W. F., E. W. Hornung, J. E. Kunzler, and T. R. Rubin (1960), The thermodynamic properties of aqueous sulfuric acid solutions and hydrates from 15 to 300K.1, *Journal of the American Chemical Society*, *82*(1), 62–70, doi:10.1021/ja01486a014.

Graf, H.-F., B. Langmann, and J. Feichter (1998), The contribution of earth degassing to the atmospheric sulfur budget, *Chemical Geology*, *147*(12), 131–145, doi:10.1016/S0009-2541(97)00177-0.

Graf, H.-F., Q. Li, and M. A. Giorgetta (2007), Volcanic effects on climate: revisiting the mechanisms, *Atmos. Chem. Phys.*, *7*(17), 4503–4511, doi:10.5194/acp-7-4503-2007.

Gunson, M. R., et al. (1996), The atmospheric trace molecule spectroscopy (ATMOS) experiment: Deployment on the ATLAS space shuttle missions, *Geophysical Research Letters*, *23*(17), 23332336, doi:10.1029/96GL01569.

Guo, S., G. J. S. Bluth, W. I. Rose, I. M. Watson, and A. J. Prata (2004), Re-evaluation of SO2 release of the 15 june 1991 pinatubo eruption using ultraviolet and infrared satellite sensors, *Geochemistry, Geophysics, Geosystems*, *5*(4), n/an/a, doi:10.1029/2003GC000654.

Halmer, M., H.-U. Schmincke, and H.-F. Graf (2002), The annual volcanic gas input into the atmosphere, in particular into the stratosphere: a global data set for the past 100 years, *Journal of Volcanology and Geothermal Research*, *115*(34), 511–528, doi:10.1016/S0377-0273(01)00318-3.

Hamill, P., E. J. Jensen, P. B. Russell, and J. J. Bauman (1997), The life cycle of stratospheric aerosol particles, *Bulletin of the American Meteorological Society*, *78*(7), 1395–1410, doi:10.1175/1520-0477(1997)078⟨1395:TLCOSA⟩2.0.CO;2.

Hauglustaine, D. A., C. Granier, G. P. Brasseur, and G. Mgie (1994), The importance of atmospheric chemistry in the calculation of radiative forcing on the climate system, *Journal of Geophysical Research: Atmospheres*, *99*(D1), 11731186, doi:10.1029/93JD02987.

Heckendorn, P., D. Weisenstein, S. Fueglistaler, B. P. Luo, E. Rozanov, M. Schraner, L. W. Thomason, and T. Peter (2009), The impact of geoengineering aerosols on stratospheric temperature and ozone, *Environmental Research Letters*, *4*(4), 045,108, doi:10.1088/1748-9326/4/4/045108.

Hoffmann, M. R., and J. G. Calvert (1985), *Chemical Transformation Modules for Eulerian Acid Deposition Models: Volume II, the Aqueous-phase Chemistry*, Atmospheric Sciences Research Laboratory, Office of Research and Development, US Environmental Protection Agency.

Hommel, R., C. Timmreck, and H. F. Graf (2011), The global middle-atmosphere aerosol model MAECHAM5-SAM2: comparison with satellite and in-situ observations, *Geoscientific Model Development*, *4*(3), 809–834, doi:10.5194/gmd-4-809-2011.

Höpfner, M., et al. (2013), Sulfur dioxide (SO_2) as observed by MIPAS/Envisat: temporal development and spatial distribution at 1545 km altitude, *Atmos. Chem. Phys.*, *13*(20), 10,405–10,423, doi:10.5194/acp-13-10405-2013.

Jacob, D. J. (1986), Chemistry of OH in remote clouds and its role in the production of formic acid and peroxymonosulfate, *Journal of Geophysical Research: Atmospheres*, *91*(D9), 98079826, doi:10.1029/JD091iD09p09807.

Jacobson, M. Z., and J. H. Seinfeld (2004), Evolution of nanoparticle size and mixing state near the point of emission, *Atmospheric Environment*, *38*(13), 1839–1850, doi:10.1016/j.atmosenv.2004.01.014.

Junge, C. (1974), Sulfur budget of the stratospheric aerosol layer, in *International Conference on Structure, Composition and General Circulation of the Upper and Lower Atmospheres and Possible Anthropogenic Perturbations, Melbourne, Australia*, p. 85100.

Junge, C. E., and J. E. Manson (1961), Stratospheric aerosol studies, *Journal of Geophysical Research*, *66*(7), 21632182, doi:10.1029/JZ066i007p02163.

Junge, C. E., C. W. Chagnon, and J. E. Manson (1961), Stratospheric aerosols, *Journal of Meteorology*, *18*(1), 81–108, doi:10.1175/1520-0469(1961)018⟨0081:SA⟩2.0.CO;2.

Kasten, F. (1968), Falling speed of aerosol particles, *Journal of Applied Meteorology*, *7*(5), 944–947, doi:10.1175/1520-0450(1968)007⟨0944:FSOAP⟩2.0.CO;2.

Kettle, A. J., and M. O. Andreae (2000), Flux of dimethylsulfide from the oceans: A comparison of updated data sets and flux models, *Journal of Geophysical Research: Atmospheres*, *105*(D22), 26,79326,808, doi:10.1029/2000JD900252.

Kettle, A. J., et al. (1999), A global database of sea surface dimethylsulfide (DMS) measurements and a procedure to predict sea surface DMS as a function of latitude, longitude, and month, *Global Biogeochemical Cycles*, *13*(2), 399–444, doi:10.1029/1999GB900004.

Kettle, A. J., U. Kuhn, M. von Hobe, J. Kesselmeier, and M. O. Andreae (2002), Global budget of atmospheric carbonyl sulfide: Temporal and spatial variations of the dominant sources and sinks, *Journal of Geophysical Research: Atmospheres*, *107*(D22), ACH 25–1ACH 25–16, doi:10.1029/2002JD002187.

Kodera, K. (1994), Influence of volcanic eruptions on the troposphere through stratospheric dynamical processes in the northern hemisphere winter, *Journal of Geophysical Research: Atmospheres*, *99*(D1), 12731282, doi:10.1029/93JD02731.

Krueger, A. J., L. S. Walter, P. K. Bhartia, C. C. Schnetzler, N. A. Krotkov, I. Sprod, and G. J. S. Bluth (1995), Volcanic sulfur dioxide measurements from the total ozone mapping spectrometer instruments, *Journal of Geophysical Research: Atmospheres*, *100*(D7), 14,05714,076, doi:10.1029/95JD01222.

Kulmala, M., and A. Laaksonen (1990), Binary nucleation of watersulfuric acid system: Comparison of classical theories with different H2SO4 saturation vapor pressures, *The Journal of Chemical Physics*, *93*(1), 696–701, doi:doi:10.1063/1.459519.

Labitzke, K., and M. P. McCormick (1992), Stratospheric temperature increases due to pinatubo aerosols, *Geophysical Research Letters*, *19*(2), 207210, doi:10.1029/91GL02940.

Lamarque, J.-F., et al. (2010), Historical (18502000) gridded anthropogenic and biomass burning emissions of reactive gases and aerosols: methodology and application, *Atmos. Chem. Phys.*, *10*(15), 7017–7039, doi:10.5194/acp-10-7017-2010.

Lanzante, J. R., and M. Free (2008), Comparison of radiosonde and GCM vertical temperature trend profiles: Effects of dataset choice and data homogenization*, *Journal of Climate*, *21*(20), 5417–5435, doi:10.1175/2008JCLI2287.1.

Leung, F.-Y. T., A. J. Colussi, M. R. Hoffmann, and G. C. Toon (2002), Isotopic fractionation of carbonyl sulfide in the atmosphere: Implications for the source of background stratospheric sulfate aerosol, *Geophysical Research Letters*, *29*(10), 112–1112–4, doi:10.1029/2001GL013955.

Lin, S.-J., and R. B. Rood (1996), Multidimensional flux-form semi-lagrangian transport schemes, *Monthly Weather Review*, *124*(9), 2046–2070, doi:10.1175/1520-0493(1996)124⟨2046:MFFSLT⟩2.0.CO;2.

McCormick, M. P., L. W. Thomason, and C. R. Trepte (1995), Atmospheric effects of the mt pinatubo eruption, *Nature*, *373*(6513), 399–404, doi:10.1038/373399a0.

Miller, Y., R. B. Gerber, and V. Vaida (2007), Photodissociation yields for vibrationally excited states of sulfuric acid under atmospheric conditions, *Geophysical Research Letters*, *34*(16), n/an/a, doi:10.1029/2007GL030529.

Mills, M. J., O. B. Toon, and S. Solomon (1999), A 2D microphysical model of the polar stratospheric CN layer, *Geophysical Research Letters*, *26*(8), 11331136, doi:10.1029/1999GL900187.

Minnis, P., E. F. Harrison, L. L. Stowe, G. G. Gibson, F. M. Denn, D. R. Doelling, and W. L. Smith (1993), Radiative climate forcing by the mount pinatubo eruption, *Science*, *259*(5100), 1411–1415, doi:10.1126/science.259.5100.1411, PMID: 17801273.

Mlawer, E. J., S. J. Taubman, P. D. Brown, M. J. Iacono, and S. A. Clough (1997), Radiative transfer for inhomogeneous atmospheres: RRTM, a validated correlated-k model for the longwave, *Journal of Geophysical Research: Atmospheres*, *102*(D14), 16,66316,682, doi:10.1029/97JD00237.

Murphy, D. M., D. S. Thomson, and M. J. Mahoney (1998), In situ measurements of organics, meteoritic material, mercury, and other elements in aerosols at 5 to 19 kilometers, *Science*, *282*(5394), 1664–1669, doi:10.1126/science.282.5394.1664, PMID: 9831550.

Narsimhan, G., and E. Ruckenstein (1985), The brownian coagulation of aerosols over the entire range of knudsen numbers: Connection between the sticking probability and the interaction forces, *Journal of Colloid and Interface Science*, *104*(2), 344–369, doi:10.1016/0021-9797(85)90044-X.

Neely, R. R., J. M. English, O. B. Toon, S. Solomon, M. Mills, and J. P. Thayer (2011), Implications of extinction due to meteoritic smoke in the upper stratosphere, *Geophysical Research Letters*, *38*(24), n/an/a, doi:10.1029/2011GL049865.

Niemeier, U., C. Timmreck, H.-F. Graf, S. Kinne, S. Rast, and S. Self (2009), Initial fate of fine ash and sulfur from large volcanic eruptions, *Atmos. Chem. Phys.*, *9*(22), 9043–9057, doi:10.5194/acp-9-9043-2009.

Nightingale, P. D., G. Malin, C. S. Law, A. J. Watson, P. S. Liss, M. I. Liddicoat, J. Boutin, and R. C. Upstill-Goddard (2000), In situ evaluation of air-sea gas exchange parameterizations using novel conservative and volatile tracers, *Global Biogeochemical Cycles*, *14*(1), 373387, doi:10.1029/1999GB900091.

Notholt, J., et al. (2005), Influence of tropospheric SO2 emissions on particle formation and the stratospheric humidity, *Geophysical Research Letters*, *32*(7), n/an/a, doi:10.1029/2004GL022159.

Ozolin, I. E. (1992), Modeling diurnal variations of trace gases in the atmosphere and the procedure of diurnal averaging in photochemical models, *Akademiia Nauk SSSR Fizika Atmosfery i Okeana*, *28*, 135–143.

Prinn, R. G., et al. (2005), Evidence for variability of atmospheric hydroxyl radicals over the past quarter century, *Geophysical Research Letters*, *32*(7), L07,809, doi:10.1029/2004GL022228.

Ramanathan, V., P. J. Crutzen, J. T. Kiehl, and D. Rosenfeld (2001), Aerosols, climate, and the hydrological cycle, *Science*, *294*(5549), 2119–2124, doi:10.1126/science.1064034, PMID: 11739947.

Randel, W. J., et al. (2009), An update of observed stratospheric temperature trends, *Journal of Geophysical Research: Atmospheres*, *114*(D2), n/an/a, doi:10.1029/2008JD010421.

Rasch, P. J., P. J. Crutzen, and D. B. Coleman (2008), Exploring the geoengineering of climate using stratospheric sulfate aerosols: The role of particle size, *Geophysical Research Letters*, *35*(2), n/an/a, doi:10.1029/2007GL032179.

Rayner, N. A., D. E. Parker, E. B. Horton, C. K. Folland, L. V. Alexander, D. P. Rowell, E. C. Kent, and A. Kaplan (2003), Global analyses of sea surface temperature, sea ice, and night marine air temperature since the late nineteenth century, *Journal of Geophysical Research: Atmospheres*, *108*(D14), n/an/a, doi:10.1029/2002JD002670.

Read, W. G., L. Froidevaux, and J. W. Waters (1993), Microwave limb sounder measurement of stratospheric SO2 from the mt. pinatubo volcano, *Geophysical Research Letters*, *20*(12), 12991302, doi:10.1029/93GL00831.

Rinsland, C. P., M. R. Gunson, M. K. W. Ko, D. W. Weisenstein, R. Zander, M. C. Abrams, A. Goldman, N. D. Sze, and G. K. Yue (1995), H2SO4 photolysis: A source of sulfur dioxide in the upper stratosphere, *Geophysical Research Letters*, *22*(9), 11091112, doi:10.1029/95GL00917.

Rinsland, C. P., et al. (1996), Trends of OCS, HCN, SF6, CHClF2 (HCFC-22) in the lower stratosphere from 1985 and 1994 atmospheric trace molecule spectroscopy experiment measurements near 30N latitude, *Geophysical Research Letters*, *23*(17), 23492352, doi:10.1029/96GL01234.

Robock, A. (2000), Volcanic eruptions and climate, *Reviews of Geophysics*, *38*(2), 191219, doi:10.1029/1998RG000054.

Robock, A., L. Oman, and G. L. Stenchikov (2008), Regional climate responses to geoengineering with tropical and arctic SO2 injections, *Journal of Geophysical Research: Atmospheres*, *113*(D16), n/an/a, doi:10.1029/2008JD010050.

Robock, A., D. G. MacMartin, R. Duren, and M. W. Christensen (2013), Studying geoengineering with natural and anthropogenic analogs, *Climatic Change*, *121*(3), 445–458, doi:10.1007/s10584-013-0777-5.

Roeckner, E., et al. (2003), The atmospheric general circulation model ECHAM 5. PART i: Model description, *Tech. rep.*, Max-Planck-Institute for Meteorology, Hamburg.

Rosen, J. M. (1971), The boiling point of stratospheric aerosols, *Journal of Applied Meteorology*, *10*(5), 1044–1046, doi:10.1175/1520-0450(1971)010⟨1044:TBPOSA⟩2.0.CO;2.

Rozanov, E. V., V. A. Zubov, M. E. Schlesinger, F. Yang, and N. G. Andronova (1999), The UIUC three-dimensional stratospheric chemical transport model: Description and evaluation of the simulated source gases and ozone, *Journal of Geophysical Research*, *104*(D9), doi:10.1029/1999JD900138.

Russell, P. B., et al. (1996), Global to microscale evolution of the pinatubo volcanic aerosol derived from diverse measurements and analyses, *Journal of Geophysical Research: Atmospheres*, *101*(D13), 18,74518,763, doi:10.1029/96JD01162.

Sander, S., et al. (2011), *Chemical Kinetics and Photochemical Data for Use in Atmospheric Studies, Evaluation No. 17*, JPL Publication 10-6, Jet Propulsion Laboratory, Pasadena.

Seinfeld, J. H., and S. N. Pandis (2006), *Atmospheric chemistry and physics: from air pollution to climate change*, J. Wiley, Hoboken, N.J.

Smith, S. J., J. van Aardenne, Z. Klimont, R. J. Andres, A. Volke, and S. Delgado Arias (2011), Anthropogenic sulfur dioxide emissions: 18502005, *Atmos. Chem. Phys.*, *11*(3), 1101–1116, doi:10.5194/acp-11-1101-2011.

Solomon, S. (1999), Stratospheric ozone depletion: A review of concepts and history, *Reviews of Geophysics*, *37*(3), 275–316, doi:10.1029/1999RG900008.

Solomon, S., R. R. Garcia, F. S. Rowland, and D. J. Wuebbles (1986), On the depletion of antarctic ozone, *Nature*, *321*(6072), 755–758, doi:10.1038/321755a0.

Solomon, S., J. S. Daniel, R. R. Neely, J.-P. Vernier, E. G. Dutton, and L. W. Thomason (2011), The persistently variable Background stratospheric aerosol layer and global climate change, *Science*, *333*(6044), 866–870, doi:10.1126/science.1206027.

SPARC (2006), SPARC report no. 4, assessment of stratospheric aerosol properties (ASAP), *WCRP-124 WMO/TD No. 1295, SPARC Report No. 4, edited by: Thomason, L. and Peter, Th., WMO.*

Stenke, A., M. Schraner, E. Rozanov, T. Egorova, B. Luo, and T. Peter (2013), The SOCOL version 3.0 chemistryclimate model: description, evaluation, and implications from an advanced transport algorithm, *Geoscientific Model Development*, *6*(5), 1407–1427, doi:10.5194/gmd-6-1407-2013.

Stier, P., et al. (2005), The aerosol-climate model ECHAM5-HAM, *Atmos. Chem. Phys.*, *5*(4), 1125–1156, doi:10.5194/acp-5-1125-2005.

Stott, P. A., and R. S. Harwood (1993), An implicit time-stepping scheme for chemical species in a global atmospheric circulation model, *Annales Geophysicae*, *11*, 377–388.

Stowe, L. L., R. M. Carey, and P. P. Pellegrino (1992), Monitoring the mt. pinatubo aerosol layer with NOAA/11 AVHRR data, *Geophysical Research Letters*, *19*(2), 159162, doi:10.1029/91GL02958.

Sze, N. D., and M. K. W. Ko (1979), CS_2 and COS in the stratospheric sulphur budget, *Nature*, *280*(5720), 308–310, doi:10.1038/280308a0.

Sze, N. D., and M. K. W. Ko (1980), Photochemistry of COS, CS_2, CH_3SCH_3 and H_2S: implications for the atmospheric sulfur cycle, *Atmospheric Environment (1967)*, *14*(11), 1223–1239, doi:10.1016/0004-6981(80)90225-5.

Tabazadeh, A., O. B. Toon, S. L. Clegg, and P. Hamill (1997), A new parameterization of H_2SO_4/H_2O aerosol composition: Atmospheric implications, *Geophysical Research Letters*, *24*(15), 19311934, doi:10.1029/97GL01879.

Takigawa, M., M. Takahashi, and H. Akiyoshi (2002), Simulation of stratospheric sulfate aerosols using a center for climate system Research/National institute for environmental studies atmospheric GCM with coupled chemistry 1. nonvolcanic simulation, *Journal of Geophysical Research: Atmospheres*, *107*(D22), AAC 1–1AAC 1–11, doi:10.1029/2001JD001007.

Textor, C., H.-F. Graf, C. Timmreck, and A. Robock (2004), *Emissions from Volancoes in Emissions of Chemical Compounds and Aerosols in the Atmosphere*, Kluwer, Dordrecht, The Netherlands.

Thomason, L. W., L. R. Poole, and T. Deshler (1997), A global climatology of stratospheric aerosol surface area density deduced from stratospheric aerosol and gas experiment II measurements: 1984–1994, *Journal of Geophysical Research: Atmospheres*, *102*(D7), 8967–8976, doi:10.1029/96JD02962.

Thomason, L. W., S. P. Burton, B.-P. Luo, and T. Peter (2008), SAGE II measurements of stratospheric aerosol properties at non-volcanic levels, *Atmos. Chem. Phys.*, *8*(4), 983–995, doi:10.5194/acp-8-983-2008.

Thomson, W. (1871), LX. on the equilibrium of vapour at a curved surface of liquid, *Philosophical Magazine Series 4*, *42*(282), 448–452, doi:10.1080/14786447108640606.

Thornton, D. C., A. R. Bandy, B. W. Blomquist, J. D. Bradshaw, and D. R. Blake (1997), Vertical transport of sulfur dioxide and dimethyl sulfide in deep convection and its role in new particle formation, *Journal of Geophysical Research: Atmospheres*, *102*(D23), 28,50128,509, doi:10.1029/97JD01647.

Timmreck, C., H.-F. Graf, and I. Kirchner (1999a), A one and half year interactive MA/ECHAM4 simulation of mount pinatubo aerosol, *Journal of Geophysical Research: Atmospheres*, *104*(D8), 93379359, doi:10.1029/1999JD900088.

Timmreck, C., H.-F. Graf, and J. Feichter (1999b), Simulation of mt. pinatubo volcanic aerosol with the hamburg climate model ECHAM4, *Theoretical and Applied Climatology*, *62*(3-4), 85–108, doi:10.1007/s007040050076.

Timmreck, C., H.-F. Graf, S. J. Lorenz, U. Niemeier, D. Zanchettin, D. Matei, J. H. Jungclaus, and T. J. Crowley (2010), Aerosol size confines climate response to volcanic super-eruptions, *Geophysical Research Letters*, *37*(24), n/an/a, doi:10.1029/2010GL045464.

Tisdale, R. T., D. L. Glandorf, M. A. Tolbert, and O. B. Toon (1998), Infrared optical constants of low-temperature H_2SO_4 solutions representative of stratospheric sulfate aerosols, *Journal of Geophysical Research: Atmospheres*, *103*(D19), 25,35325,370, doi:10.1029/98JD02457.

Trepte, C. R., and M. H. Hitchman (1992), Tropical stratospheric circulation deduced from satellite aerosol data, *Nature*, *355*(6361), 626–628, doi:10.1038/355626a0.

Trepte, C. R., R. E. Veiga, and M. P. McCormick (1993), The poleward dispersal of mount pinatubo volcanic aerosol, *Journal of Geophysical Research: Atmospheres*, *98*(D10), 18,56318,573, doi:10.1029/93JD01362.

Turco, R. P., P. Hamill, O. B. Toon, R. C. Whitten, and C. S. Kiang (1979), A one-dimensional model describing aerosol formation and evolution in the stratosphere: I. physical processes and mathematical analogs, *Journal of the Atmospheric Sciences*, *36*(4), 699–717, doi:10.1175/1520-0469(1979)036⟨0699:AODMDA⟩2.0.CO;2.

Turco, R. P., R. C. Whitten, O. B. Toon, J. B. Pollack, and P. Hamill (1980), OCS, stratospheric aerosols and climate, *Nature*, *283*(5744), 283–285, doi:10.1038/283283a0.

Vaida, V., H. G. Kjaergaard, P. E. Hintze, and D. J. Donaldson (2003), Photolysis of sulfuric acid vapor by visible solar radiation, *Science*, *299*(5612), 1566–1568, doi:10.1126/science.1079297, PMID: 12624265.

Vehkamäki, H., M. Kulmala, I. Napari, K. E. J. Lehtinen, C. Timmreck, M. Noppel, and A. Laaksonen (2002), An improved parameterization for sulfuric acidwater nucleation rates for tropospheric and stratospheric conditions, *Journal of Geophysical Research*, *107*(D22), 4622, doi:10.1029/2002JD002184.

Vernier, J.-P., L. W. Thomason, T. D. Fairlie, P. Minnis, R. Palikonda, and K. M. Bedka (2013), Comment on "Large volcanic aerosol load in the stratosphere linked to asian monsoon transport", *Science*, *339*(6120), 647–647, doi:10.1126/science.1227817, PMID: 23393247.

Walcek, C. J. (2000), Minor flux adjustment near mixing ratio extremes for simplified yet highly accurate monotonic calculation of tracer advection, *Journal of Geophysical Research: Atmospheres*, *105*(D7), 93359348, doi:10.1029/1999JD901142.

Walcek, C. J., and G. R. Taylor (1986), A theoretical method for computing vertical distributions of acidity and sulfate production within cumulus clouds, *Journal of the Atmospheric Sciences*, *43*(4), 339–355, doi:10.1175/1520-0469(1986)043⟨0339:ATMFCV⟩2.0.CO;2.

Weisenstein, D. K., M. K. W. Ko, N.-D. Sze, and J. M. Rodriguez (1996), Potential impact of SO2 emissions from stratospheric aircraft on ozone, *Geophysical Research Letters*, *23*(2), 161164, doi:10.1029/95GL03781.

Weisenstein, D. K., G. K. Yue, M. K. W. Ko, N.-D. Sze, J. M. Rodriguez, and C. J. Scott (1997), A two-dimensional model of sulfur species and aerosols, *Journal of Geophysical Research*, *102*(D11), 13,019–13,035, doi:10.1029/97JD00901.

Weisenstein, D. K., J. E. Penner, M. Herzog, and X. Liu (2007), Global 2-d intercomparison of sectional and modal aerosol modules, *Atmos. Chem. Phys.*, *7*(9), 2339–2355, doi:10.5194/acp-7-2339-2007.

Yue, G. K., L. R. Poole, P.-H. Wang, and E. W. Chiou (1994), Stratospheric aerosol acidity, density, and refractive index deduced from SAGE II and NMC temperature data, *Journal of Geophysical Research: Atmospheres*, *99*(D2), 37273738, doi:10.1029/93JD02989.

Acknowledgement

First of all I would like to express my gratitude to Thomas Peter for all the practical support and warm encouragements for me throughout my PhD study in Zurich. He is always patient and guides me step by step, like when I encountered difficulties in chemistry. I enjoyed very much the discussions with him, especially, weekly skype meetings during his sabbatical leave. I benefit a lot from his challenging questions, and gradually grow into a climate scientist (from a mathematician). Again thanks for his tremendous help in finalizing my thesis during the busy period.

Special thanks go to Eugene Rozanov for his hospitality during my visits in Davos (although I never took his suggestion to ski there), his introduction to SOCOL, his great support during the entire model development of SOCOL-AER, and his fruitful discussions and valuable comments on this work.

Many thanks also go to Mian Chin for accepting to examine my thesis.

Further I would like to thank Debra Weisenstein for her excellent collaboration and her constant support during my PhD study. I also want to thank her for the hospitality during my stay in Lexington, MA. Thanks a lot to Beiping Luo for discussions on microphysics related topics, which contributed substantially to this thesis.

Many thanks to Andrea Stenke and Julien Anet for helping me in SOCOL. Many thanks also to the whole SOCOL family, Florian Arfeuille, Marco Calisto, Ancelin Coulon, Fiona Tummon, Laura Revell, and Timofei Sukhodolov. I thank my officemates, Angela Meyer, Yvonne Boose, and all the institute members for the nice atmosphere at IAC. Thanks also to my ex-officemates, Shubha Pandey and Harald Rieder for the nice moments in New York and Denver, and Pia Soonsin for a great time in Bangkok.

Many thanks to Petra Forney and Eva Choffat for taking care of the administrative issues. Especially to Petra Forney for helping in finding accommodation when I moved to Zurich. Thanks also to the IT team, especially to Urs Beyerle and his support for installing softwares.

Further thanks to Yao and Walter for taking care of me at the flat. To my friends with a 'Dr.' title, Kaya, Yanfei, Hong, Youyou, Qiang and many others for their support.

Warmest thanks to my family. To my mother and my father for their unconditional care and love. Finally to Alice, for her support, for her trust, for her love.